Strongly coupled quark-gluon plasma in heavy ion collisions

Edward Shuryak

Rev. Mod. Phys. **89**, 035001 — Published 19 July 2017

DOI: 10.1103/RevModPhys.89.035001

Strongly coupled Quark-Gluon Plasma in Heavy Ion Collisions

Edward Shuryak

Department of Physics and Astronomy,
Stony Brook University,
Stony Brook, New York 11794-3800,
USA

(Dated: April 7, 2017)

A decade ago, a brief summary of the field of the relativistic heavy ion physics could be formulated as the discovery of *strongly-coupled* Quark-Gluon-Plasma, sQGP for short, a near-perfect fluid with surprisingly large entropy-density-to-viscosity-ratio. Since 2010, the LHC heavy ion program added excellent new data and discoveries. Significant theoretical efforts have been made to understand these phenomena. Now there seems to be a need to consolidate what we have learned and formulate a list of issues to be studied next. Studies of angular correlations of two and more secondaries reveal higher harmonics of flow, identified as the sound waves induced by the initial state perturbations. Like in cosmology, detailed measurements and calculations of these correlations helped to make our knowledge of the explosion much more quantitative. In particular, their damping had quantified the viscosity. Other kinetic coefficients – the heavy quark diffusion constants and the jet quenching parameters – also show *enhancements* near the critical point $T \approx T_c$. Since densities of QGP quarks and gluons strongly decrease at this point, these facts indicate large role of non-perturbative mechanisms. e.g. scattering on monopoles. New studies of the pp and pA collisions at high multiplicities reveal collective explosions similar to those in heavy ion AA collisions. These "smallest drops of the sQGP" revived debates about the initial out-of-equilibrium stage of the collisions and mechanisms of subsequent equilibration.

CONTENTS

I. INTRODUCTION

The history of the ultrarelativistic heavy ion collisions can be roughly divided into three periods:
(i) *formulation of the scientific goals and forming the community*; from the 1950s to the year 2000, the start of operation of Relativistic Heavy Ion collider (RHIC) ;
(ii) *crucial experimental and theoretical developments* during 2000-2004, reaching the goal of QGP production and first estimates of its properties;
(iii) the *last decade*, 2005-now.

This review attempts to provide theoretical and experimental summaries in the last decade. It is mostly addressed to people belonging to heavy ion community. The experts can skip most of the Introduction and proceed directly to the next sections. Readers new to the field should read the rest of the Introduction, and perhaps some original literature referenced there. Some pedagogical material on heavy ion terminology, relativistic hydrodynamics, and holographic models is placed in the Appendix sections at the end of the paper.

Experimental results, from RHIC and now Large Hadron Collider (LHC), continue to provide answers to old question and add new puzzles. While looking through the talks at the latest Quark Matter conferences, one observes a relative weakness of the theory: this review tries to elucidate current trends. It is not a comprehensive summary of the field. Several important directions are not covered because (in my opinion) they had not yet matured to a conclusive stage. One such direction is related with fluctuations in the gauge topology and chiral magnetic effect. Another is the RHIC beam energy scan, with emphasis on critical fluctuations aimed at possible location of the critical point. There are also other topics not covered simply because of my personal limitations and interests.

A. Before RHIC

Perhaps the first question one asks in the field is *whether a tiny system created in high energy collisions, of nucleons or nuclei, can indeed be large enough to be treated as macroscopically large.* An affirmative answer would mean that some new form of matter is produced, close to its equilibrium. A negative answer would imply that one deals with a multiparticle system far from equilibrium.

Already in the 1950s, when only the very first hints on multi-particle production reactions were detected in cosmic ray events, three famous physicists conjectured that the answer to the previous question would be positive. (Fermi, 1951) argued that a strongly interacting system of particles should rapidly equilibrate, and predicted that multiplicity should grow with (CM) energy $\sqrt{s}$ as $N \sim s^{1/4}$. (Pomeranchuk, 1951) replied immediately: if the interaction is strong enough for rapid equilibration, then the particles would be able to leave the system only at what we now call the freezeout conditions. (Landau, 1953) elegantly connected the initial stage of Fermi with the final stage of Pomeranchuck via *relativistic hydrodynamics.* He pointed out that in the expected quasi-adiabatic expansion the entropy must be preserved, and thus Fermi's prediction for entropy/multiplicity generation should hold.

In a later review, Landau related these expectations of very strong coupling at high momenta scales, as expected from QED and other QFT's known at the time. This last argument has been dramatically reversed two decades later, when asymptotic freedom of non-Abelian gauge theories and QCD was discovered by Gross,Politzer, and Wilczek in 1973. This discovery initiated studies of the high temperature, T, (or large chemical potential, μ, or both) limit of hadronic matter using perturbative diagrams and their re-summations. It has been found that, unlike vacuum fluctuations of the gluon fields providing the asymptotic freedom or *anti-screening*, thermal fluctuations of both gluon and quark fields lead to *screening* in matter, thus it was called "Quark-gluon plasma", QGP for short. For early reviews on finite-T QCD see (Gross *et al.*, 1981; Shuryak, 1980). Very hot QGP is now referred to as *weakly coupled* (wQGP). While the simplest from theoretical perspective, it is not yet reached even at the highest temperatures reached at the LHC collider.

While during the 1970s and 80s the field and its conferences was mostly ran by theorists, appropriate experimental observables were high on the agenda. Collective hydrodynamical *explosion in the transverse plane*, and *penetrating probes* (photons and dileptons) were emphasized (Shuryak, 1980). Important QGP signals suggested

in the 1980s were the *jet quenching* (Bjorken, 1982) and *subsequent melting* of charmonium and bottonium states (Matsui and Satz, 1986).

Two "experimental homes" of the field are the European center for nuclear research near Geneva, known by its French abbreviation CERN, and Brookhaven National Laboratory (BNL) on Long Island, New York. The first round of fixed target experiments started in both places soon led to realization that the collision energy is insufficient and thus heavy ion colliders are needed. The decision of the US nuclear physics community was to build Relativistic Heavy Ion Collider (RHIC), completed in 2000, initially with four detectors: larger STAR and PHENIX and smaller PHOBOS and BRAMHS.

Prior to the RHIC era, it was widely assumed that the wQGP regime extends down to the phase transition point. Numerical simulations of QCD-like theories on supercomputers, using space- (Euclidean) time discretization – "lattice QCD" for short – had provided first-principle results on QCD thermodynamics[1] A cross-over transition at

$$T_c \approx 155\, MeV \tag{1}$$

separate confining phase with broken chiral symmetry restoration from QGP region at $T > T_c$. The same value is observed experimentally, as "chemical freezeout" defining the composition of outgoing hadrons.

Most QCD theorists were skeptical, predicting that RHIC program – aimed at production of new form of matter – would basically fail. Perturbative estimates in the framework of various parton cascades indicated an unrealistically long equilibration time, and predicted "firework of minijets" rather than a collective explosion.

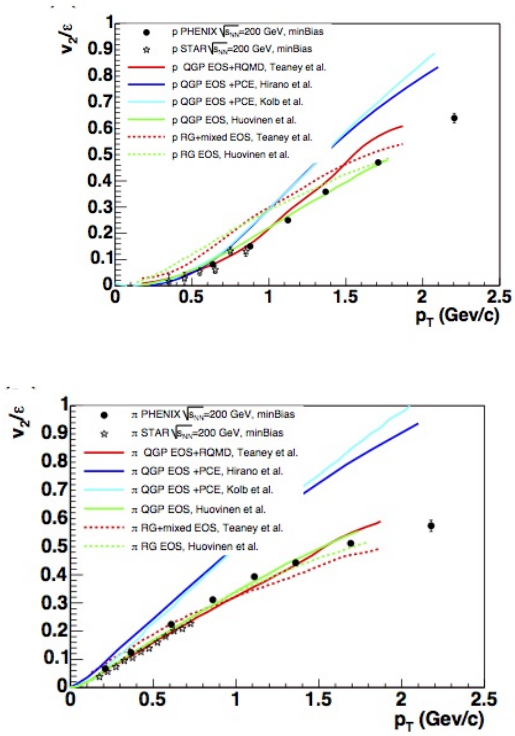

FIG. 1 (color online) From PHENIX white paper (Adcox *et al.*, 2005): elliptic flow parameter v_2, the experimental data versus the hydrodynamical predictions, for pions (upper plot) and protons (lower plot).

B. RHIC runs in years 2000-2005 and sQGP paradigm

From the very first RHIC data, it became clear that what is seen is a rather spectacular collective explosion, with *spectra* and especially the *elliptic flows* found to be in excellent agreement with predictions of relativistic hydrodynamics. Especially successful were its versions supplemented by hadronic cascade at freezeout (Hirano *et al.*, 2006; Teaney *et al.*, 2001a,b). All relevant dependences – as a function of[2] transverse momentum $p_\perp$, centrality, particle mass, rapidity and collision energy – were well reproduced.

It took a few years to document the extent of *jet quenching*, but by 2004 the case for "quark-gluon plasma discovery" had been officially made, in a theory workshop at Brookhaven and then in summarizing "white papers" produced by all four RHIC collaborations. Those, especially by PHENIX (Adcox *et al.*, 2005) and STAR (Bellwied, 2005), are written as extensive reviews and can both be recommended as a pedagogical introduction to the field.

Perturbative parton cascades and hydrodynamics made very different predictions for the elliptic flow parameter[3] v_2. Let us mention one of them: the dependence on the transverse momentum $v_2(p_\perp)$. Parton model describes colliding nucleons and nuclei in terms of "partons", quarks and gluons with certain fraction of the total momentum x and "resolution scale" Q. For large enough $Q \gg 1\, GeV$ parton-parton scattering locally knows only the direction of the impact parameter $\vec{b}$ toward the parton it scatters with, but not the overall impact parameter of two nuclei. So high $p_\perp$ partons are, to first approximation, distributed isotropically in azimuthal angle ϕ. Only the low $p_\perp$ partons, with wavelength comparable to the

[1] The thermodynamic quantities such as energy density and pressure are briefly introduced in Appendix.

[2] For the readers who may need it, some explanation of what those variables are can be found in the Appendix.

[3] See appendix A for the definition.

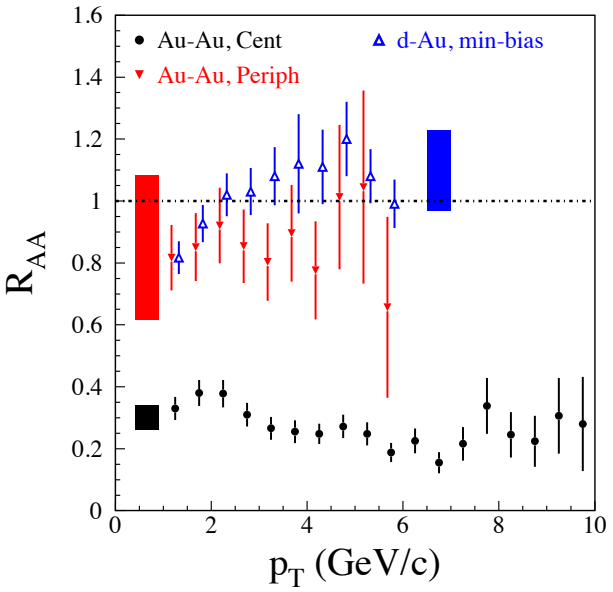

FIG. 2 (from historic PHENIX white paper (Adcox *et al.*, 2005)) The ratio R_{AA} of the yield of high $p_\perp$ hadrons in dAu and $AuAu$ collisions to the expected one according to parton model scaling. Strong deviation from one of this ration indicate the jet quenching phenomenon.

size of the overlapping regions of both nuclei, $1/p_\perp \sim R$, may have a substantial anisotropy in ϕ. So, in the first approximation, such models have no reasons for v_2 to increase with $p_\perp$. Furthermore, since next-order inelastic production of new partons dominates over their absorption, it was predicted that more partons appear in the *longest* direction of the overlap "almond", $\phi = \pm\pi/2$, so v_2 was predicted to be *negative*.

Hydrodynamics, on the other hand, predicts an anisotropic explosion driven by the pressure gradient. The largest gradient is in shorter direction of the almond $\phi = 0, \pi$, so v_2 was predicted to be *positive*. Furthermore, larger $p_\perp$ particles originate from the edge of the fireball moving toward the observer. The consequence of such "splash" geometry is that v_2 was predicted to *increase* linearly with $p_\perp$. The observed dependence of the elliptic flow parameter v_2 for pions and protons on the particle transverse momentum are shown in Fig.1: so v_2 does grow linearly with p_t, reaching large value ~ 0.2 as predicted by hydrodynamics.

Note, that while the agreement is quite good through the whole kinematic region shown in this plot, theoretical curves stop at $p_\perp = 2\,GeV$. Indeed, even the bravest theorists at the time had not dared to venture beyond it, since it was commonly expected that above such $p_\perp$ one would enter a jet-dominated regime. Yet hydro-dominated region was found to extend to $p_\perp \sim 4\,GeV$, and the transition to power-like jet regime in fact is observed only at $p_\perp > 10\,GeV$. It turned out that the jet yield, and with it contributions to hard particle spectra, are strongly suppressed by jet quenching. This phenomenon is demonstrated by Fig.2, also taken from PHENIX white paper (Adcox *et al.*, 2005).

These observations and conclusions were of course scrutinized in the years to come, and the range and degree of the agreement with this picture in fact only increased. In particular, the ellipticity parameter v_2 has been measured using correlations of several (4,6 etc) particles, confirming a conclusion that this is truly collective phenomenon. Indeed *all* thousands of secondaries do share the same anisotropic distribution in a given event.

These data, and their comparison with theoretical approaches, had created a new paradigm called "strongly coupled" Quark-Gluon-Plasma, sQGP for short. In order to quantify it, one needs to introduce certain *kinetic coefficients*, parameters describing deviations from ideal hydrodynamics in an expansion in gradients. The first one, the *shear viscosity* entering the Navier-Stokes first-order term, is usually mentioned as a ratio to the entropy density, since both are $O(T^3)$ in scale-invariant QGP. Since the viscosity is inversely proportional to scattering cross section times the density, we prefer to use the inverse ratio, entropy-density-to-viscosity. Its value turned out to be unexpectedly large

$$\frac{s}{\eta} \approx 5 - 10 \gg 1 \tag{2}$$

Thus the sQGP is among "the most perfect fluid" known.

The only "competitor" to sQGP, with comparably large entropy-to-viscosity ratio, is the so called "unitary gas" of trapped fermionic atoms, with the scattering length $a \to \infty$. Both of such fluids demonstrated spectacular elliptic flows. Note that those two fluids are at the opposite end of the scales known to physics: sQGP has T measured in fraction of GeV while T of the unitary gas is measured in nK, or 22 orders of magnitude smaller. Yet the scale hardly matter: in fact both of them are nearly scale-invariant by themselves. The unusual kinetic parameters of them are two major puzzles of modern manybody physics.

To understand why it was unexpected, it is convenient to compare it to various predictions. Kinetic theory (valid for weak coupling) would interpret this dimensionless ratio as the product of the particle density, transport cross section and inverse power of the mean velocity

$$\frac{s}{\eta} \sim \frac{n\sigma_{transport}}{T\bar{v}} \tag{3}$$

or, a bit simpler, as the ratio of interparticle separation to the mean free path. In a kinetic regime the latter is larger, so this ratio is expected to be small. More specifically, in weakly coupled plasma (Arnold *et al.*, 2003) it is

$$\frac{s}{\eta} = \frac{g^4 log(2.42/g)}{5.12} \tag{4}$$

Since it was derived assuming the "electric scale" is small compared to momenta, $M_D \sim gT \ll T$, it should perhaps be used only [4] for $g < 1$. This expression, valid at high T, was not intended to be used at $T \sim T_c$, where the density of quarks and gluons are suppressed by confinement, the vanishing Polyakov line $< P(T \to T_c) > \to 0$. The contribution of the gluon-gluon scattering to the (inverse) ratio η/s including this effect is shown in the lower part of Fig. 3.

The non-perturbative models (see Fig.3) predict otherwise: s/η has a *peak* at T_c. Qualitatively similar behavior of kinetic coefficients is known for other fluids near their phase transitions (see examples in (Csernai *et al.*, 2006)). The peak in shear viscosity correlates with similar peaks claimed for other kinetic parameters – heavy quark diffusion constant we will discuss in section X, the jet quenching parameter $\hat{q}$ to be discussed in XI, see Fig.57.

C. The first runs of LHC

The European nuclear and particle physicists decided to share the same Large Hadron Collider (LHC). One detector – ALICE – was built specially for heavy ion conditions, capable to work with high multiplicities reaching 10000 or so in an event. Two other collaborations, CMS and ATLAS, although built mostly for high energy physics goals, both include subgroups focused on heavy ions as well.

The first runs of the LHC were expected with obvious interest. At one hand, the energy of this collider is about a factor of 20 higher than of RHIC, which leads to about twice larger multiplicity. Hydrodynamics predicted stronger flows: indeed, at the LHC conditions relatively "stiff" QGP play larger role than "soft" matter near and below the critical point T_c. On the other hand, entering a higher T domain means higher momentum scale, reaching well over 1 GeV, where many colleagues expected the onset of asymptotic freedom and perturbative regime.

The first LHC run took place in 2010; radial and elliptic flows stronger than at RHIC were observed, confirming the hydrodynamic predictions once again. More recently the energy of LHC has been doubled: and collective effects like elliptic flow get further enhanced as well.

D. Why is sQGP so unusual?

Attempts to answer this question led to significant progress in our understanding of the finite-T QCD. Its important part are large-scale lattice gauge simulations,

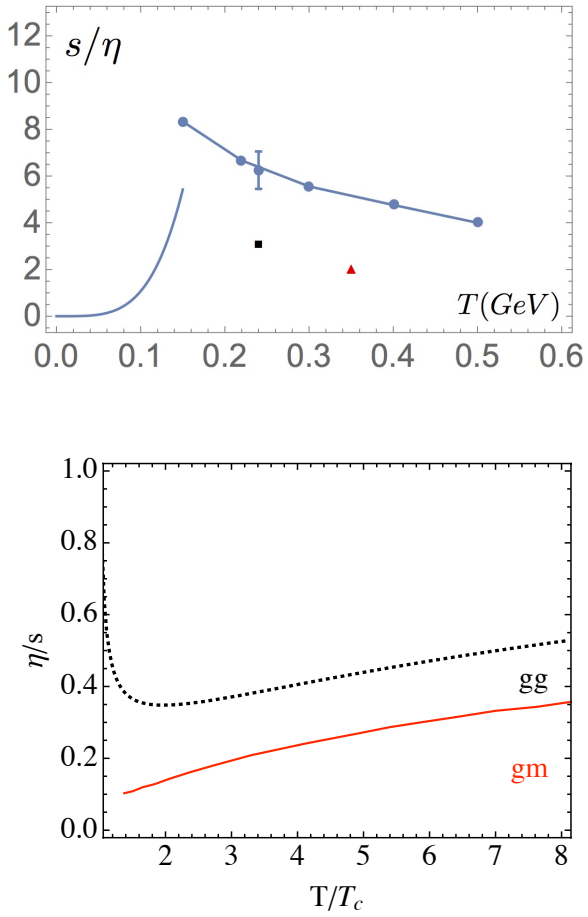

FIG. 3 Upper plot: The entropy density to viscosity ratio s/η versus the temperature $T\,(GeV)$. The upper range of the plot, $s/\eta = 4\pi$ corresponds to the value in infinitely strongly coupled $\mathcal{N}$=4 plasma (Policastro *et al.*, 2001). Curve without points on the left side corresponds to pion rescattering according to chiral perturbation theory (Prakash *et al.*, 1993). Single (red) triangle corresponds to molecular dynamics study of classical strongly coupled colored plasma (Gelman *et al.*, 2006a), single (black) square corresponds to numerical evaluation (Nakamura and Sakai, 2005) on the lattice. The single point with error bar correspond to the phenomenological value extracted from the data, see text. The series of points connected by a line correspond to gluon-monopole scattering (Ratti and Shuryak, 2009). Lower plot: The inverse ratio η/s as a function of the temperature normalized to its critical value T/T_c. The solid line marked *gm* correspond to gluon-monopole scattering (Ratti and Shuryak, 2009), same as in the upper plot, the dashed line shows the perturbative gluon-gluon scattering.

which not only quantified the thermodynamical quantities of QGP and located confinement and chiral symmetry breaking phase transitions, but also elucidated physics of certain non-perturbative and topological effects. Presenting all of that systematically goes well beyond the present paper, which is focused on heavy ion

[4] See Fig.4 and discussion there of this point.

collisions. Instead we outline in this section the main ideas proposed, on a non-technical intuitive level.

At high T the asymptotic freedom limits the coupling at scale T, while plasma screening reduces interaction below the momentum scale gT: so QCD regime is amenable to perturbative description. As T decreases, toward the end of the QGP phase at T_c , the effective coupling grows. Opinions differ on how one should describe matter in this domain. Different schools of thought can be classified as (i) perturbative, (ii) semiclassical; (iii) dual magnetic; and (iv) dual holographic ones.

(i) A "perturbative school" suggest that as one reduces temperature from its high values down to $T \approx T_c$ nothing crucial happens. The basic conclusions based on perturbative diagrams and their re-summation hold. Quark and gluon quasiparticles are dominant, together with plasma-related phenomena like plasmon and plasmino excitation modes. Perturbative formulae qualitatively hold even when the running coupling reaches values of $\alpha_s = g^2/4\pi \sim 0.5, g \approx 2.5$ or so. In particular, using this logics for viscosity calculated perturbatively (Arnold *et al.*, 2003) one get the ratio mentioned ~ 2, only factor 2-5 lower than the data. Considering higher order processes one can recover this factor, see e.g. discussion in (Xu and Greiner, 2005).

The boundary of perturbative and non-perturbative domain is a very important subject, to which, unfortunately, not enough attention has been devoted. The pQCD diagrams provide the answer in form of a series in powers of $\alpha_s/\pi = g^2/4\pi^2$, so naively it can be used for say $\alpha_s < 1/2$. And yet, looking at the Particle Data Group plot of the running QCD coupling, one finds that all but one coupling determinations are at the scale $Q \approx 10\, GeV$ and above. The only exception, the τ lepton decays, defining $\alpha_s(Q = m_\tau)$, is based on very carefully selected combination of the vector and axial spectral densities, in which the non-perturbative effects are maximally suppressed. In general, studies of point-to-point correlation functions, from phenomenology or lattice, is the most direct source of information about relative magnitude of perturbative and non-perturbative effects. The most relevant to the question of perturbative treatment of gluons are correlators of the type

$$< G^2_{\mu\nu}(x) G^2_{\mu\nu}(0) >, \quad < G_{\mu\nu}\tilde{G}_{\mu\nu}(x) G_{\alpha\beta}\tilde{G}_{\alpha\beta}(0) >$$

As originally observed in (Novikov *et al.*, 1981), their perturbative behavior sets at a much higher scale for $Q^2 > 10\, GeV^2$. Lattice studies confirm that, and in general show that the lowest glueball masses with most quantum numbers are about 2-3 GeV, while the perturbative continuum in the spectral densities is setting in well above that.

The perturbation theory at finite T is different from its vacuum version: re-summations of new IR divergent series becomes mandatory, and the resulting series go in powers of g rather than α_s/π. Where the perturbative series are convergent depends on higher order coefficients, which are rarely known. An exceptional case is the QGP free energy, to which a lot of efforts has been invested. The first perturbative corrections, calculated by myself in 1970s, was an order of magnitude smaller than the zeroth order, so the beginning of perturbative series looked promising. Many years of efforts resulted in further terms (we will use those from (Kajantie *et al.*, 2003)) plotted as a function of the coupling g in Fig.4 , as ratios to the first $O(g^2)$ perturbative effect. From this plot the reader can judge at which coupling these series are reliable. Unfortunately, we do not yet know the magnitude of perturbative corrections to kinetic coefficients.

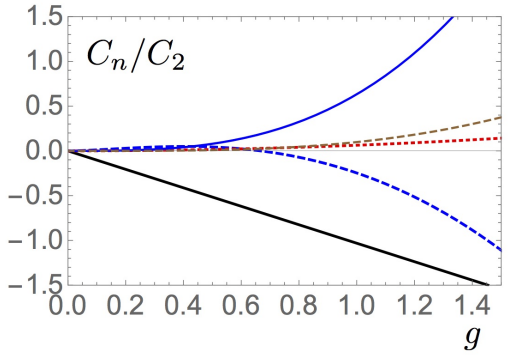

FIG. 4 Ratio of subsequent perturbative corrections to the first one $O(g^2)$: $g^3, g^4 log(g), g^4, g^5, g^6 log(g)$ are shown versus g by the black thick, blue dashed thick, red dotted, blue thin and brown dashed curves, respectively.

(ii) What can be called "the semiclassical direction" focuses on evaluation of the path integral over the fields using generalization of the saddle point method. The extrema of its integrand are identified and their contributions evaluated. It is so far most developed in quantum mechanical models, for which 2 and even 3-loop corrections have been calculated. In the case of gauge theories extrema are "instantons", complementing perturbative series by terms $\sim exp(-const/g^2)$ times the so called "instanton series" in g^2. This result in the so called *transseries*, which are not only more accurate than perturbative ones, but they are suppose to be free from ambiguities and unphysical imaginary parts which perturbative and instanton series separately have.

For the finite-temperature applications, plugging logarithmic running of the coupling into such exponential terms one finds some *power* dependences of the type

$$e^{-S} \sim exp\left(-\frac{const}{g^2(T)}\right) \sim (\frac{\Lambda}{T})^{power} \qquad (5)$$

So, these effects are not important at high T but explode – as inverse powers of T – near T_c.

In 1980-1990's it has been shown how instanton-induced interaction between light quarks *break the chiral symmetries*, the $U_A(1)$ explicitly and $SU(N_f)$ spontaneously. The latter is understood via collectivization of fermionic zero modes, for a review see (Schafer and Shuryak, 1998). Account for non-zero average Polyakov line, or non-zero vacuum expectation value of the zeroth component of the gauge potential[5] $< A_0 >$ require redefined solitons, in which this gauge field component does not vanish at large distances. Account for this changed instantons into a set of N_c instanton constituents, the so called Lee-Li-Kraan-van Baal (LLKvB) *instanton-dyons*, or instanton-monopoles (Kraan and van Baal, 1998; Lee and Lu, 1998). It has been recently shown that those, if dense enough, can naturally generate *both* confinement and chiral symmetry breaking, see (Larsen and Shuryak, 2016; Liu *et al.*, 2015), for recent review see (Shuryak, 2016). These works are however too recent to have impact on heavy ion physics, and we will not discuss it in this review.

(iii) A "dual magnetic" school consists of two distinct approaches. A "puristic" point of view assumes that at the momentum scale of interest the electric coupling is large, $\alpha_s \gg 1$, and therefore there is no hope to progress with the usual "electric" formulation of the gauge theory, and therefore one should proceed with building its "magnetic" formulation, with weak "magnetic coupling" $\alpha_m = 1/\alpha_s \ll 1$. Working example of effective magnetic theory of such kind were demonstrated for supersymmetric theories, see e.g. (Seiberg and Witten, 1994). For applications of the dual magnetic model to QCD flux tubes see (Baker *et al.*, 1997).

A more pragmatic point of view – known as "magnetic scenario" – starts with acknowledgement that both electric and magnetic couplings are close to one, $\alpha_m \sim \alpha_e \sim 1$. So, neither perturbative/semiclassical nor dual formulation will work quantitatively. Effective masses, couplings and other properties of all coexisting quasiparticles – quarks, gluons and magnetic monopoles – can only be deduced phenomenologically, from the analysis of lattice simulations. We will discuss this scenario below in this section.

(iv) Finally, very popular during the last decade are "holographic dualities", connecting strongly coupled gauge theories to a string theory in the curved space with extra dimensions. As shown by (Maldacena, 1999), in the limit of the large number of colors, $N_c \to \infty$, it is a duality to much simpler – and weakly coupled – theory, a modification of *classical gravity*. Such duality relates problems we wish to study "holographically" to some problems in general relativity. In particular, the thermally equilibrated QGP at strong coupling is related to certain black hole solutions in 5 dimensions, in which the plasma temperature is identified with the Hawking temperature, and the QGP entropy with the Bekenstein entropy. For readers who may need it some minimal terminological introduction is given in Appendix. Section VII summarizes studies of the *out-of-equilibrium* settings, in which a bulk black hole is initially absent, but then is dynamically generated. Holographic models of the AdS/QCD types also lead to new views on the QCD strings, Reggeons and Pomerons: see section VIII.C.

Completing this round of comments, we now return to (iii), the approach focused on magnetically charged quasiparticles, and provide more details on its history, basic ideas and results.

J.J.Thompson, the discoverer of the electron, noticed that something unusual should happen already for static electric and magnetic charges existing together. While both the electric field $\vec{E}$ (pointing from the center of the electric charge e) and the magnetic field $\vec{B}$ (pointing from the center of the magnetic charge g) are static (time independent), the Pointing vector

$$S = [\vec{E} \times \vec{B}]$$

indicates that the electromagnetic field energy rotates. In fact, requiring the resulting angular momentum to be quantized, to an integer times $\hbar$, one get the Dirac condition (see below).

A.Poincare went further, allowing one of the charges to move in the field of another. The Lorentz force

$$m\ddot{\vec{r}} = -eg\frac{[\dot{\vec{r}} \times \vec{r}]}{r^3} \tag{6}$$

is proportional to the product of two charges, electric e and magnetic g. The total angular momentum of the system includes the field contribution

$$\vec{J} = m[\vec{r} \times \dot{\vec{r}}] + eg\frac{\vec{r}}{r} \tag{7}$$

Its conservation leads to unusual consequence: unlike in the case of the usual potential forces, in this case the particle motion is not restricted to the scattering plane, normal to $\vec{J}$, but to a different 2-d surface, called the *Poincare cone*.

In the quantum-mechanical setting the problems involving a pair of electrically and magnetically charged particles provides further surprises. The angular momentum of the field mentioned above must take values proportional to $\hbar$ with integer or semi-integer coefficient: this leads to famous *Dirac quantization condition* (Dirac, 1931)

$$eg = \frac{1}{2}\hbar c n \tag{8}$$

(where we keep $\hbar$, unlike most other formulae) with an integer n in the r.h.s. Dirac himself derived it differently,

[5] Note that in gauge theory at finite temperatures there is a preferable frame, in which matter is at rest. Therefore this expectation value does not contradict to Lorentz invariance of the vacuum.

arguing that the unavoidable singularities of the gauge potential of the form of the Dirac strings should be pure gauge artifacts and thus invisible. He emphatically noted that this relation was the first reason for electric charge quantization.

Many outstanding theorists – Dirac and Tamm among them – wrote papers about a quantum-mechanical version of the quantum-mechanical problem of a monopole in a field of a charge, yet this problem was fully solved only decades later (Boulware *et al.*, 1976; Schwinger *et al.*, 1976). It is unfortunate that this beautiful and instructive problem is not – to our knowledge – part of any textbooks on quantum mechanics. The key element was substitution the usual angular harmonics $Y_{l,m}(\theta,\phi)$ by other functions, which for large l,m replicates the Poincare cone rather than the scattering plane.

The resurfaced interest to monopoles in 1970s was of course inspired by the discovery of 't Hooft-Polyakov monopole solution ('t Hooft, 1974; Polyakov, 1974) for Georgi-Glashow model, with an adjoint scalar field complementing the non-Abelian gauge field. In the 2+1 dimensional theories such monopoles play the role of instantons: their long-range interaction was used by (Polyakov, 1977) to prove confinement, in a gauge theory in this dimension of space-time.

In the real world, with 3+1 space-time dimensions, the monopoles are quasiparticles. A different confinement mechanism has been conjectured ('t Hooft, 1978; Mandelstam, 1976): monopoles may undergo Bose-Einstein condensation, provided their density is large enough and the temperature sufficiently low. These ideas, known as the "dual superconductor" model, were strongly supported by lattice studies.

The monopole story continued at the level of quantum field theories (QFTs), with another fascinating turn. Dirac considered the electric and magnetic charges e,g to be some fixed parameters: but in QFTs the charges run as a function of the momentum scale. So, to keep the Dirac condition, $e(Q)$ and $g(Q)$ must be running *in the opposite directions*, keeping their product fixed. In QCD-like theories the electric coupling is small in UV (large Q) but increase toward IR (small Q).

One great example of the kind was provided by the $\mathcal{N}$=2 supersymmetric theory for which partial solution was found in (Seiberg and Witten, 1994). In this theory, possessing adjoint scalar fields, the monopoles do exist as particles with well-defined masses. Furthermore, for certain special values of the vacuum expectation value (VEV) of the Higgs field, they do indeed become massless and weakly interacting, while the electric ones – gluons and gluinos – are very heavy and strongly interacting. The corresponding low energy magnetic theory is (supersymmetric) QED, and its beta function, as expected, has the opposite sign to that of the electric theory.

Even greater examples are provided by the 4-dimensional conformal theories, such as $\mathcal{N}$=4 super-Yang-Mills. Those theories are *electric-magnetic selfdual*. This means that monopoles, dressed by all fermions bound to them, form the same spin multiplet as the original fields of the "electric theory". Therefore, the beta function of this theory should be equal to itself with the minus sign! The only solution to that is that it must be identically zero, or the theory is conformal.

Completing this brief pedagogical update, let us return to (Liao and Shuryak, 2007) paper, considering properties of a classical plasma, including both electrically and magnetically charged particles[6]. Let us proceed in steps of complexity of the problem, starting from 3 particles: a *pair* of $\pm q$ static electric charges, plus a monopole which can move in their "dipole field". Numerical integration of the equation of motion had showed that the monopole's motion takes place on a curious surface, interpolating two Poincare cones with ends at the two charges: so-to-say, two charges play ping-pong with a monopole, without even moving! Another way to explain it is by noting that an electric dipole is "dual" to a "magnetic bottle", with magnetic coils, invented to keep electrically charged particles inside.

The next example was a cell with 8 alternating static positive and negative charges – modeling a grain of salt. A monopole, which is initially placed inside the cell, has formidable obstacles to get out of it: hundreds of scattering with the corner charges happen before it takes place. The Lorentz force acting on magnetic charge forces it to rotate around the electric field. Closer to the charge the field grows and thus rotation radius decreases, and eventually two particles collide.

Finally, multiple (hundreds) of electric and magnetic particles were considered in (Liao and Shuryak, 2007), moving according to classical equation of motions. It was found that their paths essentially replicate the previous example, with each particle being in a "cage", made by its dual neighbors. These findings provide some explanation of why electric-magnetic plasma has unusually small mean free path and, as a result, an unusually perfect collective behavior.

At the quantum-mechanical level the many-body studies of such plasma are still to be done. So one has to rely on kinetic theory and binary cross sections. Those for gluon-monopole scattering were calculated in (Ratti and Shuryak, 2009). It was found that gluon-monopole scattering dominates over the gluon-gluon one, as far as transport cross sections are concerned. and produce values of the viscosity quite comparable with that is observed in sQGP experimentally, as was already shown in Fig.3 . What is also worth noting, it does predict a maximum of this ratio at $T=T_c$, reflecting the behavior of the density of monopoles.

[6] We are not aware of other attempts to study such setting, although it is hardly possible that nobody thought of it.

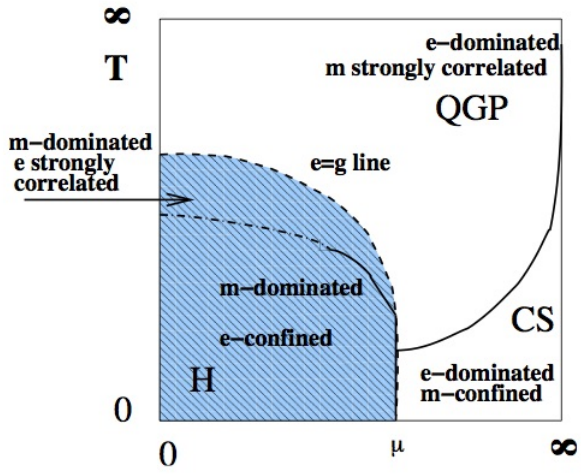

FIG. 5 A schematic phase diagram on a (compactified) plane of temperature and baryonic chemical potential, $T-\mu$, from (Liao and Shuryak, 2007). The (blue) shaded region shows magnetically dominated region $g < e$, which includes the deconfined hadronic phase as well as a small part of the QGP domain. Unshaded region includes the electrically dominated part of QGP and the color superconducting (CS) region, which has e-charged diquark condensates and is therefore "magnetically confined". The dashed line called e=g line is the line of electric-magnetic equilibrium. The solid lines indicate true phase transitions, while the dash-dotted line is a deconfinement cross-over line.

Returning to QCD-like theories which do not have powerful extended supersymmetries which would prevent any phase transitions and guarantee smooth transition from UV to IR, one finds transition to confining and chirally broken phases. Those have certain quantum condensates which divert the RG flow to hadronic phase at $T < T_c$. Therefore the duality argument must hold at least in the plasma phase, at $T > T_c$. We can follow the duality argument and the Dirac condition only half way, till $e^2/4\pi\hbar c \sim g^2/4\pi\hbar c \sim 1$. This is a plasma of coexisting electric quasiparticles and magnetic monopoles.

One can summarize the picture of the so called "magnetic scenario" by a schematic plot shown in Fig. 5, from (Liao and Shuryak, 2007). At the top – the high T domain – and at the right – the high density domain – one finds weakly coupled or "electrically dominated" regimes, or wQGP. On the contrary, near the origin of the plot, in vacuum, the electric fields are, subdominant and confined into the flux tubes. The vacuum is filled by the magnetically charged condensate, known as "dual superconductor". The region in between (relevant for matter produced at RHIC/LHC) is close to the "equilibrium line", marked by $e = g$ on the plot. (People for whom couplings are too abstract, can for example define it by an equality of the electric and magnetic screening masses.) In this region both electric and magnetic coupling are equal and thus $\alpha_{electric} = \alpha_{magnetic} = 1$: so neither the electric nor magnetic formulations of the theory are simple.

Do we have any evidence for a presence or importance for heavy ion physics of "magnetic" objects? Here are some arguments for that based on lattice studies and phenomenology, more or less in historical order:

(i) In the RHIC/LHC region $T_c < T < 2T_c$ the VEV of the Polyakov line $< P >$ is substantially different from 1. It was argued by (Hidaka and Pisarski, 2008) that $< P >$ must be incorporated into density of thermal quarks and gluons, and thus suppress their contributions. They called such matter "semi-QGP" emphasizing that say only about half of QGP degrees of freedom should actually contribute to thermodynamics at such T. And yet, the lattice data insist that the thermal energy density remains close to the T^4 trend nearly all the way to T_c.

(ii) "Magnetic scenario" (Liao and Shuryak, 2007) proposes to explain this puzzle by ascribing "another half" of such contributions to the magnetic monopoles, which are not subject to $< P >$ suppression because they do not have the electric charge. A number of lattice studies found magnetic monopoles and had shown that they behave as physical quasiparticles in the medium. Their motion definitely shows Bose-Einstein condensation at $T < T_c$ (D'Alessandro *et al.*, 2010). Their spatial correlation functions are very much plasma-like. Even more striking is the observation (Liao and Shuryak, 2008) revealing magnetic coupling which *grows* with T, being indeed an inverse of the asymptotic freedom curve.

The magnetic scenario also has difficulties. Unlike instanton-dyons we mentioned, lattice monopoles so far defined are gauge dependent. The original 'tHooft-Polyakov solution require an adjoint scalar field, absent in QCD Lagrangian, but perhaps an effective scalar can be generated dynamically. In the Euclidean time finite-temperature setting this is not a problem, as A_0 naturally takes this role, but it cannot be used in real-time applications required for kinetic calculations.

(iii) Plasmas with electric and magnetic charges show unusual transport properties: Lorenz force enhances collision rate and reduce viscosity (Liao and Shuryak, 2007). Quantum gluon-monopole scattering leads to large transport cross section (Ratti and Shuryak, 2009), providing small viscosity in the range close to that observed at RHIC/LHC.

(iv) The high density of (non-condensed) monopoles near T_c leads to compression of the electric flux tubes, perhaps explaining curious lattice observations of very high tension in the potential energy (not free energy) of the heavy-quark potentials near T_c (Liao and Shuryak, 2007), see section X.

(v) Last but not least, the peaking density of monopoles near T_c seem to be directly relevant to jet quenching, see section XI.

Completing this introduction to monopole applica-

tions, it is impossible not to mention the remaining unresolved issues. Theories with adjoint scalar fields – such as e.g. celebrated $\mathcal{N}$=2 Seiberg-Witten theory – naturally have particle-like monopole solutions. Yet in QCD-like theories without scalars the exact structure of the lattice monopole are not yet well understood. There are indications that most, if not all, of monopole physics can be taken care of via the instanton-dyons we mentioned above: in this case the role of the adjoint "Higgs" is played by the time component of the gauge potential A_4. Dyon solution is well defined and real in the Euclidean time, but would become imaginary in the Minkowski continuation: so it is not a "particle" in ordinary sense.

II. THE MAIN ISSUES IN QCD AND HEAVY ION PHYSICS

Let us start with few "super-questions" (and comments on them), which are common to the whole strong interaction physics, extending well beyond the boundaries of the heavy ion field.

I.**Can one locate the "soft-to-hard" boundary**, in whatever observables under consideration, where the transition from weak to strong coupling regimes take place?

II. Can one locate the **'micro-to- macro" boundary,** where some transition in the value of mean-free-path happens, from large (ballistic) to small (hydrodynamic) regime? In particular, which experimental observables display best this transition.

III. Can we experimentally locate **the QCD critical point**, by following higher order fluctuations/correlations?

Brief comments on them are:

(Ia) We already mentioned that large variety of correlation functions has been studied on the lattice and phenomenologically, locating transition between pQCD and non-perturbative regimes in various channels. The closest to it in experiments are hard exclusive processes, e.g. the pion and nucleon formfactors. To the highest $Q^2 \sim 4\,GeV$ measured so far, neither of them had reached quantitative agreement with the pQCD predictions. Because of its importance, the experimental studies should be continued to higher momenta, till such agreement be observed.

In the heavy ion field there exist a hotly debated "minijet" issue. While the identified jets have rather large momenta, $p_\perp > 20\,GeV$ or so, it is generally assumed that the parton description is valid down to much smaller momenta. How much smaller? Following DGLAP evolution toward small Q^2 all the way to $\sim 1\,GeV^2$ one eventually reach a negative gluon density. This and other arguments tell us that at this scale, $1\,GeV$, pQCD cannot be used. At which scale Q_{min} one has to stop is defined by the "higher twist effects", not yet studied to the extent to provide a quantitative answer.

(Ib) The elementary process fundamental for our field is *pp* scattering. Its total cross section and elastic amplitude is described by Pomeron phenomenology. The elastic amplitude is a function of the momentum transfer $t = -q^2$, its Bessel-Fourier transform is the profile function $F(b)$, depending on the impact parameter b. Small b is understood via perturbative BFKL Pomeron, while large b via some string-exchange models. In this case the experimental data actually do indicate a sharp transition between these regimes. Attempts to understand both regimes in a single AdS/QCD framework have been successful (Stoffers and Zahed, 2013). Furthermore, it has been suggested that the critical b is related to critical temperature T_c of the phase transition in the gauge theory; we will discuss this in section VIII.C.

Ic. Proceeding from elastic to inelastic collisions, when should we describe the initial snapshots of hadrons/nuclei in terms of partons (quarks and gluons) or non-perturbative effective objects (monopoles, strings)? As we will discuss, these initial effective objects produce fluctuations, which, via long-lived hydro sound modes, are visible to the detectors. Therefore, at least their number becomes experimentally observable.

(IIa) Heavy ion (AA) collisions are now complemented by "small systems", *pA* and *pp* collisions. At high enough multiplicity they display collective phenomena – radial, elliptic and even triangular flows. One would like to quantify the regime change, if possible, experimentally and theoretically. Unfortunately, so far no sharp transitions are detected.

(IIb) Where exactly is the boundary between the micro and macro theories? Textbook answer is that one can compare the micro or "mean free path" scale l to the size of the system

$$L \gg l \tag{9}$$

and if the l/L ratio is small one can use the macroscopic theories. Small phenomenological viscosity suggests that the mean free path in sQGP is few times *smaller* than the interparticle distance! By observing the smallest exploding systems, one is checking if this makes sense and is indeed the case.

III. SOUNDS ON TOP OF THE "LITTLE BANG"

A. Introductory comments on hydrodynamics

As we emphasized in the Introduction, hydrodynamical explosion of QGP is well documented: see e.g. (Heinz and Snellings, 2013). The interest has now shifted, from description of bulk of the data to special cases, with emphasis on the *limits* of the hydrodynamical description.

When one thinks of ideal hydrodynamics plus viscous corrections, it is sometimes stated that the latter, the

viscosity times the velocity gradients, should be smaller than the main terms. In fact it is not so: it the terms second (and higher order) in gradients which are neglected and thus assumed small. Navier-Stokes hydrodynamics can successfully describe rather anisotropic flows. Studies of the "anisotropic hydro", as well as an exact solution of Boltzmann equation in Gubser setting, we will discuss in section IV.C.

Another direction is the so called *higher order hydrodynamics*, attempting re-summation of certain gradient terms (Lublinsky and Shuryak, 2009), see section VII.E.

All formulations of "improved" hydrodynamics are supposed to shift its initiation to a somewhat earlier time, or promise to treat somewhat smaller systems. Yet, while the "out-of-equilibrium" initial stage get reduced, of course it can never be eliminated. The distinction between the "initial" and "equilibrated" stages is a matter of definition: but physical outputs – e.g. the total amount of entropy produced – should ideally be independent of that. Unfortunately, in practice we are still far from this ideal scenario: studies of entropy generation at an initial stage is still in its infancy.

A few other issues remains open, related with the boundary of hydrodynamical description.

One is the boundary at high p_t. The region in which hydrodynamical predictions describe the data goes roughly up to $p_\perp \sim 3\,GeV$. (Note that it includes more than 99.9% of all secondaries!) Collective flows are decreasing above this momentum, and one needs to understand why. High $p_\perp$ particles come from an edge of the fireball, where the magnitude of the flow is maximal. Using the saddle point method for Cooper-Frye integral (Blaizot and Ollitrault, 1990), one can see that the region from which such particles come shrinks, as $p_\perp$ grows. We will return to this point in connection to high multiplicity pp collisions and HBT radii, see sectionV.E. Eventually this region shrinks to a single hydrodynamic cell, of the size of a mean free path, and hydrodynamics can no longer be applied.

The viscosity effects lead to anisotropy of particle distributions induced by flow gradients (Teaney, 2003): these effects should be enhanced at the fireball's edge. Gradients add extra power of $p_\perp$, and the deviation in the flows from ideal hydrodynamics should be negative. This picture qualitatively agree with observations, but quantitative theory in the window $4 < p_\perp < 10\,GeV$ is still missing. Above it one finds a completely different – jet-dominated – physics, which is again under theoretical control.

Another issue is the "end of hydrodynamics" at the end of the collisions. Because different secondaries have very different cross sections, it has been argued that they have a *sequential freezeouts* depending on its value, see e.g. (Hung and Shuryak, 1998). Traditionally, after chemical freezeout the practical models switch from hydrodynamics to hadronic cascade, which implements it in detail.

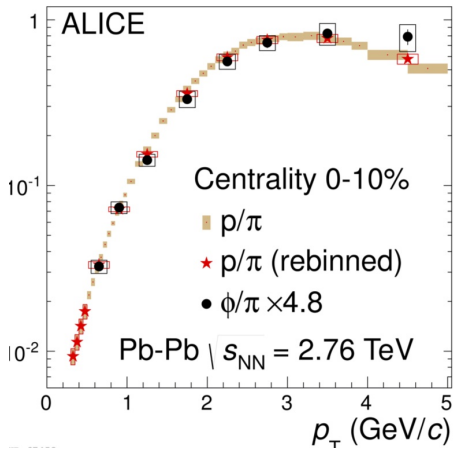

FIG. 6 Proton-to-pion and (rescaled) ϕ/π ratios, as a function of transverse momentum p_T.

But recent data, especially from ALICE, put such approach into question. The particle yields are described by chemical equilibrium so well, up to light nuclei, that little space is left to inelastic re-scatterings.

The *hydrodynamical paradigm* states that out of all individual properties of the secondary hadrons, only one – their masses – is important, as one translates from the distribution over collective flow velocities to the observed momenta. All one needs to know is that an object of mass m in a flow with velocity v has the momentum mv, plus thermal motion which also only depends on m. Let us check it, by a direct comparison of the spectra for a pair of hadrons with the same mass, with otherwise completely different quantum numbers and cross sections, e.g. p and ϕ. They can hardly be more different, a non-strange baryon versus a $\bar{s}s$ meson, so any "afterburner" code shows their late-time dynamics to be different. And yet, as the data shown in Fig.6 demonstrate, their spectra are practically identical, up to $p_\perp \sim 4\,GeV/c$.

B. Hydrodynamical response to perturbations

Now, assuming that the *average* pattern of the fireball explosion has been well established, we are going to add perturbations to it. The induced fluctuations and and their correlations is thus the next topic of our discussion.

The first method to study it is the so called event-by-event hydrodynamics, solving it for some ensemble of initial conditions. However, most of what was learned from such expensive and extensive studies can also be understood from a much simpler approach, in which one adds small and elementary perturbations on top of smooth average fireball[7] Using an analogy, instead of

[7] By no means the latter approach undermines good work which

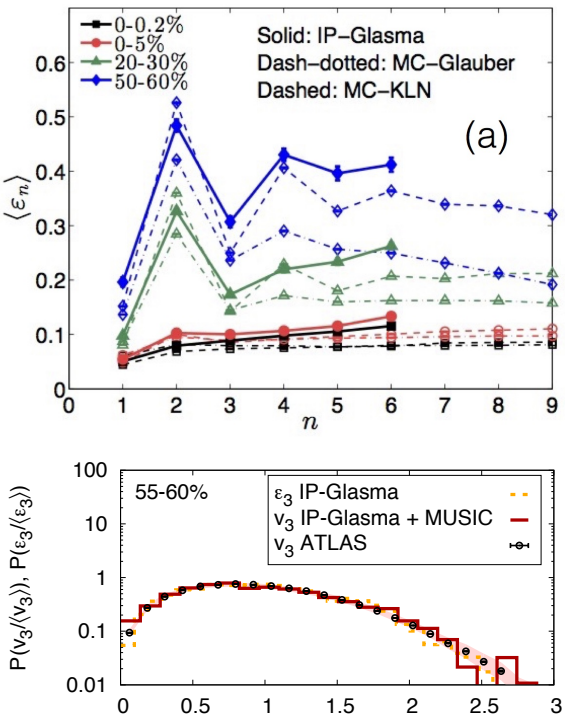

FIG. 7 (a) From (Heinz and Snellings, 2013): average deformations $< \epsilon_n >=< \cos(n\phi) >$ for various centralities using models indicated in the figure. (b)From (Schenke and Venugopalan, 2014) . Data points correspond to the event-by-event distribution of v3 measured by the ATLAS collaboration, compared to the distributions of initial eccentricities in the IP-Glasma model and the distributions of v_3 from fluid dynamic evolution with IP-Glasma initial conditions.

beating a drums forcefully, with both hands and all fingers, one may touch it gently with a drumstick, at different locations, recording the spectra and intensities of the sounds produced. Eventually, summing up all the relevant modes of excitations, one gets a complete Green function, from which a (linearized) description of *any* initial conditions follow.

In order to summarize what we have learned from fluctuation/correlation studies, one needs to go back to the data and to the results of multiple hydrodynamical calculations, separating their essence from unimportant complications. A simple pocket formula, revealing the systematics, will help us to do so.

Before we dip into details, let us formulate the main points, using my drum analogy. First of all, perturbations on top of the sQGP fireball basically are sounds, as those propagating on the drum. The main phenomenon is their viscous damping: so the value of viscosity will be the main output. Unlike the drum, the fireball is not static but exploding: therefore an oscillating behavior is superimposed on the dynamical time dependence of the amplitudes. Different excitations are excited if the drum is struck at different places; similarly we find excitation of different modes depending on their origination point.

These calculations typically start from the angular deformations of the initial state. In Fig.7(a) one finds the dependence of the mean harmonics (eccentricities)

$$\epsilon_n =< \cos(n\phi) > \tag{10}$$

where n is an integer and ϕ is the azimuthal angle. The angular brackets indicate an average over events, usually for particular centrality bin (indicated in the upper left corner as a fraction of the total cross section, which scales as bdb). The bin 0-0.2% is called the "ultra-central" one, $b \approx 0$, and $50-60\%$ are peripheral collisions. The first obvious comment to this plot is that the $n = 2$ harmonics is special, it peaks for peripheral bins, due to collision geometry. However other harmonics, and in fact *all* of them for the central bins, are basically independent of n and centrality. What this tells us is that statistically independent "elementary perturbations" (or "bumps") have small angular size $\delta\phi \ll 2\pi$, so one sees here an angular Fourier transform of the delta function.

The next observation is that the deformations are smaller for central collisions, at a few percent. This is also natural: central collisions produce larger fireballs, which have more particles and thus fluctuate less

$$< \epsilon_n > \sim \frac{1}{\sqrt{N_{cells}}} \tag{11}$$

where $N_{cells} = A_{cell}/A_{fireball}$ is the number of statistically independent cells.

Models of the initial state give not only the average deformation but also their distributions and correlations. Remarkably, the experimentally observed distributions over flows $P(v_n)$ directly reflect the distributions of the angular anisotropies $P(\epsilon_n)$ at the initial time, see e.g. ϵ_3, v_3 distributions in Fig.7(b). In other words, apparently no extra noise is generated during the hydrodynamic evolution, from the initial state ϵ_n to the final state v_n.

C. Acoustic systematics: the viscous damping

There is a qualitative difference between radial flow and higher angular harmonics. While the former monotonically grows with time, driven by the outward pressure gradient with a fixed sign, the latter are basically

the former approach does. Development of stable and causal second-order hydrodynamic codes and ensembles of initial conditions is a significant achievement. The averaging hydrodynamic results over thousands of configurations, with complicated shapes, is a lot of work, resulted in spectacular results for the v_n moments. Yet in the pedagogical review one needs to focus on the essence of the issue, in the simplest setting possible.

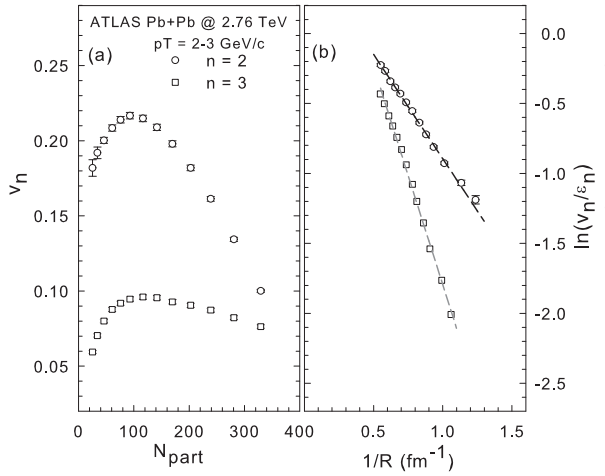

FIG. 8 (a) ATLAS data, from Ref. (Lacey *et al.*, 2013), for v_2, v_3 vs. N_{part} : (b) $ln(v_n/\epsilon_n)$ vs. $1/R$ for the same data

sounds, or density oscillations. Therefore the signal observed should, on general grounds, be the product of the two factors: (i) the amplitude reduction factor due to viscous damping and (ii) the *phase* factor containing the oscillation at the freezeout. (We will discuss the effects of the phase in the next section.)

Let us start with the "acoustic systematics" which includes only the viscous damping factor. Somewhat surprisingly, this simple expression does describe both the data and hydrodynamic calculations. More specifically, it reproduces the dependence on the viscosity value η, the size of the system R and the harmonic number n.

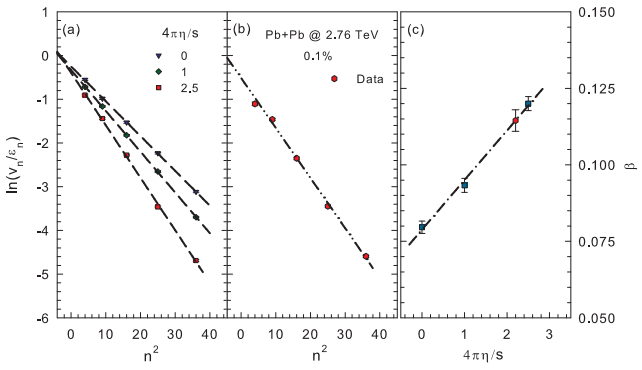

FIG. 9 (a) ATLAS data, from Ref. (Lacey *et al.*, 2013), $ln(v_n/\epsilon_n)$ vs. n^2 from viscous hydrodynamical calculations for three values of specific shear viscosity as indicated. (b) $ln(v_n/\epsilon_n)$ vs. n^2 for Pb+Pb data. The $p_\perp$ -integrated v_n results in (a) and (b) are from ATLAS 0.1% central Pb+Pb collisions at nucleon-nucleon $s_{NN} = 2.76\,TeV$; the curves are linear fits. (c) exponent vs. viscosity-to-entropy ratio $4\pi/s$ for curves shown in (a) and (b).

The expression can be motivated as follows. We had already mentioned "naive" macro and micro scales (9): now we define it a bit more accurately, by inserting the viscosity-to-entropy ratio $\eta/s = lT$ into it

$$\frac{l}{L} = \frac{\eta}{s}\frac{1}{LT} \tag{12}$$

This "true micro-to-macro ratio", corresponding to the mean free path in kinetic theory, defines the minimal size of a hydrodynamic cell.

One effect of viscosity on sounds is the damping of their amplitudes. The "acoustic damping" formula (Staig and Shuryak, 2011a) is

$$\frac{v_n}{\epsilon_n} \sim \exp\left[-Cn^2\left(\frac{\eta}{s}\right)\left(\frac{1}{TR}\right)\right] \tag{13}$$

where C is some constant. The number n appears squared because the damping includes square of the gradient, the momentum of the wave. It gives the following predictions: (i) the viscous damping is exponential in n^2; (ii) the exponent contains the product of two small factors, η/s and $1/TR$, (iii) the exponent contains $1/R$ which should be understood as the *largest* gradient in the system, often modeled[8] as $1/R = 1/R_x + 1/R_y$.

Extensive comparison of this expression with the AA data, from central to peripheral, has been done in (Lacey *et al.*, 2013) from which we borrow Fig.8 and Fig.9. The Fig.8 (a) shows the well known centrality dependence of the elliptic and triangular flows. v_2 is small for central collisions due to smallness of ϵ_2, and also small in the very peripheral bin because viscosity is large in small systems. Fig.8 (b) shows the $ln(v_n/\epsilon_n)$. As a function of the inverse system's size $1/R$, both elliptic and triangular flows show perfectly linear behavior. Further issues – the n^2 dependence as well as linear dependences of the $log(v_m/\epsilon_m)$ on viscosity value – are also very well reproduced, see Fig.9. Note that this expression works all the way to rather peripheral AA collisions with $R \sim 1\,fm$ and multiplicities comparable to those in the highest pA bins. It also seem to work to the largest n so far measured.

The acoustic damping provides correct systematics of the harmonic strength. This increases our confidence that – in spite of somewhat different geometry – the perturbations observed are actually just a form of a sound waves.

Since we will be interested not only in large AA systems but also in new – pA and pp – much smaller fireballs, one may use the systematics to compare it with the new

[8] We remind that x, y axes are transverse to the beam, and x is along the impact parameter. Thus for peripheral collisions R_x is dominant in this combination.

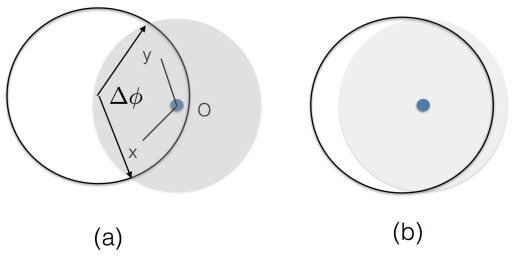

FIG. 10 The perturbation is shown by small blue circle at point O: its time evolution to points x and y is described by the Green function of linearized hydrodynamics shown by two lines. Perturbed region – shown by grey circle – is inside the sound horizon. The sound wave effect is maximal at the intersection points of this area with the fireball boundary: $\Delta\phi$ angle is the value at which the peak in two-body correlation function is to be found. Shifting the location of the perturbation, from (a) to (b), result in a rather small shift in $\Delta\phi$.

data. Using the acoustic damping formula, one can estimate how many flow harmonics can be observed in these cases. For central $PbPb$ at LHC collisions with

$$\frac{1}{TR} = \mathcal{O}(1/10) \tag{14}$$

its product of η/s is $O(10^{-2})$. One can immediately see from this expression why harmonics up to $n = O(10)$ can be observed. Proceeding to smaller systems, by keeping a similar initial temperature $T_i \sim 400\, MeV \sim 1/(0.5\, fm)$ but a smaller size R, results in a macro-to-micro parameter that is no longer small, or $1/TR \sim 1$, respectively. Note that for a usual liquid/gas, with $\eta/s > 1$, there would not be any small parameter left and one would have to conclude that hydrodynamics is inapplicable for such a small system. However, since the quark-gluon plasma is an exceptionally good liquid with a very small η/s, one can still observe flow harmonics up to $m = O(\sqrt{10}) \sim 3$. And indeed, v_2, v_3 have been observed, already in the first round of measurements! (For later data see Fig.22).

D. Waves from a point perturbation and harmonic spectra

The event-by-event hydrodynamics appears to be a very complicated problem: events have multiple shapes, described by multidimensional probability distributions $P(\epsilon_2, \epsilon_3...)$, and different spatial shapes lead to complicated deformations of the secondary spectra. Yet the analysis shows that all those shapes are however mostly due to a statistical noise, and the problem is much simpler than it naively appears to be.

The point is that the individual row of nucleons, located at different places in the transverse plane, by causality cannot possibly know about fluctuations of other rows at different locations: so their fluctuations are statistically independent. Therefore it is sufficient to study one "elementary excitation", produced by a delta-function source in the transverse plane (in reality, of the size of a nucleon) . In other words, one needs to find the Green function of the linearized hydrodynamic equations.

A particular model of the initial state expressing locality and statistical independence of "bumps" has been formulated in (Bhalerao and Ollitrault, 2006): the correlator of fluctuations is given by the Poisson local expression

$$< \delta n(x)\delta n(y) >= \bar{n}(x)\delta^2(x-y) \tag{15}$$

where $\bar{n}(x)$ is the average matter distribution. The immediate consequence of this model is that, for the central collisions (on which we focus now), ϵ_m are the same for all $m < m_{max} = O(10)$ (until the bump size gets resolved).

In order to calculate perturbations at later times one needs to apply the Green functions *twice*, describing perturbation propagating from the original source O to the observation points x and y as shown in Fig.10(a). This has been first done by (Staig and Shuryak, 2011b) analytically, for Gubser flow (see Appendix for details). One finds that the main contributions come from two points in Fig.10, where the "sound circle" intersects the fireball boundary. In single-body angular distributions those two points correspond to two excesses of particles at the corresponding two azimuthal directions. The angle between them at Fig.10(a) is about $\Delta\phi \approx 120^o$ or 2 rad. The azimuthal correlation function (Staig and Shuryak, 2011b) is shown in Fig. 11(a). One of its features is a peak at zero $\delta\phi = 0$: it is generated when both observed particles come from the same azimuthal enhancement. If two particles come from two different locations, there peaks displaced by $\Delta\phi = \pm 2$ rads. (As shown in Fig.10, if one shifts the position of perturbation from (a) to (b), the peak angle $\Delta\phi$ changes toward its maximal value, π radian, or 1/2 of the circle.)

This calculation has been made and presented[9] *before* the experimental data were shown. The experimental correlation function from ATLAS, for the "super-central bin" with the fraction of the total cross section 0-1%, is shown in Fig. 11(b). The shape of the correlator was predicted strikingly well.

While there is no need to use Fourier harmonics – I insist that the correlation function as a function of the relative angle may teach us more than harmonics, separately studied – one can certainly do so. Note that for the ultra-central collisions we now discuss the largest harmonics is v_3 (see Fig. 11(b)), not v_2. Since starting deformations ϵ_n are basically the same for all n, the difference must come from hydro, and it does. As we just

[9] At the first day of Annecy Quark Matter.

explained above using notion of the sound horizon, the angular distance between enhancements is about 120^o, not 180^o.

A very similar phenomena take place for the Big Bang sound perturbations. All hydrodynamic harmonics get excited at the initial time $t = 0$ by the Big Bang, and all got frozen out at the same time as well. The acquired phases depend on the harmonic number n, because at larger n they oscillate more rapidly. The binary correlator is proportional to $\cos^2(\phi^n_{freezout})$ and harmonics with the optimal phases close to $\pi/2$ or $3\pi/2$ values show maxima, with minima in between. Planck collaboration data on the power spectrum of the cosmic microwave Big Bang perturbations, shown in Fig. 12 as a function of harmonic number, do display a number of such maxima/minima.

The first calculation of the harmonic spectrum (Staig and Shuryak, 2011b) had similarly shown such oscillations, with the first peak close to $n = 3$ and the minimum around $n = 7$, see Fig.13(a). Subsequent study analytic linearized perturbation on top of Gubser flow (Gorda and Romatschke, 2014) produce more information about the minimum: see Fig.13(b). While the minima are clearly there for one point-like source, its location depends on the radial location of the original source r_0. Gorda and Romatschke further studied the question and found that for $r_0 \sim 5 - 6\, fm$ the minimum shifts to $m = 10$. The questions whether such minima can survive realistic ensemble average, and perhaps ever be observed experimentally, remain open. So far, high harmonics $n > 6$ remains out of reach for statistical reasons.

Currently a number of groups had developed sophisticated event-by-event hydrodynamic calculations and calculated the magnitude of harmonics: however they do so with $n = 2 - 6$, that is below the discussed minimum. It is interesting that their results are very well described by $exp(-n^2 * const)$ dependence, expected from the acoustic damping discussed above, see for example (Rose *et al.*, 2014) and Fig.14(a). Gorda and Romatschke also see this dependence, see Fig.14(b) from (Gorda and Romatschke, 2014) , but they do not agree that the coefficient to be proportional to viscosity.

Another question on these harmonic spectra: is whether there is a maximum? Thus the question reduces to the relation between $m = 2$ and $m = 3$[10] . The experiments show that $v_3 > v_2$: see ultra-central ATLAS data shown in Fig.13(a), as well as the CMS central bin data in Fig.13(b) . (The latter include slightly larger impact parameters and thus feed more geometry-related contribution to v_2.) The same conclusion stems from the both calculations just discussed, (Gorda and Romatschke, 2014; Staig and Shuryak, 2011b) at large r_0. Surprisingly, all sophisticated event-by-event studies led to the opposite conclusion, namely $v_3 < v_2$ for the ultracentral bin.

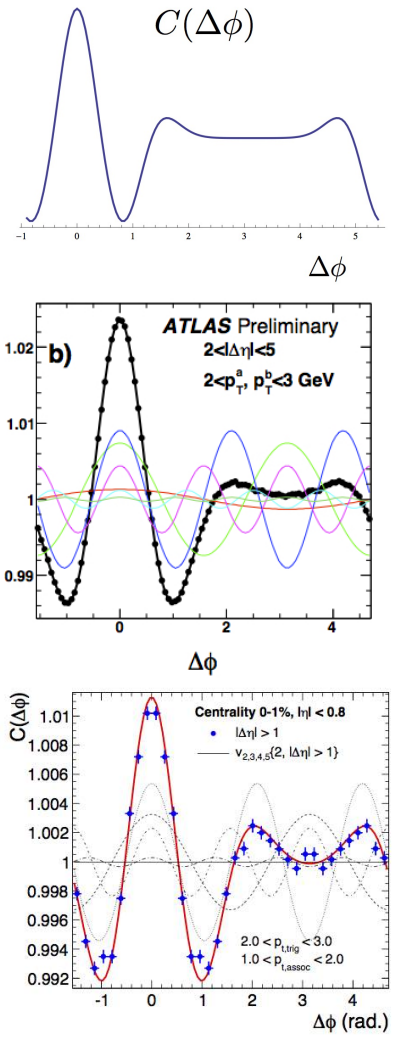

FIG. 11 (a) Calculated two-pion distribution as a function of azimuthal angle difference $\Delta\phi$, for viscosity-to-entropy ratios $\eta/s = 0.134$, from (Staig and Shuryak, 2011b). (b) from ATLAS (Jia, 2011), (c) from ALICE (Aamodt *et al.*, 2011b): All for ultra-central collisions.

The "flow harmonics", solutions of linearized equations on top of average smooth flow, should make a complete set of all possible perturbations. The functions of course depend not only on the azimuthal angle $\sim e^{im\phi}$, but on other coordinates r, η as well. For Gubser flow (see Appendix) one can use the co-moving coordinates ρ, θ, ϕ, η, derive linearized equations for perturbations, separate the dependence on all four coordinates, with nice analytic expressions for all harmonics. The flow in the transverse plane r, ϕ is nicely combined into standard angular har-

[10] The harmonics $m = 1$ is known to be especially small due to the vanishing dipole, and so it should be removed from consideration. We now discuss central collisions only, in which all effect comes from fluctuations, not the geometry.

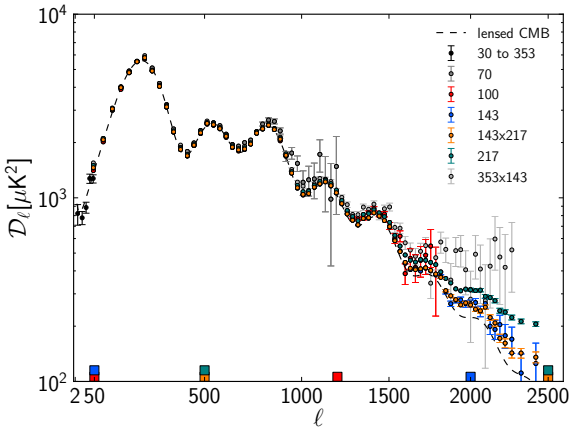

FIG. 12 Power spectrum of cosmic microwave background radiation measured by Planck collaboration (Ade *et al.*, 2014).

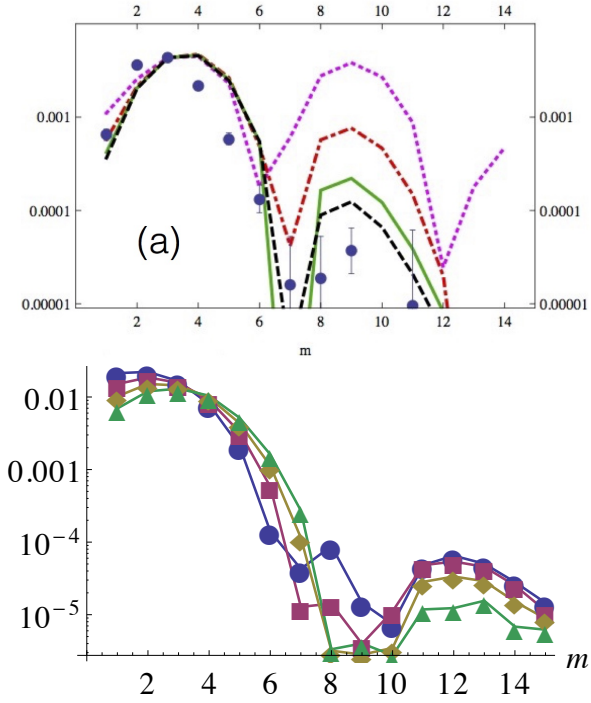

FIG. 13 (a) The lines are from analytic linearized hydrodynamic calculations of the correlation function harmonics, v_m^2, based on a Green function from a point source (Staig and Shuryak, 2011b), for four values of viscosity $4\pi\eta/s$ =0,1,1.68,2 (top to bottom at the right). The closed circles are the ATLAS data for the ultra-central bin.
(b) Calculation of harmonic flow spectra from analytic linearized hydrodynamics by (Gorda and Romatschke, 2014), at $p_\perp = 1\,GeV$ demonstrates the dependence of the minimum on the location of the perturbation $r_0 = 7.5, 8.0, 8.5, 9\,fm$, by blue circle, red square, brown diamond and green triangle, respectively.

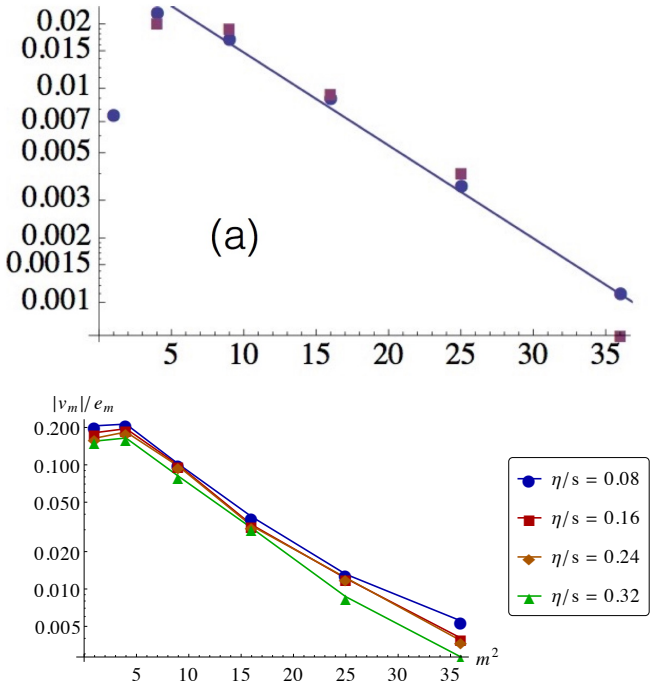

FIG. 14 (a) $v_n\{2\}$ plotted vs n^2. Blue closed circles correspond to viscous even-by-event hydrodynamics (Rose *et al.*, 2014), in "IP Glasma+Music" model, with viscosity value $\eta/s = 0.14$. The straight line, shown to guide the eye, demonstrate that "acoustic systematics" does in fact describe the results of this heavy calculation quite accurately. The CMS data for the 0-1% centrality bin, shown by the red squares, in fact display larger deviations, perhaps an oscillatory ones.
(b) The harmonics induced by a fixed perturbation at $r_0 = 4\,fm$, from (Gorda and Romatschke, 2014), for variable viscosity.

monics $Y_l(\theta, \phi)$, combining the azimuthal angle ϕ and the radial coordinate r into θ. The waves in the rapidity direction η are simple plane waves.

Can one define similarly a complete set of independent harmonics, for a generic non-Gubser setting? And, even more importantly, can those be observed? A nice step in this direction has been made by (Mazeliauskas and Teaney, 2015) using "subheading harmonics" of flow, extracted from experimental data. Here is a picture Fig.15 from that work indicating a difference between the leading and subleading triangular flows. Note that the latter gets a sign change along the radial direction, unlike the former one.

E. Detecting the interactions between harmonics

We already argued above, that the individual sources – or "bumps" as we call them – are uncorrelated, and so one should not pay attention to their interferences. The suggested picture is similar to a number of stones thrown into the pond: the produced expanding circles visibly interfere, they do not really interact with each

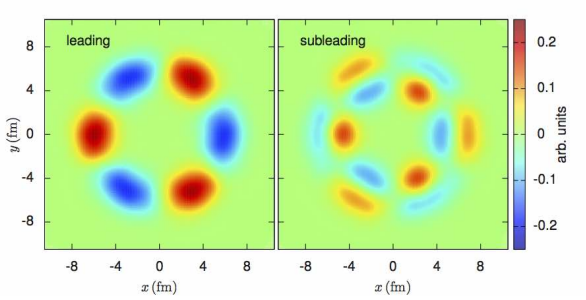

FIG. 15 The leading (left) and subleading (right) harmonics of triangular flow, from (Mazeliauskas and Teaney, 2015).

other since the amplitude is small.

Now we look at the details of this picture. First of all, how many of such "bumps" are there? For central collisions the circumference of the fireball is $2\pi R_A \approx 40\, fm$. The correlation length is perhaps the typical impact parameter in NN collisions, which at LHC energies is $b \sim \sqrt{\sigma/\pi} \sim 1.6\, fm$. So there are not more than

$$N_{sources} \approx \frac{2\pi R_A}{b} \approx 25 \tag{16}$$

independent sources.

The absolute scale of correlator harmonics in experiments is of the order of a percent, see e.g. Fig.11(b). Of course, it comes from incoherent sum over the number of sources, so one individual bump contribute only $O(10^{-3})$ into it. In the wave amplitude – one needs to take the square root – one deals with perturbation of the order of 1/30.

With such small amplitudes one might conclude that the linear theory is completely sufficient, and all nonlinear effects can be ignored. It is basically correct, but not near the fireball edge. Small waves can produce large effects at the large p_t end. Indeed, at $p_t \sim 3\, GeV$ the elliptic flow gets large $v_n \sim 0.2$ which makes angular distribution 100% asymmetric. Similarly, the non-linear interactions of flows at the edge – large p_t – are non-negligible.

For example, v_4 received a contribution proportional to ϵ_2^2, v_6 from ϵ_3^2, etc. Detailed studies of such effects can be found in (Teaney and Yan, 2012). Non-linear effects include a particularly curious case: v_1 harmonics generated by nonlinear $\epsilon_2 \cdot \epsilon_3$ interaction

These nonlinear effects do *not* originate from the nonlinear terms in the hydrodynamic equation, but from an expansion of the Cooper-Frye exponent $exp(p^\mu u_\mu/T)$, containing flow velocity, in powers of these perturbations. Obviously they become more important at high p_t. Furthermore, while the linear terms are also linear in p_t, the non-linear effects we mentioned are quadratic $\sim p_\perp^2$, etc (Teaney and Yan, 2012).

F. Event-by-event v_n fluctuations/correlations

At the beginning of this section we had already emphasized that the main source of the v_n fluctuations is that of the original perturbations ϵ_n themselves, see e.g. Fig. 7(b).

Now we return to the question: *Why does the ratios v_n/ϵ_n, evaluated by hydro, have such a small spread?*. While the practitioners of the event-by-event hydrodynamics use a huge variety of initial configurations, it turns out that just one parameter – ϵ_n – is sufficient to predict v_n. If there would be some spread in values, the distributions in v_n and ϵ_n would not match that well!

Even adopting the minimalistic model advocated above – that all perturbations come from incoherent point-like sources – it is surprising that event-by-event fluctuations of strength and locations of the "bumps" do not create any additional spread. (Or, using my drum analogy, does on get the same sound when the drum is hit in different radius?)

Trying to understand this dependence, let us come back to Fig.10. The source located at the fireball edge, fig.(a), produces correlation at $\Delta\phi \approx 2\, rad$. As emphasized previously, projected into harmonics, it will excite the $m = 3$ one, since 2 rad is about 1/3 of 2π. As the source moves inward, fig.(b), the overlap of the sound circle and the fireball edge moves to t $\Delta\phi \sim \pi$, and the leading excitation becomes elliptic $m = 2$. The calculations show that in the latter case the correlation gets much weaker. The observed shape of the correlator for ultra-central collisions does have a *minimum* at $\Delta\phi = \pi$. Finally, as the source moves further toward the fireball center (not shown in Fig.10), the correlation appears at all angles equally, and its contributions to $m \neq 0$ harmonics vanishes. In summary: the harmonics we see comes mostly from the sources located near the boundary of the fireball. The angular correlations they induce have one universal form.

The studies of flow harmonics and their correlations is a rapidly expanding field. Correlations can be divided to those sensitive to relative phases of the harmonics, and those which are not. An example of the latter is

$$SC(m,n) = < v_m^2 v_n^2 > - < v_m^2 >< v_n^2 > \tag{17}$$

ALICE provided data for $SC(4,2)$ and $SC(3,2)$, observing that $SC(4,2) > 0$ but $SC(3,2) < 0$: both qualitatively reproduced by hydrodynamical models.

This development requires the initial state model which is good enough not only to predict the mean ϵ_n, but their fluctuations and even respective correlations. Suppose we do so using the Bhalerao-Ollitrault relation (15): the results depend on integrals like $\int d^2 r r^P \bar{n}(r)$ with large powers $P = 6, 8$. Thus the correlations are again coming from the very surface of the fireball at the initial time. Their absolute magnitude suffer from signif-

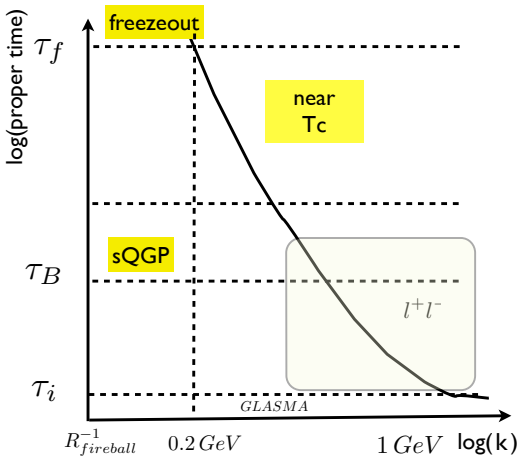

FIG. 16 The log-log plane proper time τ – sound momentum k. The solid curve indicates the amplitude damping by a factor e: only small-k sounds thus survive till freeze out. The shadowed region on the right corresponds to that in which sonomagnetoluminiscence effect may produce extra dileptons.

icant uncertainties, but the angular shapes and normalized correlators of harmonics can still be under control.

G. The map of the sounds

The number of gauge field harmonics needed to describe the initial state is rather large, counted in hundreds, much exceeding the number of sound modes we detect at freezeout. In Fig.16 we show a map of those, in terms of momentum (rather than angular momentum). The curved line – corresponding to "acoustic systematics" discussed above – show their lifetime. This curve crosses the freezeout time: smaller k waves can be observed at freezeout. Larger k cannot: they are weakened due to viscous damping. (A suggestion to detect those via the MSL process will be discussed in section IX.B.)

Fluctuation-dissipation theorem tells us that while the initial perturbations are damped, new ones should be produced instead. There should therefore be some noise, producing sounds continuously during the whole hydrodynamical evolution. Studies of the resulting "hydrodynamics with noise" has been demonstrated by (Young *et al.*, 2015). Unfortunately, the authors have not separated the "initial time sounds" from the "late time ones". Perhaps that can be experimentally separated via studies of the azimuth+rapidity correlations, exploring the fact that the former lead to rapidity-independent modes, and the latter are rapidity-localized.

(Shuryak and Staig, 2013b) suggested that late-time fluctuations may be generated by collapsing QGP clusters inside the hadronic phase. Those collapse events should happen because the QGP phase gets unstable in the bulk, once the temperature cools to $T < T_c$. This phenomenon is similar to the celebrated bubble collapse studied by Rayleigh.

Shocks/sounds are also expected to be created by jets depositing its energy into the ambient matter. How those are propagated via sounds is worked out by (Shuryak and Staig, 2013a).

H. Sounds in the loops

The hydrodynamical longitudinal pressure waves – the sounds – are the best quasiparticles we have. They are Goldstone modes, related with the spontaneous breaking of the translation invariance by matter, and thus their interaction fallows certain pattern familiar from the pion physics. For large wavelengths they have a long lifetime, exceeding the freezeout time. Therefore, in both the Little and the Big Bangs, one can observe "frozen" traces of the initial perturbations, provided one looks at large enough wavelengths.

Because the sounds have their own long lifetimes and travel far, one may ask how an ensemble of sounds would behave, given such long times. In other fields of physics a theory developed for this questions is called "the acoustic turbulence". Furthermore, one may add to hydrodynamical equations a Langevin-type noise term, with some Gaussian distribution, and formulate the resulting theory as path integral, or in the QFT-like form. Progress along this direction has been summarized in a review (Kovtun, 2012). Discussion of formal issues cannot be made in this review, however, and thus I illustrate the physics involved by one example only, also from (Kovtun *et al.*, 2011).

Recall that matter viscosity can be defined via certain limit of the stress tensor correlator, known as the Kubo formula. Kovtun et al calculated a "loop corrections" to this correlator induced by the equilibrium sounds. Technically the calculation is done as follows: in the $< T^{\mu\nu}T^{\mu'\nu'} >$ correlator one substitute hydrodynamical expression for stress tensor containing sound perturbation velocities and make it into a loop diagram with the "sound propagators"

$$\Delta^{mn} = \int d^4x e^{-ip_\alpha x^\alpha} < u^m(x)u^n(0) > \qquad (18)$$

for two pairs of the velocities. (We use latin indices indicating that they are only space-like here. For shear viscosity those used are $m = x, n = y$). Skipping the derivation I jump to the answer obtained from this calculation, which can be put into the form of loop correction to the viscosity

$$\delta\eta_{loop} = \frac{17}{120\pi^2}\frac{p_{max}T(\epsilon+p)}{\eta_0} \qquad (19)$$

which is UV divergent and thus includes p_{max}, the largest momentum for sound which still makes sense. What

is important here is that the zeroth-order viscosity enters into the denominator. This should not be surprising: a very good liquid with small η_0 support very long-lived sounds, which can transfer momentum at relatively large distances, which means they produce *large* contribution[11] to the effective viscosity.

The same correlator of stress tensors, in the "sound approximation" similar to that used above, has been used (Kalaydzhyan and Shuryak, 2015) to calculate the on-shell rate of sound+sound $\rightarrow$ gravity waves, from sounds generated by QCD and/or electroweak cosmological phase transition.

Completing this section we would like to remind the reader about existence of other hydrodynamical modes, the rotational [12] ones. Rotational modes on top of the Bjorken flow were discussed by (Floerchinger and Wiedemann, 2011): under certain conditions one hydrodynamic mode does become unstable. Other unstable hydrodynamical modes appear for non-central collisions with rotation (Csernai *et al.*, 2014) . More studied of these instabilities are however necessary to see whether such instabilities can indeed be observed.

IV. THE PRE-EQUILIBRIUM STATE, GLOBAL OBSERVABLES AND FLUCTUATIONS

A. Perturbative vs non-perturbative models

A theory of the early stage should be able to
(i) specify certain wave function of the colliding particle, in a wide rapidity range;
(ii) explain what happens during the collision time ;
(iii) explain how the produced state evolves into the final observed hadronic state.

It is perhaps fair to say that approaches based on the weak coupling (pQCD) has been able to explain (i) and (ii), but not (iii). Strong coupling approaches, AdS/CFT especially, explains (iii) but not the first two.

More specifically, the perturbative (pQCD) regime is natural for hard processes, for which the QCD running coupling is weak. Already in the 1970s pQCD developed a *factorization framework*, which divided production amplitudes into "past","during", and "after" parts. The "past" and "after" parts are treated empirically, by structure (or distribution) and fragmentation functions. The "during", near-instantaneous, part is described by the explicit partonic processes under consideration.

The strength of this approach is based on the separation of hard and soft scales, by some normalization scale μ, on which the final answer should not depend. Dependence of PDFs and fragmentation functions on μ is described by the renormalization group tool, Dokshitser-Gribov-Lipatov-Altarelli-Parisi (DGLAP) evolution. Using it, one can tune the hard scale Q to pertinent kinematics. It works well for truly hard processes such as jet production at $Q > 10\,GeV$. In the "mini-jets" domain, at $Q \sim$ few GeV, "higher twist" $1/Q^n$ corrections are large and not yet under theoretical control.

The described pQCD framework has also serious restrictions as well. The factorized PDFs by definition describe the *average* nucleon (or nucleus). As soon as a particle is touched – e.g. the impact parameter (multiplicity bin) is selected – factorization theorems are no longer applicable. The absence of good practical models describing partonic state with fluctuations remains a problem: e.g. for understanding pp collisions with multiplicity several times the average. As we will discuss below in detail, pQCD can hardly be used for assessing the transverse plane distributions/correlations of partons.

For "baseline" soft processes – minimally biased pp, pA collisions with low multiplicity – the phenomenological models describing QCD string production and fragmentation are rather successful. The Lund model has branched into various "event generators", such as PYTHIA, popular among experimentalists. Their key feature is independent string fragmentation. However, new experiments focused on high multiplicity events, found correlation phenomena clearly going beyond the reach of these event generators.

In the case of very high multiplicity – e.g. central pA, AA – the initial conditions for hydrodynamics are smooth and defined given by the nuclear shape. The main parameter one needs to know about the preequilibrium stage is the total amount of the *entropy* generated. So far this is treated with some empirical coefficients, entropy/parton, not yet derived.

In the next approximation one accounts for quantum fluctuations, in the positions of the nucleons as well as in the cross sections, via versions of the Glauber eikonal models. They provide well defined and reasonable predictions for initial state perturbations ϵ_n, generating flow harmonics via hydrodynamics. The GLASMA-based models include more fluctuations, resolving partonic substructure of the nucleons: its relevance for the results is at the moment unclear.

Partonic description of the initial state of the collision at asymptotically high parton density evolved into the so called Color-Glass-Condensate (CGC)- GLASMA paradigm (McLerran and Venugopalan, 1994). Since at any transverse location the number of colored objects involved can be considered large, the color charge fluctuation should also become large, producing strong gauge fields, the CGC. When the gluonic fields become so strong that the occupation numbers reach $O(1/\alpha_s)$, the nonlinear commutator term in non-Abelian gauge

[11] Other examples of the most penetrating modes dominating transport are ballistically moving phonons in liquid helium or neutrinos in a supernova.

[12] It is well known that those are central e.g. for the atmospheric turbulence.

fields is as large as linear ones, and so one should use *classical* nonlinear Yang-Mills equations. GLASMA is a state made of such random classical fields, starting from CGC at the collision time and then evolving as the system expands, until the occupation numbers reduce to $O(1)$. The model remains valid provided the scale of the (2-dimensional) parton density $n \sim Q_s^2$, known as a *saturation momentum*, remains large compared to non-perturbative QCD scale. At early time the charges in each "glasma cell" separate longitudinally, producing longitudinal electric and magnetic fields. Cells of area $\sim 1/Q_s^2$ are statistically independent and fluctuate with their own Poisson-like distributions. The explicit modeling of the resulting field, from cells in the transverse plane, is now known as an $impact-parameter$ (IP) glasma models.

High-multiplicity initial states then evolve into sQGP, which undergo hydrodynamical expansion. Reducing the multiplicity, one expects to find a regime in which the system is too small to have the hydrodynamical stage. Howe would one see that?

Let us illustrate it by one particular observable, the *elliptic* flow v_2. Suppose there is no sQGP stage: partons – gluons and quarks – simply become mini-jets after the collision, more or less like the Weizsacker-Williams photons do in QED. Correlations in the collision, related to the impact parameter plane, will produce certain v_n moments. Let us discuss their $p_\perp$ dependence.

Hard partons at large momentum scale $Q > Q_s$, exceeding the saturation scale of GLASMA, cannot possibly know about other cells and geometry: those would be produced isotropically in the transverse plane and do not contribute to v_n. If they re-interact later, the resulting showers contributing a *negative* correction to v_2. Softer partons, with momenta $Q \sim 1/R \ll Q_s$, will know about the "overlap almond" shape of the initial state: their distribution will be anisotropic, perhaps even with v_2 of the order of several percents as observed. Thus the prediction would be basically flat $v_2(p_\perp)$ below Q_s and *decreasing* as $p_\perp > Q_s$, perhaps to negative values. Unfortunately, in practice implementation of these ideas are difficult. The Q_s value for small systems in question is in the range 2.5-3 GeV, close to the maxima produced be the flow. Experiments show v_n extending to higher $p_\perp \sim 5\,GeV$, confusing the situation.

Strong-coupling models of the initial stage and equilibrated matter fall into two categories. One is classical strongly-coupled plasmas (Gelman *et al.*, 2006a). Its main feature is that the so called plasma parameter is large

$$\Gamma = \frac{V_{interaction}}{T} > 1 \tag{20}$$

and therefore the potential energy of a particle exceeds its kinetic energy. Simulations and experiments with QED strongly coupled plasmas show that for relevant $\Gamma = 1 - 10$ one deals with *strongly correlated liquids*. Screening in this regime was studied by (Gelman *et al.*, 2006b), and viscosity and diffusion constant by (Liao and Shuryak, 2007). The second – much wider known – strong coupling framework is based on holography and AdS/CFT correspondence.

B. Centrality, $E_\perp$ and fluctuations

Let us briefly remind some basic facts about the global observables and their fluctuations. One of the first practical questions for AA collisions is the determination of centrality classes, related to observables like the number of participant nucleons N_p, correlated to total multiplicity N or transverse energy $E_\perp$. The N_p is defined via measurements of near-forward going neutrons, by forward-backward calorimeters, complementing observables determined from the central mid-rapidity detectors. Correlation plots between all of them and precise cuts defining the centrality classes are defined by each collaboration in their technical reports.

Historically, the ratio of the $E_\perp$ rapidity distributions for AA and pp collisions were fitted by a parameterization

$$\frac{dE_\perp^{AA}}{d\eta}/\frac{dE_\perp^{pp}}{d\eta} = (1-x)\frac{N_p}{2} + xN_{coll} \tag{21}$$

with a parameter x interpreted as an admixture of the "binary collisions" N_{coll} to the main "soft" term, proportional to the number of participants. But we now know that a "hard" interpretation of this last term is questionable: the "hard" power-like component of the particle spectra is actually orders of magnitude smaller than would be needed for it.

One possibility can be that such interpretation is correct at early time, yet with subsequent equilibration jets are quenched and disappear from spectra, however an extra entropy generated by them may still survive and contribute to the total multiplicity.

Another interesting interpretation for the multiplicity and $E_\perp$ distributions were provided by (Tannenbaum, 2014). The notion of participant nucleon is substituted by the "participant quark" N_{qp}. The model – an incarnation of the additive quark model of 1960s – view a nucleon as a set of 3 constituent quarks, which interact separately. Defining the number of "quark participants" N_{qp} he showed that – within a 1% accuracy (!) – it is proportional to the r.h.s. of (21). In particular, the $E_\perp$ is perfectly linear in N_{qp}, see Fig. 17(b). If so, each participant quark is connected by the QCD string to the other one, and those strings are the "clusters" or ancestors for the observed secondaries. We will return to "wounded quarks" concept in the discussion of the Pomeron in section VIII.C.)

On the other hand, the additive quark model does not agree with CGC/GLASMA picture, in which cells, or flux

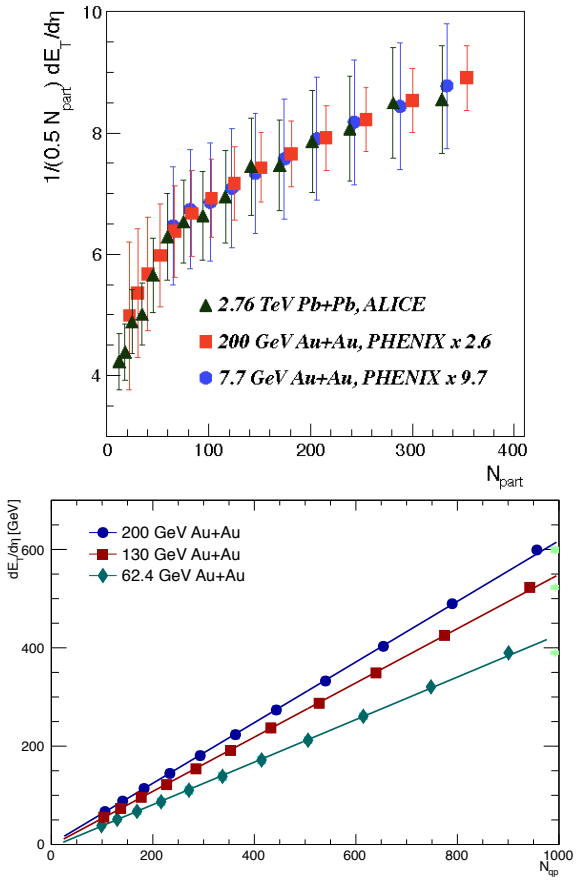

FIG. 17 Distributions over participant nucleons (a) and participant quarks (b), from (Adler *et al.*, 2014; Tannenbaum, 2014).

tubes[13] of the size $1/Q_s \times 1/Q_s$ are the statistically independent sources producing the secondaries. Presumably the CGC-glasma picture should be valid at a high density regime, while simpler Lund-type models with QCD strings (and, perhaps, constituent quarks at their ends) be true in the low density regime. The problem is in the data we do not experimentally detect any sharp transition between the two regimes.

Let us seek further guidance from phenomenology. Note that if the number of independently decaying "clusters" is N, the width of the observed distributions, should scale as $O(N^{-1/2})$. The multiplicity distributions have long tails toward large values, which are usually fitted by the negative binomial or similar distributions with two parameters, or some similar convolutions of two random processes with different parameters. Its second moment should tell us how many "progenitors" (clusters, clans, ancestors,cells) the system goes through.

Let us discuss three models: (i) the usual Glauber in which N is the number of participant nucleons N_p; (ii) the Tannenbaum's modification, based on the number of participant constituent quarks N_{pq}; (iii) and the CGC-glasma, and calculate the fluctuations.

In the last case

$$N_{GLASMA} \sim (\pi R^2) Q_s^2 \tag{22}$$

For central AA the area is geometrical Area=100 fm^2 and

$$N_p \sim 400, N_{pq} \sim 1000, N_{GLASMA} \sim 10^4 \tag{23}$$

For central pA the area is given by the NN cross section $\sigma \sim 100\, mb = 10\, fm^2$. So one gets very different number of "clusters"

$$N_p \sim 16, N_{pq} \sim 40, N_{GLASMA} \sim 10^3 \tag{24}$$

Therefore these models predict vastly different fluctuations.

A brief summary of such a comparison with data is as follows. The participant quark model describes $AuAu$ and dAu data extremely well, while for pp it underpredicts the tail of the distribution. Even 6 participant quarks – the maximal of the model – is not enough, there seems to be more "clusters" than that. The lesson is perhaps that the highest multiplicity pp is indeed the first case when "soft" models become insufficient. The models which have pQCD gluons in the wave function and hard scatterings are doing better on the "tails". In particular, Pythia (pQCD+strings) describes the high multiplicity tail of pp reasonably well.

Alternative approach to initial state fluctuations is provided by the *angular deformations* ϵ_n. We argued above that those are created by a number of statistically independent small-size sources (or "bumps"). For simplicity, like we did before, let us focus on central collisions only, where ϵ_2 is fluctuation-induced and of the same magnitude as all other harmonics. We return to these in section VI.C.

C. Anisotropy and the boundaries of hydrodynamics

The partonic initial state leads to the initial out-of-equilibrium stage of the collision which is highly anisotropic in momentum distribution. However, during the collisions, partons are naturally separated in time according to different rapidities, and create "floating matter", in which a spread of longitudinal momenta is *smaller* than the transverse one. At later hydrodynamical stage, the viscosity effects reduce such anisotropy. Knowledge of the viscosity value allows one to calculate

[13] These McLerran-Venugopalan "flux tubes" should not be confused with the QCD strings: the former exist in dense deconfined phase, are classical and not quantized, have arbitrary fluctuating field strength, and thus do not have an universal tension.

the anisotropy at this stage, provided its initial value is known.

What happens in between is still a matter of debate. Weak coupling approaching –partonic cascades – predict anisotropy to be rising to large values, while the strong coupling (holographic) approaches lead to rapid convergence to small values, consistent with hydrodynamics. For a discussion see e.g. (Martinez and Strickland, 2010)) and subsequent papers.

The issue of anisotropy has two practical aspects. The experimental one – to which we return in section IX.C – is a question how one can experimentally monitor the anisotropy of matter, at various stages of the evolution. The theoretical question is whether one can extend the hydrodynamical description for strongly anisotropic matter. Recently there were significant development along the line of the so called *anisotropic hydrodynamics*, or aHydro. The idea (Florkowski and Ryblewski, 2011; Martinez and Strickland, 2010) is to introduce the asymmetry parameter into the particle distribution, and then, from the Boltzmann equation, derive an equations of motion for it, complementing the equations of the hydrodynamics. Solutions of various versions of hydrodynamics were compared to the exact solution of the Boltzmann equation itself, derived for Gubser geometrical setting by (Denicol *et al.*, 2014). This paper contains many instructive plots, from which I selected the normalized temperature shown in Fig.18 and the sheer stress Π^{ξ}_{ξ} shown in Fig.19 . In both cases the pairs of points correspond to small and very high viscosity values, separated by two orders of magnitude and roughly representatives of the strongly and weakly coupled regimes.

Gubser's variable ρ is the "time" coordinate. In all four plots one can see that all curves coincide in the interval $-2 < \rho < 2$, but deviate from each other both at large negative values, corresponding to the very early stages, and for large positive ones, corresponding to very late times. In fact, all practical applications of hydrodynamics were indeed made inside this interval of ρ, with other regions being "before formation" and "after freezeout".

Solutions for two – hugely different - viscosities show a very similar trends. Israel-Stuart hydrodynamics seems to follow solution of the Boltzmann equation quite well. Even the free streaming regime is not very far from all hydros and exact Boltzmann: this would be surprising for the reader if we did not already know that the radial flow – unlike higher harmonics – can indeed be "faked". If these authors would calculate the elliptic and higher flows, the results would be quite different. One would expect that for $4\pi\eta/s = 100$ higher harmonics would be completely obliterated. The plots for the shear stress show different behaviors for small and large viscosity, but again all curves coincide inside the "hydro window" of $-2 < \rho < 2$. Even going well outside that domain, we never see discrepancies between them by more than 20%.

The overall conclusion one can draw from all of those impressive works is quite simple: all versions of hydrodynamics used in practice are very accurate for realistic viscosities $4\pi\eta/s \approx 2$ and the times the hydrodynamics is actually applied.

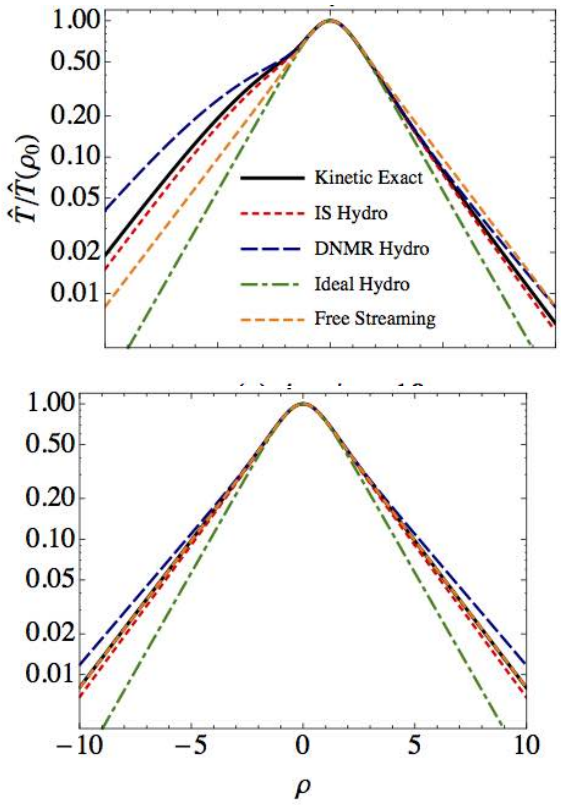

FIG. 18 From (Denicol *et al.*, 2014): the normalized temperature for $4\pi\eta/s = 1, 100$, upper and lower plots, respectively. The meaning of different curves is explained in the upper plot.

V. THE SMALLEST DROPS OF QGP

We have emphasized a certain gap that still exists between weak and strong couplings estimates of the equilibration time and viscosity. Such issues should play an enhanced role in experiments with systems smaller than AA collisions and should clarify *the limits of hydrodynamics*.

Let us start this discussion with another look at the spatial scale corresponding to the shortest sound wavelength, for the highest n of the v_n observed. Azimuthal harmonic are waves propagating along the fireball $surface$. Therefore, successful description of the n-th harmonics implies that hydrodynamics is still applicable at a wavelength scale $2\pi R/n$. Taking the nuclear radius as $R \sim 6\, fm$ and the largest harmonics so far observed $n = 6$, one finds that the scale under consideration is larger than $O(1\, fm)$. So, it is still not small enough to resolve the nucleon substructure. That is why there is

little difference between the initial states of the Glauber model (described in terms of nucleons) from those generated by GLASMA models (operating on a parton level) .

Why don't we see harmonics with larger $n > 6$? Higher harmonics suffer stronger viscous damping. The limitation is due to current statistical limitations of the data sample, and is thus unrelated with the limits of hydrodynamics.

In principle, one could have studied AA collisions with smaller and smaller A, decreasing the system size smoothly, while preserving the overall geometry. However, historically the development was not that smooth: unexpected discovery of the so called "ridge" at the LHC in very small systems – pp with high multiplicity trigger– provided a look at the opposite extreme case.

Before we go into details, let us see how small these systems really are. At freezeout the size can be directly measured, using the so called $femtoscopy$ method (see Appendix for some explanations). The corresponding data are shown in Fig.20, which combines the traditional 2-pion with more novel 3-pion correlation functions of identical pions.

An overall growth of the freezeout size with multiplicity, roughly as $< N_{ch} >^{1/3}$, is expected if the freezeout density is an universal constant. While for AA collisions this simple idea indeed works, the pp, pA data apparently form a different line, with significantly smaller radii. Apparently those two systems get frozen at higher density,

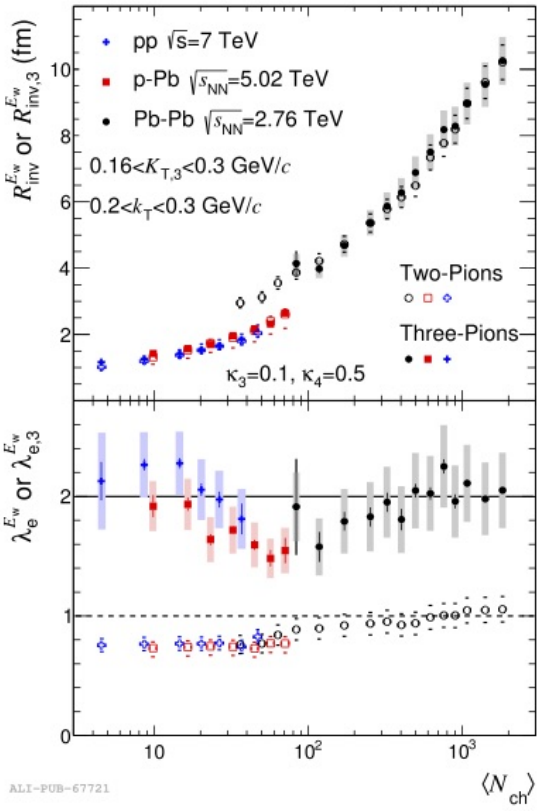

FIG. 20 Alice data on the femtoscopy radii (From (Grosse-Oetringhaus, 2014)) (upper part) and "coherence parameter" (lower part) as a function of multiplicity, for $pp, pPb, PbPb$ collisions.

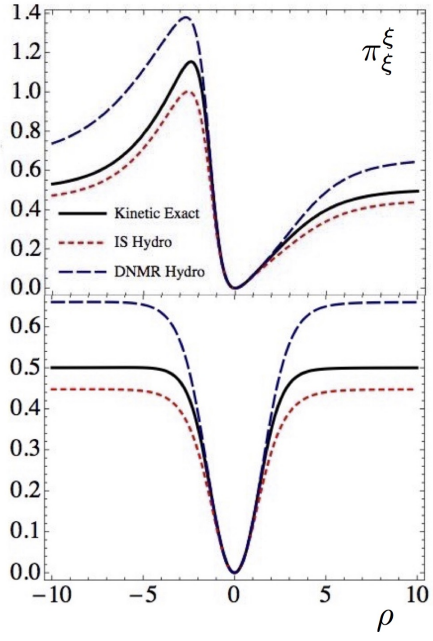

FIG. 19 From (Denicol *et al.*, 2014): the shear stress π^{ξ}_{ξ} versus coordinate ρ, for viscosity $4\pi\eta/s = 1, 100$, the upper and the lower plots, respectively.

compared to AA, but why? To understand that recall the *freezeout condition*: "the collision rate becomes comparable to the expansion rate"

$$< n\sigma v >= \tau^{-1}_{coll}(n) \sim \tau^{-1}_{expansion} = \frac{dn(\tau)/d\tau}{n(\tau)} \qquad (25)$$

Higher density means larger l.h.s., and thus a larger r.h.s.. So, pp, pA high-multiplicity systems are more "explosive", with larger expansion rate! We will indeed argue below that this conclusion is also confirmed by radial flow measured by particle spectra, as well as the HBT radii.

But why are those systems "more explosives"? Where is the room for that, given that even the measured final size of these objects is *smaller* than in peripheral AA (which show only a rather modest radial flow). The only space left is at the beginning: those systems must obviously *start accelerating earlier*, from *even smaller* size than seen by femtoscopy, to produce strong collective flow at freezeout.

Another puzzle is why central pA – a collision of a proton with about 16 others – appears to be so similar in size and collective flows to (same multiplicity) pp, a collision of only two protons. We will turn to its discussion

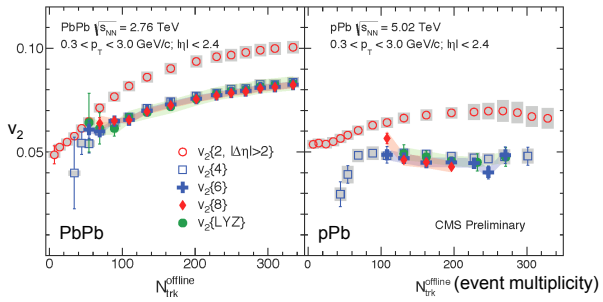

FIG. 21 CMS data (de Cassagnac, 2014) for v_2 calculated using 2,4,6, 8 particle correlations, as well as Lee-Yang zeroes (basically all particles). Good agreement between those manifest collectivity of the phenomenon.

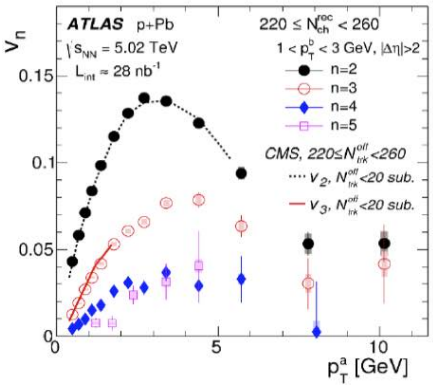

FIG. 22 v_n for $n-2,3,4,5$ versus $p_\perp$ in GeV, for high multiplicity bin indicated on the figure. The points are from ATLAS, lines from CMS (presentation at QM2015).

in section V.C.

A. Collectivity in small systems

The first discovery – in the very first LHC run – was due to the CMS collaboration (Khachatryan *et al.*, 2010) which found a "ridge" correlation in high multiplicity pp events. A special trigger was required because, unfortunately, the effect was first seen only in events with a probability $P \sim 10^{-6}$ [14]. Switching to central pA collisions, the CMS observed a similar ridge there, now with much higher probability, few percent instead of $P \sim 10^{-6}$ (Chatrchyan *et al.*, 2013) . By subtracting central minus peripheral correlations, ATLAS CMS and ALICE groups soon all found, that the observed "ridge" is accompanied by the "anti-ridge" in the other hemisphere, concluding the phenomenon is a familiar elliptic flow, $v_2 cos(2\phi)$ deformation.

The PHENIX collaboration at RHIC also found a ridge-like correction in central dAu collisions, with the v_2 value about twice *larger* than in pPb at LHC. This difference was soon attributed to different initial conditions, for d and p beams, since the former produce a "double explosion" by its two nucleons. Quantitative hydrodynamical studies, such as (Bozek, 2012) , confirmed this simple idea. It was later was additionally confirmed by collisions of He^3Au as well.

The best set of data, which established *collectivity* of the flow in pA "beyond a reasonable doubt", came from CMS (de Cassagnac, 2014). Their v_2 measurements from 4,6 and 8 particle correlators are shown in Fig.21.

Taking collectivity for granted, one can further ask if the v_2 observed is caused by the pre-collision correlations or by the after-collision collective flows. A very nice control experiment testing this is provided by dA and He^3A collisions. Two nucleons in d are in average far from each other and 2 MeV binding is so small that one surely can ignore their initial state correlations. So, whatever the "initial shape" effect in pp, in dA it should be *reduced* by $1/\sqrt{2}$ because two shapes cannot be correlated. It should be reduced further in He^3A by $1/\sqrt{3}$, if the same logic holds.

Hydrodynamical predictions are opposite: double (or triple) initial explosions still lead to one common fireball, with the initial anisotropies *larger* than in pA. Data from RHIC by PHENIX and STAR on dAu, He^3Au do indeed show such an *increase* of the v_2, v_3, relative to pAu, again in quantitative agreement with hydrodynamics (Bozek and Broniowski, 2014; Nagle *et al.*, 2014).

ATLAS was able to perform the first measurements of higher harmonics $v_n, n = 4, 5$ in central pPb, see Fig. 22. Except at very high $p_\perp$, those two harmonics seem to be comparable in magnitude: it is the first contradiction to "viscous damping" systematics.

B. Pedagogical digression: scale invariance of sQGP and small systems

Acceptance of hydrodynamical treatment of "small system explosions" is psychologically hard for many. One asks how is it possible to treat a fireball, of size less than 1 fm, as a macroscopic one[15].

So let us take a step back from the data and consider the issue of scales. If one takes smaller and smaller cells of ordinary fluid – such as water or air – eventually one

[14] Dividing the cost of LHC, $\sim \$10^{10}$ by the number of recorded pp events $\sim 10^{10}$ one finds that an event costs about a dollar each. Therefore, high multiplicity pp events under consideration cost about a million dollar each, and one needs thousands of them to construct a correlation function!

[15] Note that just 15 years ago the same question was asked about systems of 6 fm size.

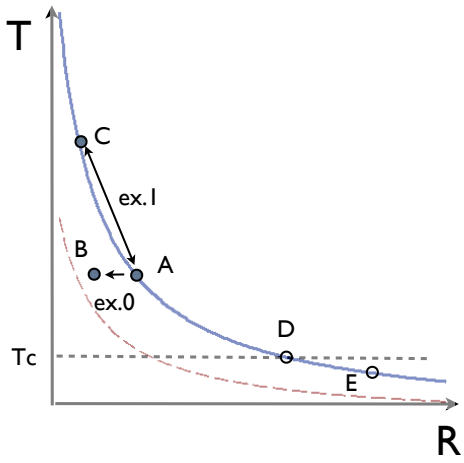

FIG. 23 (color online) Temperature T versus the fireball size R plane. Solid blue line is the adiabatic $S = const$, approximately $TR = const$ for sQGP. Example 1 in the text corresponds to reducing R, moving left $A \to B$. Example 2 is moving up the adiabatic $A \to C$. Example 3 corresponds to adiabatic expansion, such as $A \to E$,$C \to E$. If in reality C corresponds to pA, the freezeout occurs at the earlier point D.

reaches the atomic scale, beyond which water or air, as such, do not exist: at some scale one resolves the individual molecules. But QGP is *not* like that: it is made of essentially massless quarks and gluons which have no scale of their own. The relevant scale is given by only one parameter T – thus QGP is approximately scale invariant. (The second scale Λ_{QCD} only enters via logarithmic running of the coupling, which is relatively slow and can in some approximation be ignored.)

As lattice numerical calculations show (see e.g. Fig.64), at $T > 200\,MeV$ the QGP thermodynamics is approximately scale invariant[16] : $\epsilon/T^4, p/T^4$ are approximately T-independent. The comparison of LHC to RHIC data further suggests that similar scaling $\eta/T^3 \sim const$ holds for viscosity as well. (although with less accuracy so far). Thus, as a first approximation one may assume that QGP does not have a scale of its own. This means that it would show *exactly the same behavior* if conditions related by the scale transformation

$$R_A/R_C = \xi, T_A/T_C = \xi^{-1} \tag{26}$$

are compared.

Consider a *thought experiment 1*, in which we compare two systems on the same adiabatic A and C. For scale invariant sQGP the points A, C are related by this scale transformation mentioned above, and have the same entropy [17] . Assuming the scale transformation is an approximate symmetry, one expects the same dynamical evolution. A smaller-but-hotter plasma ball C will explode in exactly the same way as its larger-but-cooler version A.

Let us now proceed to *thought experiment (2)*, which is the same as above but in QCD, with a running coupling. In the sQGP regime it leads to (very small, as lattice tells us) running of s/T^3, some (unknown) running of η/T^3, etc. The most dramatic effect is however not the running coupling *per se*, but the lack of supersymmetry, which allows for the chiral/deconfinement phase transition, out of the sQGP phase at $T > T_c$ to hadronic phase at $T < T_c$. The end of the sQGP explosion D thus has an *absolute scale*, not subject to a scale transformation!

So let us consider two systems A,C of the same total entropy/multiplicity, both initiated in the sQGP phase, with initial conditions related by the scale transformation. Their evolution would be the same, until the larger/cooler one reaches $T \approx T_c$, where scale invariance of their evolution ends! So, the final result of the explosions are not the same. In fact, the smaller/hotter system has an advantage over the larger/cooler one, since the *larger* ratio of the initial and final scales T_i/T_f let it be accelerated more.

The hydrodynamic expansion does not need to stop at the phase boundary D. In fact large systems, as obtained in central AA collisions are known to freezeout at $T_f < T_c$, down to 100 MeV range (and indicated in the sketch by the point E. However small systems, obtained in peripheral AA or central pA seem to freezeout at D.

Brief summary: We expect hydrodynamics to work as well in smaller system, due to approximate scale invariance of sQGP. Including deviations from scale invariance, one finds that small systems should explode even more violently, compared to larger/cooler systems, since larger fraction of time is spent in the sQGP phase.

Another meaning of the term "small systems" is applied when not the actual size but entropy/multiplicity is reduced. Deviations from hydrodynamics in such cases are seen as higher viscous corrections. For recent discussion of those issues see (Romatschke, 2016; Spalinski, 2016).

C. Comparison of the peripheral AA,

[16] At $T < 200\,MeV$ there is no scale symmetry: there is significant change instead. It is of course taken into account in hydrodynamics and will be discussed later, e.g. in the section on HBT radii.

[17] Note, that the holographic models interpret the "RG scale" as an extra 5-th coordinate. The evolution in scale is thus depicted as "gravitational falling" of particles,strings, fireballs etc along this coordinate. In this language, our two systems fall similarly in the same gravity, but since the smaller system starts "higher", it gets larger velocity at the same "ground level", given by a fixed scale T_c.

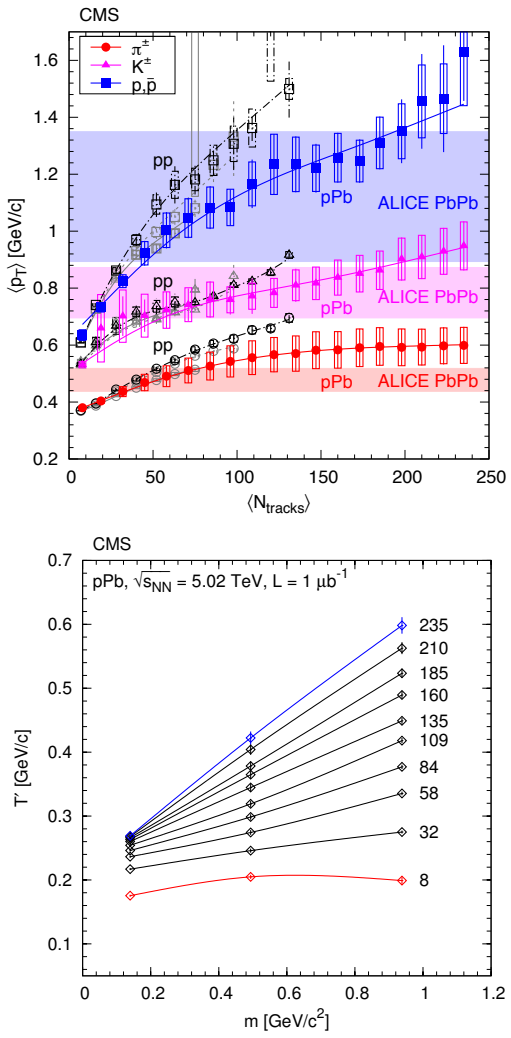

FIG. 24 (color online) (From (Chatrchyan *et al.*, 2014).) (a) Average transverse momentum of identified charged hadrons (pions, kaons, protons; left panel) and ratios of particle yields (right panel) in the range $|y| < 1$ as a function of the corrected track multiplicity for $|\eta| < 2.4$, for pp collisions (open symbols) at several energies, and for pPb collisions (filled symbols) at $\sqrt{s_{NN}} = 5.02\,TeV$. (b) The slopes of the $m_\perp$ distribution T' (in GeV) as a function of the particle mass. The numbers on the right of the lines give the track multiplicity.

central pA and high multiplicity pp

From thought experiments with some ideal systems, let us return to reality. We will do it in two steps, starting in this section with "naive" estimates for three cases at hand, based on standard assumptions about the collision dynamics, and then returning to more model-dependent discussion in the next subsections.

We want to evaluate the *initial* transverse radii and parton densities, not that of the fireball at freezeout, after a hydrodynamic expansion. The multiplicity is however the *final* one, but – due to (approximate) entropy conservation during hydrodynamics – we think of it as a proxy for the entropy at all times. Entropy generated by viscosity *during* expansion is relatively small and can be corrected for, if needed.

(i) Our most studied case, the central $AuAu$ or PbPb, is the obvious benchmark. With the total multiplicity about $N_{AA} \approx 10^4$ and transverse area of nuclei $\pi R_A^2 \approx 100\,fm^2$ one gets the density per area

$$n_{AA} = \frac{N}{\pi R_A^2} \sim 100\,fm^{-2} \tag{27}$$

This can be transformed into entropy if needed, in a standard way.

(ii) Central pA (up to a few percent of the total cross section) has CMS track multiplicity of about 100. Accounting for unobserved range of $p_\perp, y$ and neutrals increases it by about factor 3, so $N_{pA}^{central} \sim 300$. The area now corresponds to the typical impact parameter b in pp collisions, or $\pi < b^2 >= \sigma_{pp} \approx 10\,fm^2$. The density per area is then

$$n_{pA}^{central} = \frac{N_{pA}^{central}}{\sigma_{pp}} \sim 30\,fm^{-2} \tag{28}$$

or 1/3 of that in central AA. Using the power of LHC luminosity CMS can reach – as a fluctuation with the probability 10^{-6} — another increase of the multiplicity, by a factor of 2.5 or so, up to the density N_{pA}^{max}/σ_{pp} in AA. Another approach used is a comparison of central pA with peripheral AA of the same multiplicity, or more or less same number of participants, or similar matter density.

(iii) Now we move to the last (and most controversial) case, of the high multiplicity pp collisions. (Needless to say the density is very low for min.bias events.) "High multiplicity" at which CMS famously discovered the "ridge" starts from about $N_{pp}^{max} > 100 * 3$ (again, 100 is the number of CMS recorded tracks and 3 is extrapolation outside the detector covered).

The big question now is: *what is the area?* Unlike in the case of central pA, we don't utilize standard Glauber and full cross section (maximal impact parameters). We instead address a fluctuation which has small probability. In fact, nobody knows the answer to this question. Based on the profile of pp elastic scattering (to be discussed in section VIII.C), it should correspond to impact parameter b in the black disc regime. If so $\pi b_{b.d.}^2 \sim 1/2\,fm^2$, which leads to density per area

$$n_{pp}^{max} \approx \frac{N_{pp}^{max}}{\pi b_{b.d.}^2} \sim 600\,fm^{-2} \tag{29}$$

Other evidences about glue distribution in a proton comes from HERA diffractive production, especially of $\gamma \to J/\psi$. They also suggest a r.m.s. radius of only $0.3\,fm$, less than a half of electromagnetic radius.

Brief summary: in terms of the initial entropy density one expects the following order of the densities-per-area involved

$$\frac{dN^{pA}_{maximal}}{dA_\perp} \sim \frac{dN^{AA}_{peripheral}}{dA_\perp} \ll \frac{dN^{AA}_{central}}{dA_\perp} \ll \frac{dN^{pp}_{maximal}}{dA_\perp} \tag{30}$$

One may expect that the radial flow follows the same pattern: yet the data show it is *not* the case.

D. The size and radial flow puzzle for central pA

The simplest consequence of the radial flow is an increase in mean transverse momentum. CMS data as a function of multiplicity are shown in Fig.24(a). While pp and pA data are shown by points, the AA ones (from ALICE) are shown by shaded areas. (The most central ones correspond to the upper edge of this shaded region.)

The next experimental signature of the radial flow is that the blue-shifts it induces modify spectra of secondaries of different mass differently. While light pions retain their exponential shape of the p_t spectra, only with a blue-shifted slope,

$$T' = T_f e^{\kappa} \tag{31}$$

the spectra of massive particles change their shape. Eventually, for very heavy particles (e.g. d or other nuclei), their thermal motion is negligible and their spectra depend completely on collective velocities. Their distribution has a characteristic peak at the fireball's edge, with $v = v_{max}$, and thus the $p_\perp$ spectra develop a peak at $p_\perp = m v_{max}$.

More specifically, flow creates "violation of the $m_\perp$ scaling" (Shuryak and Zhirov, 1979). The $m_\perp$ slopes T', defined by the exponential form (above certain p_t)

$$\frac{dN}{dydp_\perp^2} = \frac{dN}{dydm_\perp^2} \sim exp(-\frac{m_\perp}{T'}) \tag{32}$$

are very sensitive indicators of the radial flow. A sample of such slopes for pA collisions, from CMS, is shown in Fig.24. Note that for low multiplicity bins (marked by 8 and 32 at the bottom-right) one sees the same T' for all secondaries: this is the $m_\perp$ scaling: the flow is absent. This behavior is natural for independent string fragmentation, rescattering or glasma models.

Flow manifests itself at higher multiplicity bins, in which the slopes T' are mass-dependent . As seen from Fig.24(b), they are growing approximately linearly with the particle mass. The effect gets more pronounced with multiplicity: this is the sign of stronger collective flow. Note that for the most central pA bin this slope *exceeds*[18]

[18] Predicted to happen before the data: check version v1 of (Shuryak and Zahed, 2013).

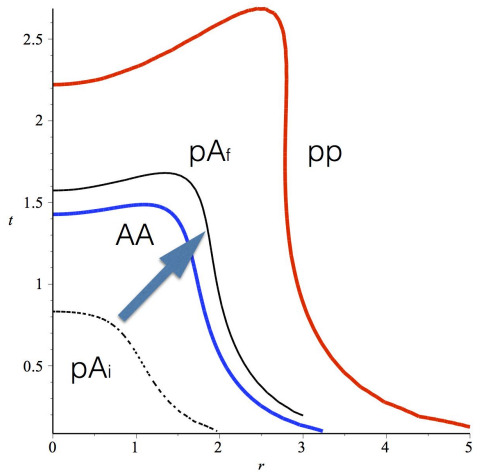

FIG. 25 (color online) The freezeout surface in universal dimensionless time t and radial distance r coordinates. (Blue) thick solid line in the middle corresponds to central AA (PbPb) collisions, (red) thick solid line on the top to the highest multiplicity pp . Two (black) thin ones correspond to central p Pb case, before and after collapse compression, marked pA_i, pA_f respectively. The arrow connecting them indicates the effect of multi string collapse.

those in central $PbPb$ collisions at the LHC, the previous record-violent explosion!

This gives rise to what we call *the radial flow puzzle*. Indeed, naive estimates of densities in the previous subsection may suggest that the explosion in highest multiplicity pA case should still be *weaker* than in AA. Indeed, both the system is smaller and the initial entropy density seem to be smaller as well. Yet the data show the opposite: the observed radial flow strength (expressed via the magnitude of the transverse rapidity) follows a different pattern

$$y_\perp^{AA,central} < y_\perp^{pA,central} < y_\perp^{pp,highest} \tag{33}$$

Hydrodynamics is basically a bridge, between the initial and the final properties of the system. For the radial flow dependence on the size of the system it is convenient to follow Ref. (Shuryak and Zahed, 2013) based on Gubser's flow , see section B.2 . One single analytic solution describes all cases considered: we will proceed from the dimensional variables $\bar\tau, \bar r$ with the bar to the dimensionless variables

$$t = q\bar\tau, \;\; r = q\bar r \tag{34}$$

rescaled by a factor q, with the dimension of an inverse length. In such variables there is a single Gubser solution of ideal relativistic hydrodynamics, for the transverse velocity (B29) and the energy density (B30).

Recall our thought experiment (1) of the subsection V.B: two collisions which are conformal copies of each

other merge into a single one in these dimensionless variables. In fact, the blue line[19] marked AA in Fig.25 corresponds not only to central PbPb collisions but actually to any other AA collisions at the LHC. The two black lines are for the pPb case: they both have $T_f = 170\,MeV$ and the same multiplicity but different scale parameters: $q = 1/1.6\,fm$ for the lower dotted line but twice smaller initial size $q = 1/0.8\,fm$ for the upper (thin solid black) line. As an arrow indicates, in order to explain the observed higher explosion velocity one has to move the curve above the blue line. This implies that hydrodynamics must be initiated from smaller "compressed" size, according to "spaghetti collapse" scenario we will discuss in section V.B. If this is done, the freezeout surface "jumps over" our AA benchmark blue line, and its radial flow gets stronger. The maximal transverse velocities on these curves (located near the turn of the freezeout surface downward) are

$$v_\perp^{pAu} = 0.56 < v_\perp^{AA} = 0.81 < v_\perp^{pAu,f} = 0.84 \qquad (35)$$

The upper red line is our guess for the maximal multiplicity pp collisions, assuming its $q = 1/0.5\,fm$: it has even stronger radial flow, with maximal $v_\perp^{pp} \approx 0.93$. So, paradoxically, small systems are in fact larger than AA in the appropriate dimensionless variables, and that is why their radial flow is better developed.

In summary: the observed pattern of radial flow magnitude can be explained if the initial size of the pA system is significantly reduced compared to the naive estimates of the preceding section.

E. Radial flow in high multiplicity pp

According to our estimates of the densities per area made above, it is much higher for high multiplicity pp than for AA collisions. The initial state must be in a GLASMA state, if there is one. Unfortunately we have little theoretical guidance about the size. After all, in this subsection we discuss fluctuations with a probability $\sim 10^{-6}$! Lacking good theory guidance, one may invert our logic and proceed phenomenologically:
(i) The first phenomenological input – the mean $p_\perp$ and spectra of the identified particles – are shown in Fig.24. The absolute magnitude of the flows at freezeout – radial, v_2, v_3 – can thus be evaluated from the data.
(ii) Then one can "solve hydrodynamics backwards", and determine which initial conditions are required to generate it.
(iii) For consistency, one can calculate the absolute values of the radii provided by the femtoscopy. The observed radii show a decrease with the increase of the

[19] For the record, its parameters are $q = 1/4.3\,fm, \hat{\epsilon}_0 = 2531, T_f = 120\,MeV$.

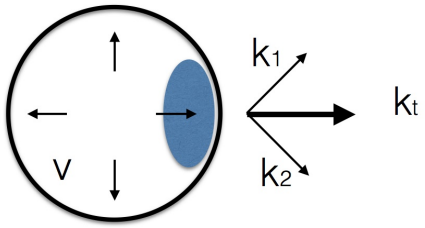

FIG. 26 Sketch of the radial flow (arrows directed radially from the fireball center) explaining how it influences the HBT radii. At small k_t the whole fireball (the large circle) contributes, but at larger k_t one sees only the part of the fireball which is co-moving in the same direction as the observed pair. This region – shown by shaded ellipse – has a smaller radii and anisotropic shape, even for central collisions.

(total) transverse momentum $\vec{k_1} + \vec{k_2} = \vec{k_\perp}$ of the pair (Makhlin and Sinyukov, 1988). Modification of the argument is explained in a sketch shown in Fig.26. At small $k_\perp$ the detector sees hadrons emitted from the whole fireball, but the larger is $k_\perp$, the brighter becomes its small (shaded) part in which the radial flow is (a) maximal and (b) has the same direction as $\vec{k_t}$. This follows from maximization of the Doppler-shifted thermal spectrum $\sim \exp\left(p^\mu u_\mu / T_{freezeout}\right)$.

This effect has been calculated (Hirono and Shuryak, 2015) and compared with the ALICE HBT data (Aamodt *et al.*, 2011a) shown in Fig.27. Strong flow in high multiplicity pp collisions is directly visible in the data. The effect is best seen in the "out"-directed radius R_{out} (the top plot). While low multiplicity data (connected by the blue dashed line) are basically independent on the pair momentum, at high multiplicity (stars and red dashed line) they decrease by a rather large factor. Another consequence of the flow is anisotropy of radii. In the bottom plot the ratio of two radii are shown. At small multiplicity it is always 1 – that is the source is isotropic – but at high multiplicity the source becomes anisotropic, the radii in two directions are quite different, with their ratio dropping to about 1/3, at the largest k_t. Thus, a direct consequence of the flow is that only 1/3 of the fireball emits pairs of such momenta.

In Fig.28 we show a series of calculations in which the initial QGP stage of the collision is modeled by numerical hydrodynamics solution close to Gubser analytic solution with variable parameter q. (The late stages need to deviate from Gubser since near T_c the EOS is very different from conformal $\epsilon = 3p$ assumed in Gubser's derivation).

Brief summary: Unlike central pA, the highest multiplicity pp events are significantly denser/hotter than central AA. Very strong radial flow, seen in spectra of identified particles and HBT radii, require very small, sub femtometer, initial size of the system. In spite of

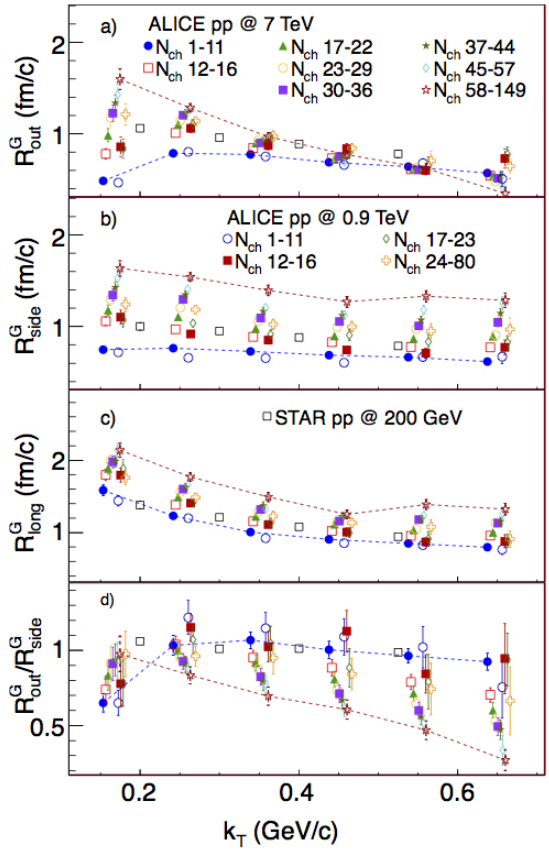

FIG. 27 HBT radii versus the pair transverse momentum k_T, for various multiplicities of the pp collisions, from ALICE (Aamodt *et al.*, 2011a).

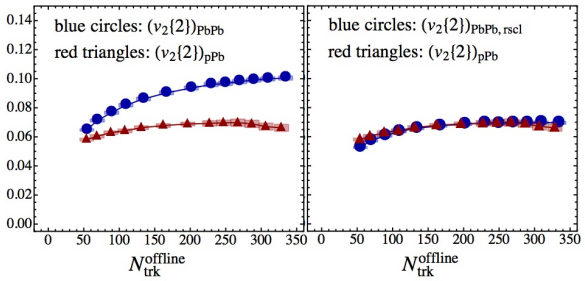

FIG. 29 The integrated $v2\{2\}$ for $PbPb$ and pPb vs. multiplicity from [23]. Left: Original values. Right: The fluctuation dependent elliptic flow, with the geometrical part subtracted. This geometrical part was calculated using the Phobos Glauber Model and is not a fit.

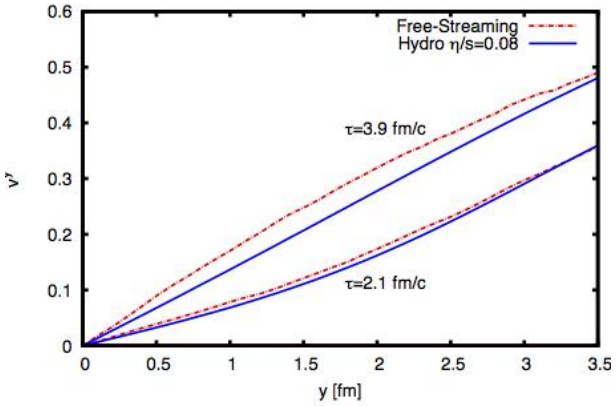

FIG. 30 Comparison of the flow profile, for hydrodynamics and free streaming , from (Romatschke, 2015).

high cost associated with those events, their studies are justified because here we produce the most extreme state of matter ever created in the lab.

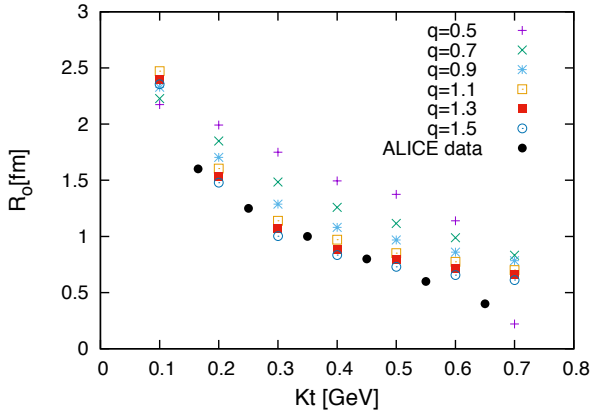

FIG. 28 From (Hirono and Shuryak, 2015): HBT radii compared to ALICE data (closed circles), for solutions starting with different initial size of the fireball, indicated by Gubser scale parameter q (which is inversely proportional to the size).

F. Can flows in small systems be "fake"?

The question of what I call "the fake flow" and subsequent development is due to (Romatschke, 2015) who considered consequences of a scenario in which quarks and gluons at the QGP phase have no interactions, they "free stream" from the point of the initial scattering to the hadronization surface. At this surface the system switches to hadronic phase, treated by standard hadronic cascade code.

In Fig.30 one sees a comparison of the radial flow profiles of the two cases, with and without interaction at the QGP phase. One can see that the profiles are in fact very similar, becoming linear Hubble-like as time goes on. In fact free streaming generates even a bit stronger flow, because free streaming uncouples from longitudinal direction, and equilibrated medium does not. Comparing particle spectra and HBT radii Romatschke shows that

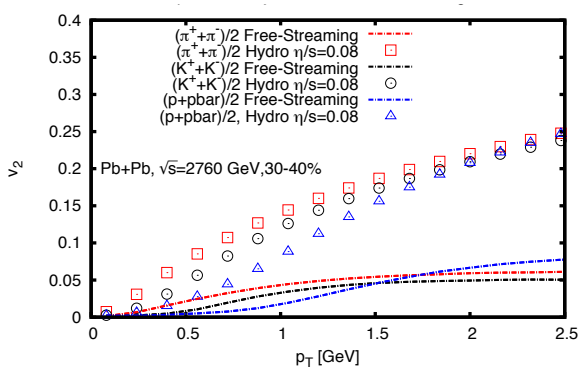

FIG. 31 Comparison of the flow harmonic, for hydrodynamics and free streaming for PbPb collisions, from (Romatschke, 2015).

this "fake" radial flow is indeed *indistinguishable* from the hydrodynamics.

What about flow harmonics? The results for $PbPb$ collisions are shown in Fig.31. As one can see, without hydrodynamics these disappear. This is not surprising since if there is no hydrodynamics then there are no sound waves, and initial bumps are simply dissolved without a trace.

In fact it is an interesting question how *any* v_n can be generated in the free streaming. The initial momentum distribution of partons is isotropic, and so it must be related to the interaction after hadronization. Romatschke found that indeed before hadronization they are absent. However two component of $T_{\mu\nu}$, the flow $\sim u_\mu u_\nu$ part and the dissipative $\Pi_{\mu\nu}$ part, still have nonzero values which cancel each other in sum. After hadronization hadronic interaction kills the second component $\Pi_{\mu\nu} \to 0$ and reveals the effect of the first one.

Not only are the "fake" flow harmonics small, they do not show two important features of the "true" hydrodynamical ones: (i) they do not show strong increase with $p_\perp$; and (ii) they do not show strong decrease with the number $\sim exp(-n^2)$ induced by the viscosity during the time before hadronization.

So, unlike the radial flow, higher harmonics in large ($PbPb$) systems cannot be faked. What about smaller systems? Romatschke gives the results for pPb at LHC and dAu and He^3Au for RHIC energies. We show the first case in Fig.32. Again the free that the free streaming model seems to be failing for v_2, but is somewhat marginally surviving for v_3.

Summary: flow harmonics are not "faked". Yet, for small systems, taking into account remaining uncertainties of the initial stage models and thus ϵ_n values , this conclusion is not as robust as for the AA. Perhaps some scenarios, intermediate between equilibrated hydrodynamicsand free streaming, may still fit these data.

G. Shape fluctuations: central pA vs peripheral AA

Scaling relations between central pA and peripheral AA were suggested by (Baar and Teaney, 2014). Step one of their paper was prompted by the fact (noticed in the CMS paper already): that at the same multiplicity, v_3 in central pA and peripheral AA are basically the same. Some people called for new paradigms based on this fact: but in fact it is hardly surprising: equal multiplicity means equal number of participant nucleons, and thus equal fluctuations of the shape. After the geometrical contribution to v_2 in peripheral AA is removed, the remaining – fluctuation-driven – part of the elliptic flow is perfectly the same in both cases, see Fig.29.

Their second proposal is that the $p_\perp$ dependence of (the fluctuating part) of the v_n has an universal shape, and AA and pA data are only different by a scale of mean $p_\perp$

$$v_n^{pA}(p_t) = v_n^{pA}(\frac{p_\perp}{\kappa}) \tag{36}$$

where the scaling factor is defined as

$$\kappa = \frac{< p_\perp >_{pPb}}{< p_\perp >_{PbPb}} \approx 1.25 \tag{37}$$

and is due to the difference in the radial flow.

VI. EQUILIBRATION IN QCD-BASED MODELS

A. CGC and turbulent GLASMA

The idea of continuity, from a state before collision to early time after it, is most directly realized in the so called CGC-GLASMA approach. Technically it is based on the argument (McLerran and Venugopalan, 1994) that high density of partons leads to large color charge fluctuations, which should create strong color fields. If fields are

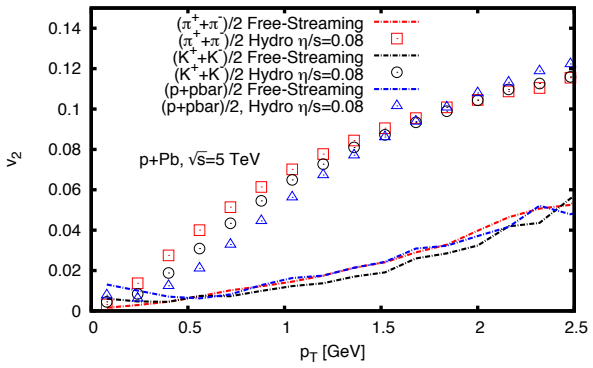

FIG. 32 Comparison of the flow harmonic, for hydrodynamics and free streaming in the pPb central bin , from (Romatschke, 2015).

strong enough, then classical Yang-Mills (YM) equations are sufficient, and those can be solved numerically. It is important that at this stage the fields get strong, the occupancy of gluons $n_g \sim 1/\alpha_s \gg 1$ and, by rescaling them, one can get the coupling out of the equations. It means that GLASMA is non-perturbative, in spite of weak coupling. It remains so until gluon occupation numbers drop to their thermal magnitude $n_g \sim 1$.

When density of gluons gets large enough and nonlinear effects become important, the GLASMA is in its "dense regime". Its boundary, shown in Fig.33 is defined by the saturation momentum $Q_s(x)$, separating it from the dilute partonic phase. $Q_s(x)$ is expected to grow with collision energy (smaller x) and higher atomic number A. At the highest LHC energies and atomic numbers its value is as large as $Q_s^2 \sim 10\,GeV^2$, believed to be in the perturbative domain. However another boundary, of the "confining regime" at the bottom of the figure, is indicated by extremely small $Q^2 < 0.03\,GeV^2$. This is unacceptable: the boundary of pQCD is in fact at least a factor 30 or more higher. There are no gluons with virtuality below 1 GeV[20]. Modern lattice simulations show that gluon effective mass in QGP is of the order of $1\,GeV$ at $T = T_c$, and grows further at $T > T_c$.

Theoretical study of parton equilibration in weak coupling domain has a long history. The "bottom up" approach (Baier *et al.*, 2001) was based on soft gluons radiated by scattered hard partons. The name reflects that thermal occupation starts from the IR end. (Note that it is opposite to the "top-down" equilibration in holographic models we will discuss below.) The main predictions of that model was the equilibration time and the initial temperature scaling with the coupling

$$\tau_{eq} \sim 1/(\alpha_s^{13/5} Q_s),\;\; T_i \sim \alpha_s^{2/5} Q_s \tag{38}$$

Some details were changed later, Weibel, Nielsen-Olesen and other instabilities which occur in the model were incorporated. Its validity domain is restricted by its core assumption of small angle scattering of the gluons, justified by large impact parameters of the order of inverse (perturbative) Debye mass. Perturbative means $M_D \approx gT \ll T$ or small $g \ll 1$. For its edge values $g = 1, \alpha_s = 1/4\pi$ the equilibration time is predicted to be very long $\tau_{eq} Q_s \sim 700$, exceeding duration of the collisions.

In the last few years several groups performed numerical studies of parton equilibration using both the Boltzmann equation or the YM field equations. Typically, in such studies the coupling constant is taken to be extremely small. In fact, so small that one can treat not only powers of α_s but even its log as a large parameter $log(1/\alpha_s) \gg 1$, allowing the total GLASMA evolution scale

$$\tau_{GLASMA} \sim \frac{log^2(1/\alpha_s)}{Q_s} \tag{39}$$

to be considered large.

Significant progress in this directions has been induced by incorporation of certain ideas from general theory of turbulent cascades. Not going into its long history, Let us just mention the Kholmogorov-Zakharov stationary power-like solutions for Boltzmann equations, for a number of systems with various waves. Another general advance is existence of the time-dependent self-similar solutions. J.Berges and collaborators developed it for scalar and gauge fields, pointing out different regimes for UV and IR-directed cascades, and identifying such regimes in impressive numerical simulations.

This body of work resulted in the following new scenario: the pre-equilibrated stage is dominated by a *non-trivial turbulent attractor* – a certain self-similar power solution – in which it spend some time before progressing toward the thermal equilibrium. An important signature of that is large momentum anisotropy, measured by the ratio $p_l/p_\perp$. One group (Epelbaum, 2014) performed a next-order GLASMA simulation, with $g = 0.5$, in which $p_l/p_\perp$ kept approximately constant value during the whole time of the simulation $\tau Q_s = 10 - 40$. Another group (Berges *et al.*, 2015) found that, at $g = 0.3$, the longitudinal pressure p_l/ϵ remains close to zero at similar times. Both results are shown in Fig.34.

Cascade simulations at larger couplings (Kurkela and Zhu, 2015) produce the results shown in Fig.35. The two sets of trajectories, shown by solid and dashed lines,

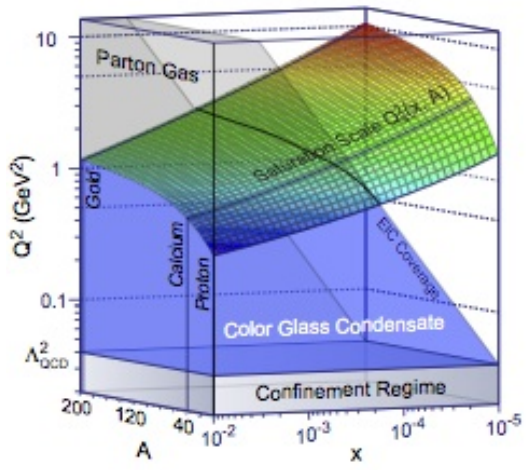

FIG. 33 The CGC phase diagram: the saturation momentum Q_s as a function of fraction of momentum x and the atomic number A, from (Lappi *et al.*, 2014).

[20] Recall that already Nambu-Jona-Lasinio model of 1961 had strong non-perturbative forces at $Q < 1\,GeV$ creating chiral symmetry breaking.

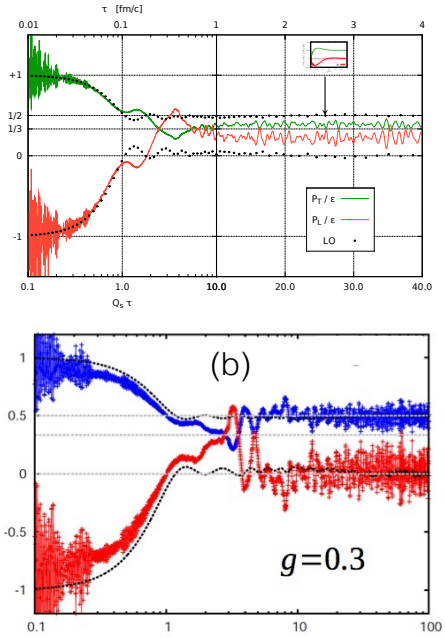

FIG. 34 (a) Upper green curve is $p_\perp/\epsilon$, lower red is p_l/ϵ, as a function of time in units of saturation scale, τQ_s, at $g = 0.5$, from (Epelbaum, 2014).
(b) Upper blue curve is $p_\perp/\epsilon$, lower red is p_l/ϵ, at $g = 0.3$, from (Berges *et al.*, 2015).

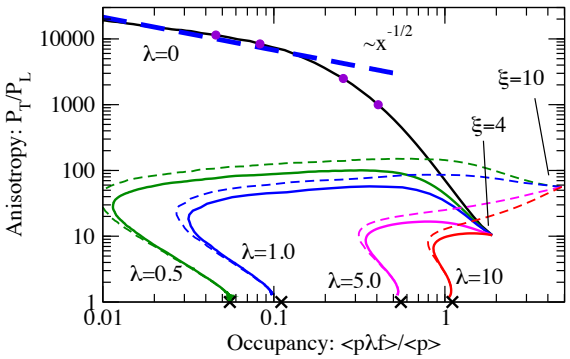

FIG. 35 From (Kurkela and Zhu, 2015): Trajectories of the systems on the occupancy-anisotropy plane for various settings. The parameter λ near curves show the corresponding 't Hooft coupling constant $\lambda = g^2 N_c$. All solid line originate from one initial distribution characterized by the anisotropy parameter $\xi = 4$, the dashed lines originate from a different point with $\xi = 10$. .

starting from two different initial distributions. At zero coupling (upper left curve) the longitudinal momenta of particles gets very small compared to the transverse, and anisotropy steadily increases. This is a scaling-like classical regime with a nontrivial fixed point. However all other paths stay more or less at the same initial anisotropy, and then rapidly turn downward, to locally isotropic distributions (marked by diagonal crosses at the bottom). Unfortunately no simulations were done with λ between 0 and 0.5: perhaps at some critical coupling a bifurcation of the trajectories happens, separating those who proceed toward the new and the equilibrium fixed points. Yet the issue is rather academic, since the realistic relevant coupling value $\alpha_s = g^2/4\pi \approx 0.3$ corresponds to 't Hooft coupling constant $\lambda = \alpha_s N_c 4\pi \approx 10$, which is the *largest* value shown in this figure (bottom right). The corresponding curve rapidly approaches the equilibrium point, with coordinates (1,1) at this figure.

B. From glasma to hydro

The weak coupling cascades discussed above predict highly anisotropic pressure $p_l \ll p_\perp$. The question is about the time during which this feature persists, before the viscous hydrodynamics becomes valid. Recent research focused on a "hydrodynamization", a convergence of the stress tensor calculated using GLASMA or parton cascade simulations to a form appropriate for hydrodynamics. In other words, the issue is the relaxation mechanism/time of the non-hydrodynamical modes, see e.g. discussion by (Keegan *et al.*, 2016). Perturbative parton cascades propose time of several fm/c, while strong coupling approaches like AdS/QCD suggest an order of magnitude shorter time, around 0.5 fm/c.

To know which value is the case one needs to do more calculations using both approaches, especially those which can be directly compared to the data. Surprisingly, there is very little discussion of how to measure "the anisotropy time" in experiment.

One particular suggestion of the author, via dilepton polarization, will be discussed in section IX.C.

Since the longitudinal pressure p_l changes most, one can perhaps study the effect of the longitudinal pressure on the rapidity distribution. Historically, the original papers of Landau had focused on the longitudinal expansion. But Landau's initial condition – the instantaneous stopping – is rather unrealistic in QCD. To quantify a realistic initial rapidity distribution, from PDFs or GLASMA theory, is still to be done.

Since the beginning of RHIC era, the time of "hydrodynamization" has been empirically derived from a comparison to data on the radial and especially the elliptic flows. It has been shown, see e.g. (Molnar and Huovinen, 2005), that the parton cascades tend to effectively dissipate anisotropies needed for the elliptic flows. This is especially true for high $p_\perp \sim 3\,GeV$ and peripheral collisions. Even for rather extreme values of the parton cross section, a cascade and hydrodynamical evolution diverge at rather early time (Molnar and Huovinen, 2005). Current round of studies based on parton cascades and

kinetic equations need to address these issues directly.

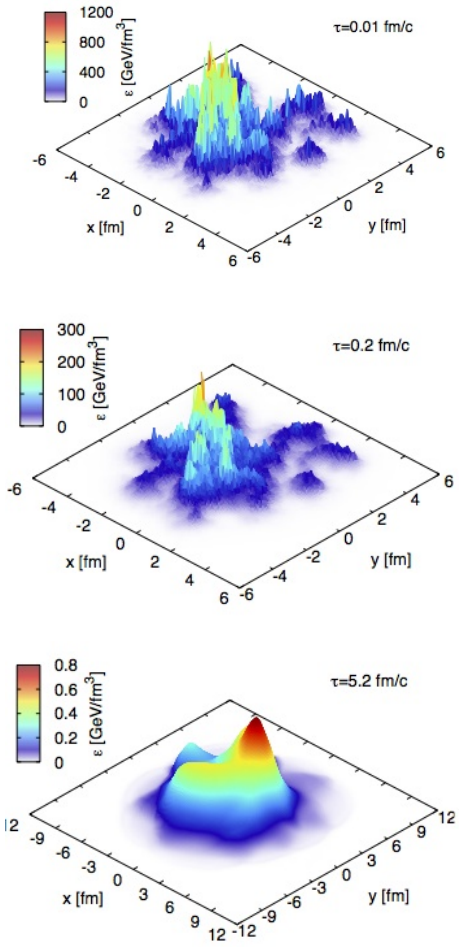

FIG. 36 From (Schenke and Venugopalan, 2014): Transverse energy profile from the IP glasma model for a semi-peripheral (b = 8 fm) Au+Au collision at s = 200 A GeV, at times τ = 0.01, 0.2, and 5.2 fm/c. From τ= 0.01 fm/c to 0.2 fm/c the fireball evolves out of equilibrium according to the Glasma model.

Fig.36 illustrates what is done in the impact parameter (IP) glasma approach. An important feature of glasma is independent fluctuations of color in different cells, which seeds the harmonic flows. At certain proper time – 0.2 fm/c in this example – glasma evolution is stopped and the stress tensor is matched to that of ideal fluid. For technical reasons the value of the viscous tensor is put to zero. How important is the selected time 0.2 fm/c ? Note that the second picture is hardly different from the first, except the overall scale of the energy density is reduced. Indeed, 0.2 fm is small distance relative to the nuclear size, and all one finds at this time is dilution due to longitudinal stretching. By starting hydrodynamics right from the second picture Schenke and collaborators implicitly assume that hydrodynamics cells can indeed be

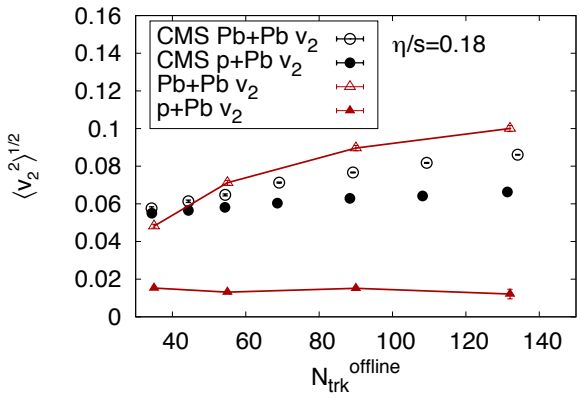

FIG. 37 (Color online) Multiplicity dependence of the root-mean-square elliptic flow coefficient v2 in Pb+Pb (open symbols) and p+Pb collisions (filled symbols) from the IP-Glasma+music model (connected triangles) (Schenke and Venugopalan, 2014) compared to experimental data by the CMS collaboration.

as small as 0.2 fm, and that their code can cope with huge gradients between the cells. (Typically hydrodynamics starts at few times later time, 0.6 fm/c or more.)

Following the evolution to the bottom figure, at time 5.2 fm/c, one finds it to be very different. The original bumps has disappeared and instead a new one at another location is formed. Indeed, sound perturbations cannot stand still and must move with a speed of sound. At intersections of "sound circles" from the primary bumps random enhancements of the density are observed. Yet since the bumps are statistically uncorrelated, those should get averaged out, at least in 2-particle correlations, and only correlations from the same circle will stay.

How many harmonics are needed to describe pictures like that shown in Fig.36 ? Taking 0.2 fm as a resolution and 4 fm as the fireball size, one finds that the upper picture requires about 20*20=400 pixels to be represented by certain stress tensor components. At the freezeout there are only several angular harmonics observed, so 99% of the information shown in those pictures does not survive till the freezeout. In the hydrodynamic simulation just described those disappear predictably, via viscous damping. It is possible that these systematics will fail at shorter wavelengths: so it is worth trying to measure higher harmonics. Other ways to observe density waves can perhaps be invented: one of such is potential observation of those in the dileptons, to be discussed below.

C. The initial state and angular correlations

The role of the initial state is greater for "small systems". When a nucleon is going along the diameter of large-A nucleus the mean number of participant nucleons is

$$< N_p >= n_0 \sigma_{NN} 2R_A \tag{40}$$

so for pPb at LHC one gets $< N_p > \approx 16$.

The question however is, where exactly in the transverse plane the deposited energy is located?

In Fig.39 we sketched two opposite models of the initial state. In (a) we show each of the N_p participants represented by N_g gluons (ignoring sea quarks and antiquarks) from their PDFs each, so the total number of partons $N_p N_g$. We assume that these gluons are randomly distributed in a spot of the size of the pp cross section. In (b) we show an alternative picture, the stringy Pomerons, in which there are no gluons but $2N_p$ QCD strings instead. Since those are "cold" (unexcited), they are shown by straight lines.

Let us estimate the deformation of the initial state in central collisions, for which there are no geometrical effects and all deformations come from the fluctuations. As discussed above, for all n one expects the same magnitude

$$\epsilon_n \sim \frac{1}{\sqrt{N}} \tag{41}$$

where $N = N_p N_g$ for (a) and $N = N_p$ for (b). Evaluating N_g from PDF's at LHC energy includes integration from $x_{min} \sim 10^{-3}$ to 1: one gets roughly the ratio

$$\frac{\epsilon_n^{(b)}}{\epsilon_n^{(a)}} \sim \frac{1}{\sqrt{N_g}} \sim 4 \tag{42}$$

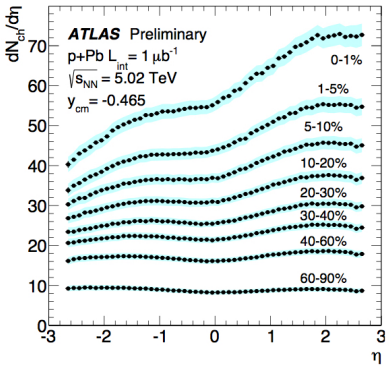

FIG. 38 Rapidity distribution in pPb collisions for different centrality classes, from "Measurement of the centrality dependence of the charged particle pseudorapidity distribution in proton-lead collisions", ATLAS-CONF-2013-096, https://cds.cern.ch/record/1599773 .

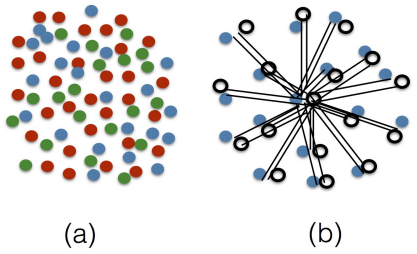

FIG. 39 Sketch of the initial state in central pA collisions. The plot (a) corresponds to IP-glasma model, with colored circles representing multiple gluons. Fig.(b) is for $N_p = 16$ Pomerons, each represented by a pair of cold strings. The open circles are quarks and filled blue circles are diquarks.

The elliptic and triangular flows in (very peripheral) AA and central pA studied by (Schenke and Venugopalan, 2014) demonstrated that the (IP)-glasma model does a very good job for the former case, but strongly underpredicts fluctuations in the latter case, see Fig. 37.

As we already discussed above, in the peripheral AA ϵ_2 is large, O(1), in any model, and in order to get the right v_2 one has to have the correct viscosity – which apparently these authors have. The central pA is indeed the test case: we argued above that the density is not yet large enough to apply the IP-glasma model, while the stringy Pomeron model should be applicable instead. If so, using (42) we should increase the v_2 by a factor of 4, which brings it to an agreement with the CMS measurements. We thus conclude that the stringy model Fig.39(b) is preferable over the picture (a), the uncorrelated gluons.

Above, we simplistically assumed a Glauber picture in which each wounded nucleon (or a participant) interacts with the projectile proton by a single Pomeron. Note that one gluon exchange generates (at least) *two* strings. If strings be simply stretched longitudinally, till they fragment independently, the rapidity distributions would be flat (rapidity independent) for all centrality classes. This is not the case, as is seen in ATLAS data shown in Fig.38. As one can see, the peripheral bins have flat rapidity distribution: few strings are produced, and those are extended through all rapidities. Yet central bins for pPb have rather asymmetric distributions, with larger multiplicity at the Pb side.

In the Pomeron language, this is explained by the "fan diagrams", in which one Pomeron can split into two. The "triple Pomeron vertex" is, however small, preventing development of extensive "Pomeron cascades". The multiplicity difference between the r.h.s. and the l.h.s. of the plot is not too dramatic, it certainly is not proportional to N_p scaling. For example, for the most commonly used centrality bin 1-5% the rapidity density $dn_{ch}/d\eta$ changes from about 35 to 55, across the rapidity interval shown in

this figure. If on the Pb end there are say $N_s > 2N_p \approx 40$ strings, then on the p end there are not one or few, but approximately 20 strings. Since the area on the l.h.s. is reduced by an order of magnitude or so, and the number only by factor 2, it is by far more dense system than the r.h.s.! One may further asks if flows, and development of collectivity, do depend on rapidity. So far we do not see any evidences for that. For example, the famous v_2 "ridge" is rapidity-independent.

Finally, briefly about the case of high multiplicity pp collisions. We do not yet know ϵ_n in this case. Theoretical predictions for pp cover the whole range: from elongated transverse string (Bjorken *et al.*, 2013) predicting large $\epsilon_2 \sim 1$ to a IP-glasma or "string ball" picture (Kalaydzhyan and Shuryak, 2014c) which predicts very small ϵ_2 instead. Experiment does give v_2, v_3 for 2 particle correlations, but 4,6 particle correlators are still beyond the reach for statistical reasons.

D. Multi-string dynamics

A version of the initial state theory, alternative to glasma picture at high density, is the old Lund model, represented by event generators such as PYTHIA. It is supposed to be applicable for lower matter density, remaining in the confined phase. Multiple color charges, moving relativistically from each other after collisions, are connected by multiple QCD strings. As they are rapidly stretched longitudinally, the strings become nearly parallel to each other.

Note that in both GLASMA and string pictures the color fields have similar longitudinal structure: one difference though is that GLASMA also have longitudinal magnetic fields. GLASMA state dynamics leads to interesting oscillations shown in Fig.40 from (Florkowski and Ryblewski, 2014): we will return to its analog in the string model using holography later. predicted, see

Transition between the two pictures –GLASMA and a

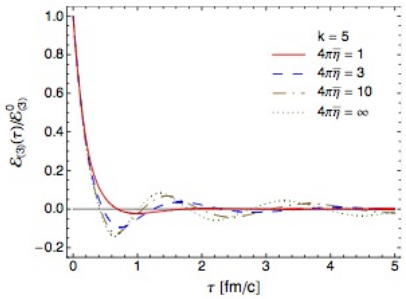

FIG. 40 Oscillation of the energy density in simulations starting from "glasma"-like initial conditions. $k = 5$ is the number of fluxes through the flux tubes, from (Florkowski and Ryblewski, 2014) .

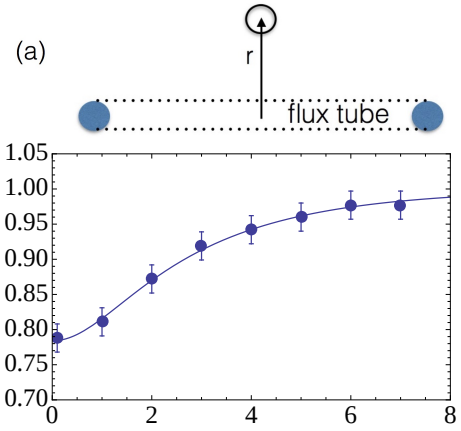

FIG. 41 (Color online). (a) Static quark-antiquark pair are indicated by shaded circles: those are connected by the flux tube (QCD string). At distance r from the tube the local value of the quark condensate $\bar{q}q(r)$ is measured. (b) Normalized chiral condensate as a function of the coordinate r transverse to the QCD string (in lattice units). Points are from the lattice calculation (Iritani *et al.*, 2014). The curve is the expression (44) with $C = 0.26$, $s_{string} = 0.176\,\text{fm}$.

multi-string state to be called a "spaghetti" – is expected when the string diluteness parameter become of the order 1, so they can no longer be separated. This is expected to happen at

$$\frac{N_{string}}{Area} \sim \frac{1}{\pi r_{string}^2} \sim 10\, fm^{-2} \tag{43}$$

where in the numerical value we use the field radius in the string $r_s \approx 0.17\, fm \sim 1\, GeV^{-1}$ from lattice measurements.

Collective interaction between the QCD strings in a "spaghetti state" has been studied by (Kalaydzhyan and Shuryak, 2014c). Analysis of the lattice data made there confirmed that the string interaction at large distances is mediated by the lightest scalar σ, similar to long-distance forces between nucleons. Specifically, the shape of the quark condensate around the string is well described by

$$\frac{\langle \bar{q}q(r_\perp) W\rangle}{\langle W\rangle \langle \bar{q}q\rangle} = 1 - CK_0(m_\sigma \tilde{r}_\perp)\,, \tag{44}$$

(where K_0 is the modified Bessel function and the "regularized" transverse distance $\tilde{r}_\perp$ is

$$\tilde{r}_\perp = \sqrt{r_\perp^2 + s_{string}^2}\,, \tag{45}$$

which regulates the Coulomb singularity $\sim \ln(r_\perp)$ at small $r_\perp$), see Fig. 41. The sigma mass value used is $m_\sigma = 600$ MeV.

Since the strings are almost parallel to each other, the problem is reduced to the set of point particles in a 2d plane with the 2d Yukawa interaction. From the fit (44)

one can see (Kalaydzhyan and Shuryak, 2014c), that the main parameter of the string-string interaction (in string tension units) is numerically small,

$$g_N\sigma_T = \frac{\langle\sigma\rangle^2 C^2}{4\sigma_T} \ll 1\,, \tag{46}$$

typically in the range $10^{-1} - 10^{-2}$. Therefore it was correctly neglected in the situations, for which the Lund model has been originally invented – when only $\mathcal{O}(1)$ strings are created.

Collective interaction plays a role when this smallness can be compensated by a large number of strings. As seen from Fig. 41, a magnitude of the quark condensate $\sigma = |\langle\bar{q}q\rangle|$ at the string position is suppressed by about 20% of its vacuum value. So, in a "spaghetti" state one should think of the quark condensate suppression of about 0.2 times the diluteness, which is still less than 1.

On the other hand, about 5 overlapping strings would be enough to eliminate the condensate and restore the chiral symmetry. If $N_s > 30$ strings implode into an area several times smaller than σ_{in}, then the chiral condensate will be eliminated inside a larger region of 1 fm in radius, or about 3 fm^2 in area. This is nothing but a hot QGP fireball.

As discussed above, the strings can be viewed as a 2D gas of particles (in transverse plane) with unit masses at positions $\vec{r}_i$. The forces between them are given by the derivative of the energy (44), and so

$$\ddot{\vec{r}}_i = \vec{f}_{ij} = \frac{\vec{r}_{ij}}{\tilde{r}_{ij}}(g_N\sigma_T)m_\sigma 2K_1(m_\sigma\tilde{r}_{ij}) \tag{47}$$

with $\vec{r}_{ij} = \vec{r}_j - \vec{r}_i$ and "regularized" $\tilde{r}$ (45). In the simulations a classical molecular dynamics code was used.

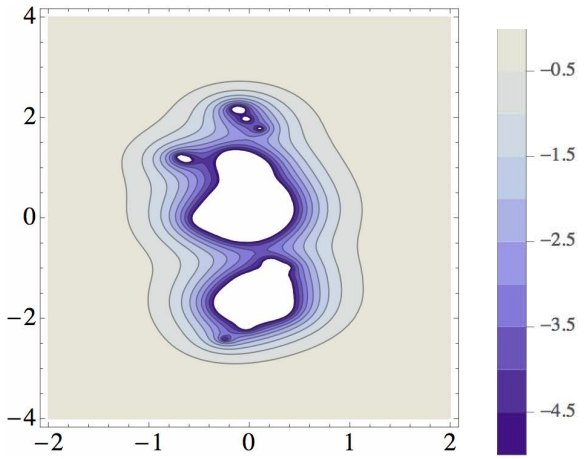

FIG. 42 (Color online) Instantaneous collective potential in units $2g_N\sigma_T$ for an AA configuration with $b = 11$ fm, $g_N\sigma_T = 0.2$, $N_s = 50$ at the moment of time $\tau = 1\,\mathrm{fm}/c$. White regions correspond to the chirally restored phase.

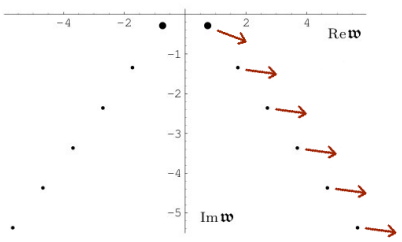

FIG. 43 A set of frequency modes, on ω complex plane, from (Kovtun and Starinets, 2005). Dots are for a particular wave vector k, arrows indicate the direction of motion as k increases.

The evolution consists of two qualitatively distinct parts: (i) early implosion, which converts potential energy into the kinetic one, which has its peak when fraction of the particles "gravitationally collapse" into a tight cluster; and (ii) subsequent approach to a "mini-galaxy" in virtual quasi-equilibrium. Only the first one is physical, as the imploded spaghetti has density sufficient for production of QGP fireball, and after that explodes hydrodynamically. The whole scenario thus resembles the supernovae: an implosion, leading to a more violent explosion later.

In Fig. 42 we show an example of the instantaneous collective potential produced by the strings in the transverse plane. The white regions correspond to the values of potential smaller than $-5\cdot 2g_N\sigma_T(\mathrm{fm}^{-1}) \approx -400\,MeV$, i.e. the chiral symmetry can be completely restored in those regions. A sufficiently strong gradient of this potential can cause quark pair production, similar to Schwinger process in an electric field. One particle may fall into the well and another may fly away, a phenomenon analogous to Hawking radiation near the black hole.

VII. HOLOGRAPHIC EQUILIBRATION

A. Near equilibrium

The holographic equilibrium setting includes the so called "AdS-black hole" metric, with its horizon located at the 5-th coordinate $z_h = 1/\pi T$, so the gauge theory – located at the $z = 0$ boundary feels the Hawking radiation temperature T[21].

Gravity waves propagating in the AdS background metric have certain dispersion relations $\omega(\vec{k})$ with cal-

[21] Some readers may be confused by the known fact, that Hawking radiation leads to evaporation of black holes (BH). Indeed, one BH, placed in asymptotically flat background, cannot heat up an infinite Universe, and it does evaporate. But the AdS metric is basically a finite box, and in this case BH can be in static equilibrium state with the "heated" Universe.

culable real and imaginary parts, an example is shown in Fig.43. Such quasinormal[22] modes are known for various examples of BHs for a long time, these particular ones were calculated by (Kovtun and Starinets, 2005) . In this channel, the lowest eigenvalue, shown by larger dots, is close to the origin and describes the sound mode. For reference we mention several known terms at small k (from (Lublinsky and Shuryak, 2009))

$$\frac{\omega}{2\pi T} = \pm\frac{\tilde{k}}{\sqrt{3}}\left[1+\left(\frac{1}{2}-\frac{\ln 2}{3}\right)\tilde{k}^2 - 0.088\,\tilde{k}^4\right] - \frac{i\tilde{k}^2}{3}\left[1-\frac{4-8\ln 2+\ln^2 2}{12}\,\tilde{k}^2 - 0.15\,\tilde{k}^4\right], \qquad (48)$$

where $\tilde{k} \equiv (k/2\pi T)$. First, note that at small k the imaginary viscous term is very small[23] $Im\omega \sim k^2$. Second, the dispersive correction to the speed of sound – the k^2 term in the first square brackets – has positive coefficient. Thus AdS/CFT predicts that one sound wave can decay into two. Third: note that higher order corrections to viscosity are both negative. This is in contrast to some popular second order ad hoc schemes such as Israel-Stuart.

All other "non-hydrodynamical" modes have large $Im(\omega)/(2\pi T) = O(1)$. During time of the order of $z_h \sim 1/(2\pi T)$ they all disappear since they "fall into the black hole"[24] . The essence of the AdS explanation for the rapid equilibration is thus simple: any objects (non-hydro modes) become invisible as they are absorbed by the black hole. The only[25] remaining memory is their total mass, which BH transforms into the appropriate amount of Bekenstein entropy.

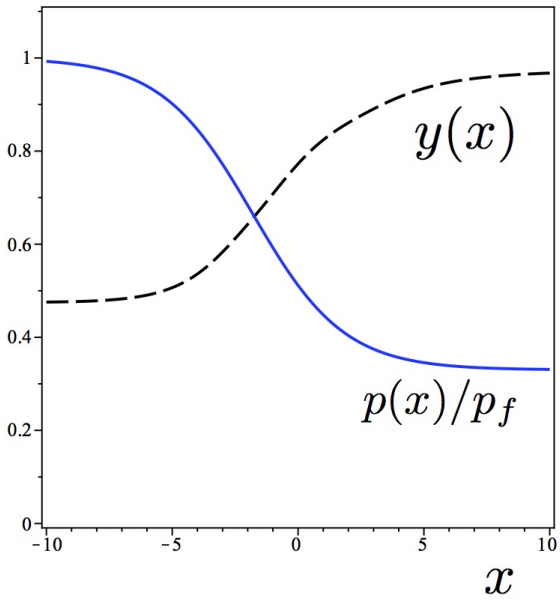

FIG. 44 (From (Shuryak, 2012b).) Profile of a strong shock in QGP in its rest frame, according to the Navier-Stokes hydrodynamics, as a function of the coordinate normal to the shock front. The time goes right to left, so the left-hand side shows the final values of the observables, while the right-hand side shows the initial ones. The pressure, shown by the (blue) solid line, is in units of its asymptotic value: thus the curve jumps to 1 on the left side. The flow rapidity, shown by the (black) dashed line, is reduced. The process is thus rapid formation of hotter denser QGP by influx of cooler and more dilute one.

B. Out of equilibrium 1: the shocks

Shocks are the classic examples of out-of-equilibrium phenomena. They traditionally are divided into two categories: weak and strong. In the former case the difference between matter before and after the shock is small. Weak shock can be treated hydrodynamically, e.g. using the Navier- Stokes (NS) approximation. Strong shocks have finite jumps in matter properties. Their profiles have large gradients: so one needs some more powerful means to solve the problem, not relying on hydrodynamics, which is just an expansion in gradients.

The reason we put this example as number one is because it is the only one which can be considered in *stationary approximation*. Indeed, in the frame which moves with the velocity of the shock, its profile is *time-independent*.

Strong shocks in AdS/CFT setting were discussed by (Shuryak, 2012b). An example with the Navier-Stokes profile is shown in Fig.44. Fluxes of the total energy and momentum are tuned to be the same, from the left to the right side of the picture. One may think of it as a low-density QGP entering on the right with higher rapidly, gets suddenly excited into a higher density QGP, floating out more slowly. It resembles a picture seen from a cockpit of a supersonic jet.

In the AdS/CFT setting, one can solve the problem from the first principles, by solving the Einstein equations. Since the setting has an extra holographic dimension z, even static solution depends not on one but on two variables: the longitudinal coordinate x and z. Not going into details, the surprising conclusion was that all corrections the Navier-Stokes profile of the shock happen to be small, at a scale of few percent, even without any apparent small parameter in the problem.

[22] Like wave functions of the α-decaying nuclei, when energy is complex the wave function grows in space and is not normalizable– thus the name. In nuclear physics there are called quasistationary states.

[23] We used that fact above, in the section on the "acoustic damping" phenomenology.

[24] It is amusing to note that a puzzling process of QGP equilibration is, in the AdS/CFT setting, simply "problem number one" in physics, the Galilean stones falling in gravity field.

[25] Plus all conserved charges, if they are there.

(Another tool used to correct the NS solution was the so called "re-summed hydrodynamics" (Lublinsky and Shuryak, 2009): it also lead to corrections at the percent level. Unfortunately, the accuracy I had on AdS/CFT solution was insufficient to tell whether both agree or not.)

The lesson is that all higher order gradient corrections to the NS solution have strong tendency to cancel each other.

C. Out of equilibrium 2: the falling shell

This setting of a falling matter shell was proposed by (Lin and Shuryak, 2008b). It is in a way complementary to the previous one: there is dependence on time t but no dependence on space x because the shell's motion occurs along the holographic 5-th direction z.

The physical meaning of this motion is as follows. First of all, recall that the 5-th coordinate $z = 1/r$ corresponds to a momentum "scale". Small values near the boundary (large r) corresponding to the UV end of the scales, while large z, small r corresponds to the IR or small momenta. Since everything happens much quicker in the UV as compared to IR, the equilibration process naturally proceeds from UV to IR, also known as "top-down" equilibration. The gravity force in the AdS is directed accordingly.

One can imagine that this process can in some sense be reduced to a thin "equilibration shock wave", propagating in the z direction. The key idea of the paper (Lin and Shuryak, 2008b) was that this shock can be thought of as a certain external objects – a shell or an elastic membrane – falling *under its own weight*. (See the sketch in Fig.45(a)). If this is the case, the total energy of the membrane is *conserved* (potential energy goes into kinetic). The consequences of this are very important: while the shell is falling toward the AdS center, the metric – both above and below the membrane – is actually time independent, as it depends only on its total mass. So there is no need to solve the Einstein equations[26]. In the case of an extreme black hole at the AdS center (the blue dot in Fig.45(a)) the solution consists of (i) thermal Schwarzschield-AdS metric above the shell and (ii) "empty vacuum" or the AdS_5 solution below it.

The only equation that needs to be solved are those describing motion of the shell itself, $r(t) = 1/z(t)$. It is not so trivial to derive, since the coordinates used below and and above the shell are discontinuous. Fortunately, a thin shell collapse has already been solved in the general relativity: in literature it is the so called "Israel junction" condition. The shell equation of motion in time of the distant observer t is given by

$$\frac{dz}{dt} = \frac{\dot{z}}{\dot{t}} = \frac{f\sqrt{(\frac{\kappa_5^2 p}{6})^2 + (\frac{3}{2\kappa_5^2 p})^2(1-f)^2 - \frac{1+f}{2}}}{\frac{\kappa_5^2 p}{6} + \frac{3}{2\kappa_5^2 p}(1-f)} \tag{49}$$

where $\kappa_5^2 p$ is the product of the 5-dim gravity constant and the shell elastic constant, and $f = 1 - z^4/z_h^4$ is the standard BH function of the thermal AdS background.

The shell starts falling with zero velocity from certain hight, and then gets accelerated to nearly speed of light. Finally, near the horizon position $z \to z_h$ there appears a "braking phenomenon": the shell slows down to velocity zero. This breaking is standard feature stemming from the use of the distant observer time, familiar from Schwarzschiled metric.

After solution is found, one can calculate what different observers at the boundary – that is, in the gauge theory – will see. In particular, one may ask if/how such an observer can tell a static black hole (the thermal state with stationary horizon) from that with a falling shell?

A *"one-point observer"* O_1 Fig.45(b) would simply see stress tensor perturbation induced a gravitational propagator indicated by the red dashed line. Since the metric above the shell is thermal-AdS, such observer will see the *time-independent* temperature, pressure and energy density, corresponding to static final equilibrium. Yet more sophisticated *"two-point observers"* O_2, O_3 can measure certain correlation functions of the stress tensors. They will see contributions both from gravity waves propagating along the line shown by the solid line above the shell, that is in the thermal metrics, as well as from waves propagating along the path shown by the dashed line which penetrate *below* the shell: those would notice deviations from equilibrium. Solving for various two-point

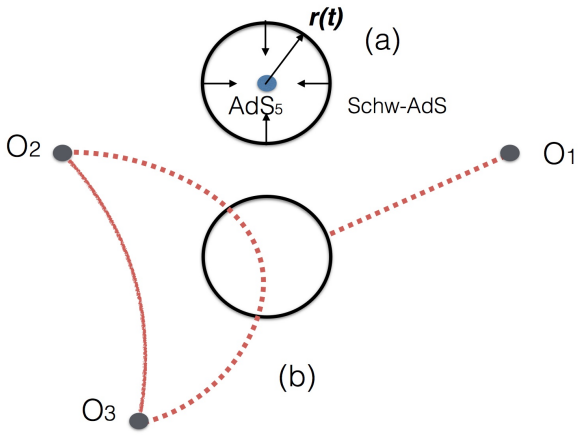

FIG. 45 (a) A sketch of a falling shell geometry. Its radius $r(t) = 1/z(t)$ which is used in the text. (b) Single-point observer O_1 and the two-point observers O_2, O_3

[26] It is instructive to recall the Newton's proof that a massive sphere has the outside field the same as a point mass, and that there is no gravity inside the sphere. This is also true if the sphere is falling. It also remains true in general relativity.

functions in the background with falling shell/membrane we found these deviations. They happen to be oscillating as a function of the wave frequency. This observation, first puzzling, is explained (Lin and Shuryak, 2008b) by finite "echo" times due to a signal reflected from the shell. So, one can experimentally observe an echo, coming from the 5-th (non-existing) dimension!

For further discussion of the scenarios of top-down equilibration, with infalling scalar fields etc – the reader is referred to subsequent literature, e.g. (Balasubramanian *et al.*, 2011).

D. Out of equilibrium 3: anisotropic plasma

Our next example, due to Chesler and Yaffe, is a setting in which one starts with some *anisotropic* but homogeneous metric, and follows its relaxation to equilibrium, for summary see (Chesler and Yaffe, 2014). The metric is diagonal, with time dependent but space-independent components, the resulting Einstein equations are solved numerically.

Rapid relaxation to equilibrium thermal-AdS solution is observed. A number of initial states can be compared, selected with the same equilibrium energy density (or horizon, or T) at late time. While at early time the momentum asymmetry can be very large – say, an order of magnitude – it becomes exponentially small with time. Any deviations from equilibrium are strongly red-shifted as they approach the horizon.

There are no hydrodynamical modes since the setting is homogeneous. The lowest mode has frequency $\omega = (2.74 + i3.12)\pi T$. So, the strongly coupled QGP has the "isotropization time" is as short as

$$\tau_{isotropization} \sim \frac{0.1}{T} \tag{50}$$

E. Out of equilibrium 4: rapidity independent collisions

The picture of "debris" created in the bulk after a high energy collision, forming a small black hole falling toward the AdS center (Shuryak *et al.*, 2007) related the exploding/cooling fireball in the real world to a hologram of the black hole horizon moving away from the boundary. The specific solution discussed in that paper was spherically symmetric, and thus more appropriate for cosmology than for heavy ion applications.

A more appropriate setting with "falling" horizons, corresponding to the Bjorken hydro solution (see Appendix) was developed by (Janik and Peschanski, 2006) . In this case, the horizon is rapidity independent and has time-dependent location $z_h(\tau)$. At late time The solution of Einstein equation reproduces Bjorken hydro, because

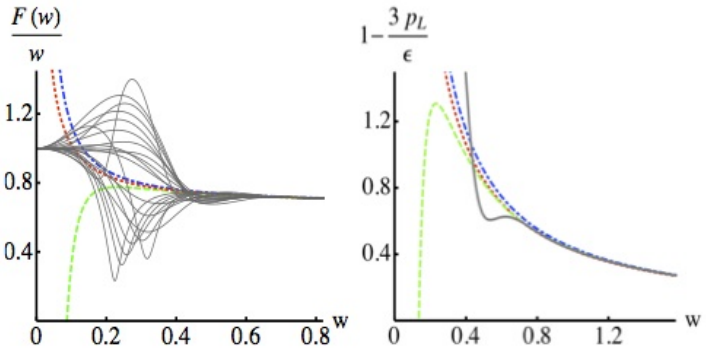

FIG. 46 (left) From (Heller *et al.*, 2012): The temperature evolution combination $dlog(w)/dlog\tau$ for different initial conditions (black thin curves) converging into a universal function of $w = T\tau$, compared to hydro. (right) The pressure anisotropy for one of the evolutions compared to 1-st (NS), 2-nd and 3-ed order hydrodynamics.

at $\tau \to \infty$

$$z_h(\tau) = 1/\pi T(\tau) \sim \tau^{1/3} \tag{51}$$

The variable $w = T\tau$ has the meaning of the macro-to-micro scale ratio. At late time $\tau \to \infty$ it grows, indicating that the system becomes more macroscopic and hydrodynamics becomes more accurate. The question is when exactly the hydrodynamical description becomes valid and *with what accuracy*.

Fig.46 from (Heller *et al.*, 2012) shows the time evolutions of many initial states, all approaching the same hydrodynamical solution. Fig.46(left) shows that this happens via convergence to certain *universal function* of the variable $w = \tau\, T$ defined by

$$\frac{dw}{d\ln\tau} \;=\; F(w)\,, \tag{52}$$

Existence of such universality is the essence of the "resummed hydro" (Lublinsky and Shuryak, 2009). Depending on the required degree of accuracy, one may assign a specific initial value of w at which the "hydrodynamics starts", in the range $w_i = 0.4..-0.6$. The plot on the right demonstrates that at such time the anisotropy is still large and viscosity is important.

The lesson from this work can be better explained by comparing its result to naive expectations, that hydrodynamics starts when macro and micro times are the same, $w = \tau T > 1$, and that the accuracy of hydrodynamics should be bad, O(100%). Calculations show instead that at *twice smaller* time $w \sim 1/2$ the accuracy of (the lowest-order Navier-Stokes) hydro suddenly becomes quite good, to a few percent!

Why is it so? While gradients are not yet small at that time, the combined effect of all of them is. Lublinsky-Shuryak re-summation provides an answer: the higher

gradient series has alternating signs, it can be Pade resummed a la a geometric series to a decreasing function.

The issue has its practical aspect, related to one of the first observations made at the first LHC $PbPb$ run. It was found that the (charged hadron) multiplicity in $PbPb$ collisions grow with energy a bit more rapidly than in pp :

$$\frac{dN^{PbPb}}{dy}(y=0,s)\sim s^{0.15} \qquad \frac{dN^{pp}}{dy}(y=0,s)\sim s^{0.11} \tag{53}$$

From the RHIC energy ($E=0.2\,TeV$) to the LHC, the double ratio

$$\frac{\frac{dN}{d\eta}|_{PbPb,LHC}\ /\ \frac{dN}{d\eta}|_{pp,LHC}}{\frac{dN}{d\eta}|_{AuAu,RHIC}\ /\ \frac{dN}{d\eta}|_{pp,RHIC}}=1.23\,. \tag{54}$$

shows a noticeable change with the energy, which calls for an explanation.

A simple form for the function $F(w)$ was proposed by (Lublinsky and Shuryak, 2011) . If known, one can calculate the entropy produced, from the time w_i on: it turns out to be about 30%. Furthermore, we get the following expression for the contribution to this double ratio $\approx 1+\frac{3[\bar\eta(LHC)-\bar\eta(RHIC)]}{2w_i+3\bar\eta(RHIC)}$ and show, that the observed growth can be naturally explained by the viscosity growth, from RHIC to LHC, predicted by a number of phenomenological models.

VIII. COLLISIONS IN HOLOGRAPHY

A. "Trapped surfaces" and the entropy production

The simplest geometry to consider is the wall-on-wall collisions, in which there is no dependence on the wo transverse coordinates, and only the remaining three – time, longitudinal (rapidity), and the holographic direction – remain in play. Needless to say, it is a very formidable problem, solved by Chasler and Yaffe via clever "nesting" of Einstein equations. The reader can find explanations in (Chesler and Yaffe, 2014).

Collisions of finite size objects are even more difficult to solve, but those historically brought a discussion of the very important issues of *trapped surface* formation and the *entropy production*. It was pioneered by (Gubser *et al.*, 2008) who considered head-on (zero impact parameter) collisions of point black holes. The setting is shown in Fig.47(a).

"Trapped surface" is a technical substitute for the horizon – for this review it is not necessary to discuss the difference – and its appearance in the collision basically means that there exists a black hole inside it. Classically, all information trapped inside it cannot be observed from outside, and lost information is *entropy*. For known static black hole solutions this area does give the black hole Bekenstein entropy.

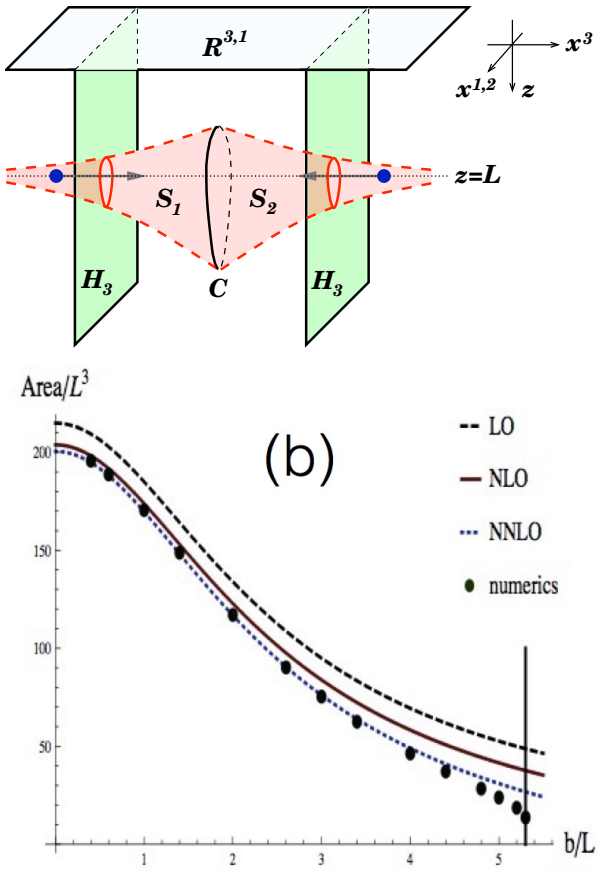

FIG. 47 (a) From (Gubser *et al.*, 2008):A projection of the marginally trapped surface onto a fixed time slice of the AdS geometry. (b) The area of the trapped surface versus impact parameter, with the comparison of the numerical studies (Lin and Shuryak, 2009) shown by points and analytic curves from (Gubser *et al.*, 2009). The vertical line shows location of the critical impact parameter b_c beyond which there is no trapped surface.

Locating this surface allows one to limit the produced entropy *from below*, by simply calculating *its area*. The reason why this entropy estimate is from below is because the trapped surface area is calculated at the *early* time $t=0$ of the collision, not at its end. No particle can get out from trapped surface, but some can get into it *during* the system's evolution, increasing the black hole mass and thus its entropy.

Gubser et al denote the distance separating colliding black hole from the boundary by L; we will discuss its physical meaning below. Naively, central collisions have only axial O(2) symmetry in the transverse plane $x_\perp$, but using global AdS coordinates these authors found a 'higher O(3) symmetry of the problem, which becomes manifest if a coordinate

$$q=\frac{\vec{x}_\perp^2+(z-L)^2}{4zL} \tag{55}$$

is used. It was shown that the 3-d trapped surface C

at the collision moment is in this coordinate a 3-sphere, with some radius q_c. If q_c is determined, the relation between the CM collision energy and Bekenstein entropy can be calculated.

For large q_c these expressions are

$$E \approx \frac{4L^2 q_c^3}{G_5}, \quad S \approx \frac{4\pi L^3 q_c^2}{G_5}, \tag{56}$$

from which, by eliminating q_c, one finds the main conclusion, the entropy grows with the collision energy as

$$S \sim E^{2/3} L^{5/3} \tag{57}$$

Note that this power is in general $(d-3)/(d-2)$, so it is directly related to the d=5, the dimension of AdS space. Note also that it is different from the 1950's prediction of Fermi/Landau who predicted $S \sim E^{1/2}$ as well as from the data, which according to (53) indicate the power of about 0.30.

Let us now return to the meaning of the parameter L. Gubser et al relate the "depth" of the colliding objects with the nuclear size, $L \sim 1/R_A$ which cannot depend on the energy. An alternative idea suggested by (Lin and Shuryak, 2009) ascribe L to the (inverse) "saturation scale", the typical parton's momenta in the wave function of the colliding objects. In this case it is related to the collision energy by

$$L \approx \frac{1}{Q_s(E)} \sim E^{-\alpha} \tag{58}$$

where $\alpha \approx 1/4$ is empirical index of the PDFs. It is especially clear if one would consider wall-on-wall collisions, in which the nuclear size R_A goes to infinity, while Q_s characterize the material of the wall made of, and remains fixed. L is not of the $O(10\,fm)$ scale, but rather two orders of magnitude smaller $O(0.1\,fm)$. Furthermore, it is expected to *decrease* with the energy $L \sim 1/Q_s(E)$. Including this modifies (57) to

$$S \sim E^{(2/3)-(5/3)\alpha} \sim E^{0.25} \tag{59}$$

which is in reasonable agreement with the observed multiplicity.

The generalization of this theory to non-central collisions (Lin and Shuryak, 2009) lead to the results shown in Fig.47(b). The figure is from (Gubser *et al.*, 2009), it shows the dependence of the trapped surface area on the impact parameter. Specifically, numerical results from (Lin and Shuryak, 2009) (points) are compared with the analytic series of curves (Gubser *et al.*, 2009), which are in excellent agreement.

From the gravity point of view the qualitative trend shown is clear: two colliding objects may merge into a common black hole only provided that the impact parameter is less than some critical value $b_c(E)$, depending on the collision energy. Indeed, with b rising, the trapped energy decreases while the total angular momentum increases, so at some point Kerr parameter exceeds 1 and thus no black hole can be formed. Interestingly, the calculation shows that it happens with a finite jump – a first order transition[27] as a function of the impact parameter.

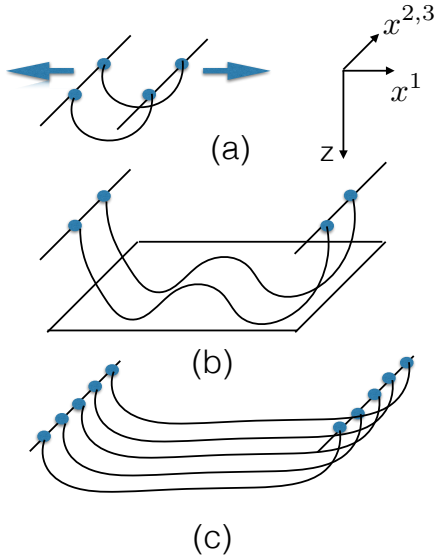

FIG. 48 (a) An early time snapshot of a pair of strings created after one color exchange. The coordinates are explained on the right: the colliding objects move with a speed of light away from each other and strings are stretched. (b) Later time snapshot, in AdS/QCD background. After strings reach the "levitation surface" – shown by a rectangular shape – they start to oscillate around it; (c) In case of high density of many strings they can be approximated by a continuous membrane.

Just a bit below critical value of the impact parameter, the trapped surface and black hole exist, and nothing indicates that at larger b none is formed. So, at $b < b_c$ a creation of QGP fireball happens, while for peripheral $b > b_c$ collisions the system remains in the hadronic phase . A jump in entropy as a function of impact parameter is rather surprising, but in fact the experimental multiplicity-per-participant plots do indeed show rapid change between non-QGP small systems and QGP-based not-too-peripheral AA collisions. It would be interesting to compare it with all available information on small systems, undergoing transition to explosive regime.

In the same paper (Lin and Shuryak, 2009) we pointed out that the simplest geometry of the the trapped surface would be that for a wall-wall collision, in which there is no dependence on transverse coordinates x^2, x^3. Thus a sphere becomes just two points in z, above and below the

[27] The first order transition stems from the large N_c approximation: this conclusion may perhaps may be modified at finite N_c. Furthermore, the problem of trapped surface in quantum gravity is way too complicated, not studied so far.

colliding bulk objects. We elaborated on this, considering collision of two infinite walls made of material with different "saturation scales" (Lin and Shuryak, 2011), and studied conditions for trapped surface formation.

B. From holographic to QCD strings

AdS/CFT is a duality with a string theory, so fundamental strings are naturally present in the bulk. Already the first calculation, made in Maldacena's original paper, the "modified Coulomb law", was based on the evaluation of the shape and total energy of a "pending string", sourced by "quarks" on the boundary.

Extension to non-static strings has been done in two papers (Lin and Shuryak, 2008a,c) . The first derived the shape of a falling string with ends moving away from each other with velocities $\pm v$, and the second calculating its hologram (stress tensor distribution) at the boundary. This study can be thought of as a strongly coupled version of the Ampere's law, with two currents rather than charges, or as a strongly coupled version of $e+e-$ annihilation into two quarks. The hologram showed a near-spherical explosion, historically an early indication that *there are no jets* at strong coupling.

These works used the setting associated with conformal gauge theory: in AdS_5 string falling continues forever. This is of course *not* what we observe in the real world, in which there is confinement and there are jets. Modern strong coupling models moved into what is collectively known as AdS/QCD , for review see e.g. (Gursoy and Kiritsis, 2008; Gursoy *et al.*, 2008). In contrast with the original AdS/CFT, the background metric is not conformally invariant and incorporates both $confinement$ in the IR and the *asymptotic freedom* in the UV. These models use additional scalar ("dilaton") field, which is also given a phenomenological potential depending on the 5-th coordinate.

In such settings, the bulk strings can "levitate" at some position z_*, at which the downward gravity force is compensated by the uplifting dilaton gradient. The hologram of such a levitating string at the boundary is *the QCD string*. Its tension, width and stress tensor distribution are all calculable. The potential between point charges is still given by a pending string. In the AdS/QCD background its energy changes from Coulombic potential at small r, to linear potential at large r, showing confinement. Furthermore, allowing fundamental fermions in the bulk – via certain brane constructions –and including their back reaction in a consistent manner, one can get the so called Veneziano limit of QCD $(N_c, N_f \to \infty, x = N_f/N_c = fixed)$ (Arean *et al.*, 2013).

Since in the UV these models also possess a weak coupling regime, one can also model perturbative glasma, by putting a certain density of color sources on the two planes, departing from each other. In such setting there would be smooth transition between two alternatives descriptions of the initial state we discussed above – from the perturbative glasma to a "spaghetti" made of the QCD strings. When time τ is small, Fig.48(a), strings are in the UV domain (at small distance $z \sim 1/Q_s$ from the boundary) their hologram is Coulombic or glasma-like. When strings fall further and reach the "levitation point" z^* they start oscillating around it (Iatrakis *et al.*, 2015a), Fig.48(b). This is very similar to oscillations discussed by Florkowski (see sect.VI.D) without AdS/QCD.

AdS/QCD predictions for string-string interaction were derived by (Iatrakis *et al.*, 2015a). We already discussed this issue in the QCD context above, concluding that its long-range attraction is dominated by the σ meson exchanges (just like between nucleons, in nuclear forces). The question is whether it is also the case in the AdS/QCD. AdS/QCD has very few fields in the bulk – gravitons, dilaton and (quark-related) "tachyon". Their quantization along the 5-th coordinate generate towers of 4-dimensional hadronic states. Hadronic masses are just quantized 5-th momentum. So, from this approach one can calculate not only the masses but also the *wave functions* in a scale space, as well as mixing between the fields. Specific issue studied by (Iatrakis *et al.*, 2015a) is the mechanism of hadronic flavorless scalars, which includes the σ and others. Without any changes in the setting of AdS/QCD we found very good description of (quite involved) mixing pattern of the scalars, which puzzled spectroscopists for decades. Since strings are gluonic objects and σ interact strongly with quarks, understanding of such mixing is crucial for obtaining realistic string-string forces.

Note that so far there is no temperature or entropy in the problem: the dynamics is given by classical mechanics of strings moving in certain backgrounds. If the number (or density) of strings becomes high enough, see Fig.48(c), one should include the back reaction of their gravity and dilaton field, or even include mutual attraction of strings. Such AdS/QCD version of multi-string dynamics (Iatrakis *et al.*, 2015b) is the holographic version of "spaghetti collapse", discussed in section VI.D following (Kalaydzhyan and Shuryak, 2014a). The bulk strings, if too many, does produce a gravitational collapse.

C. Holographic Pomeron

Description of hadronic cross sections and elastic amplitudes using Reggeons and Pomerons originates from the phenomenology, as well as from the celebrated Veneziano amplitudes. While originally derived following the resonance duality in different channels, a nearly forgotten pre-QCD ideology of 1960's, these expressions were historically very important, as they gave us the first hints on existence of QCD strings.

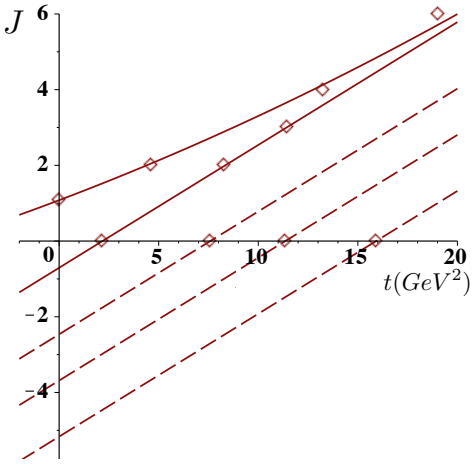

FIG. 49 Glueball masses calculated on the lattice (diamonds) organized in Regge trajectories (lines). (From (Shuryak and Zahed, 2014)).

The Pomeron is an effective object corresponding to the "leading" Regge trajectory $\alpha(t)$ which dominates the high energy asymptotics of the hadron-hadron cross sections. Fig.49 is a version of the Regge plot (angular momentum J versus the mass squared m^2) for glueballs. The Pomeron corresponds to scattering and thus has small non-physical mass $t<0$ and a non-integer J slightly above 1: the trajectory $\alpha(t)$ has of course physical states as well. It enters the elastic cross section in a form

$$\frac{d\sigma}{dt}\approx\left(\frac{s}{s_0}\right)^{\alpha(t)-1}\approx e^{\ln(s)[(\alpha(0)-1)+\alpha'(0)t]} \tag{60}$$

The two main parameters of the Pomeron have a very different origin. The intercept $\alpha(0)$ is a dimensionless index, describing the power with which the total cross section rises. Perturbative description of the Pomeron by Balitsky-Fadin-Kuraev-Lipatov (BFKL) (Kuraev *et al.*, 1977) provides perturbative $O(\alpha_s)$ value for it. The slope[28] $\alpha'(t=0)$ has dimension $[mass^{-2}]$ and is nonperturbative. Its value is related to the closed string tension $\alpha'\approx 1/(2\pi\sigma)$, roughly twice that of the slope observed in meson/baryon Reggeons, related to open strings.

So, the Pomeron phenomenology includes elements of perturbative and non-perturbative physics. To make less confusing, let us consider scattering as a function of the impact parameter b. For small color dipoles and small b the amplitude should be perturbative, due to gluon exchanges. At large $b\sim 1$ fm it should be non-perturbative: the model description of it is given in terms of a (double) string exchange.

[28] The "string scale" in the fundamental string theory is traditionally called α' still, as a historic remnant of QCD phenomenology left in it.

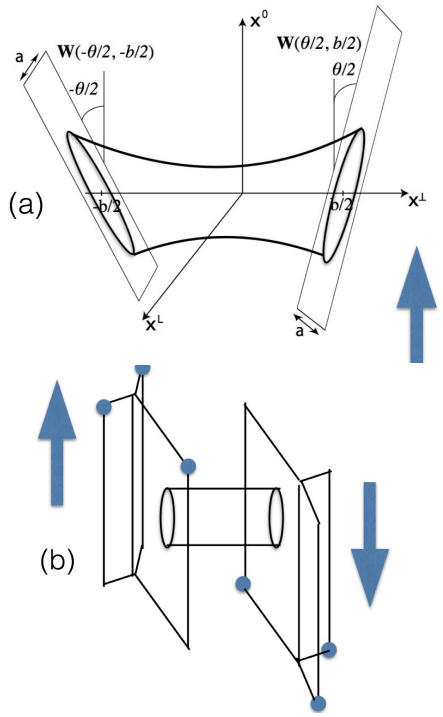

FIG. 50 (Color online) (a) Dipole-dipole scattering configuration in Euclidean space. The dipoles have size a and are b apart. The dipoles are tilted by $\pm\theta/2$ (Euclidean rapidity) in the longitudinal x_0x_L plane. (b) A sketch illustrating Pomeron exchange for baryon-baryon scattering: only one pair of quarks become "wounded quarks".

The holographic models collectively known as AdS/QCD combine strongly coupled regime in the IR (large values of the 5-th coordinate z) with weakly coupled regime in the UV, see (Gursoy and Kiritsis, 2008). The topic of this section, the "holographic Pomeron", includes in fact two different approaches to the Pomeron, which we discuss subsequently.

The first idea is to approximate the Pomeron properties via analytic continuations of the *bulk gravitons*. It may look exotic, but note that Regge trajectories are natural consequence of AdS/QCD models, and that the closest state to the Pomeron along the trajectory is $J^{PC}=2^{++}$ glueball, rather well described by these models. Recent application of the Hilbert-Einstein action to Pomeron-Pomeron-2^{++} glueball triple vertex successfully described the double diffractive production data which were puzzling for a long time, see (Iatrakis *et al.*, 2016). Even more recent are very successful applications of the tensor Pomeron for the desciption of RHIC polarized pp scattering, see (Ewerz *et al.*, 2016) and subsequent works.

We will however follow in more detail the second idea by (Basar *et al.*, 2012; Stoffers and Zahed, 2013), providing derivation of the Pomeron-induced scattering amplitude in a AdS/QCD, including both soft and hard

regimes, and thus providing interpolation between the "stringy" and the BFKL limits of the Pomeron. The semiclassical derivation of the Pomeron amplitude is given in terms of closed string production – similar to Schwinger pair production in an electric field. The string world-volume has the shape depicted in Fig.50(a): it is a "tube" connecting two flat strips, the world volume of propagating color dipoles. In Fig.50(b) we sketch a Pomeron in a collision of two nucleons, consisting of 3 quarks and 3 string, joined into a string junction. In this case a Pomeron tube "punctures" only one of the three surfaces. This produces one "wounded quark", as we discussed in connection to Tannenbaum's description of fluctuations.

Direct semiclassical derivation of the scattering amplitude (Basar *et al.*, 2012) is based on the Nambu-Goto action (the tube's area). Fig.50(a) indicate Euclidean setting in which difference in rapidity is represented by twisted angle θ between the propagation vectors of the two dipoles. Fig.50(b) illustrates a baryon-baryon scattering, in which the Pomeron tube can be connected to any of the available dipoles, explaining the concept of the "wounded quarks" we mentioned in section IV.B. More than one Pomeron means more tubes, perhaps connecting other quarks.

The classical action of this configuration provides the α' term, while the intercept $\alpha(0)-1$ is in this approach generated by the next order (one-loop) corrections due to string vibrations. The elastic amplitude squared can be cut in half, by the unitarity cut. The corresponding "tube" configurations, when cut longitudinally, provides two strings of certain length and shape. Those are two physical strings which "jumps from under the barrier" and appear in Minkowskian world. They should be used as the initial conditions for Minkowskian real-time evolution.

The same expression for the scattering amplitude has an alternative derivation from string diffusion equation, in the 5-d bulk. The 5-th coordinate in it has a meaning of the dipole size parameter, so motion in this coordinate is dual to DGLAP evolution. Scattering pp data as well as deep-inelastic *ep* (DESY data) are well reproduced by this model, see (Basar *et al.*, 2012).

It was further argued by (Shuryak and Zahed, 2014) that because the "tube" has a periodic variable resembling the Matsubara time, its fluctuations take the thermal form. Appearance of an effective temperature and entropy was a new aspect to the Pomeron problem: but once recognized the analogy to thermal strings can be exploited. It was argued that two known regimes of the Pomeron we already mentioned – long string exchange at large impact parameter b and perturbative gluon exchange at small b – should be joined by a third distinct regime, in which strings are highly excited due to the Hagedorn phenomenon. This is what happens near critical temperature in gluodynamic. The third regime is known as the mixed phase, between the confined and the deconfined phases.

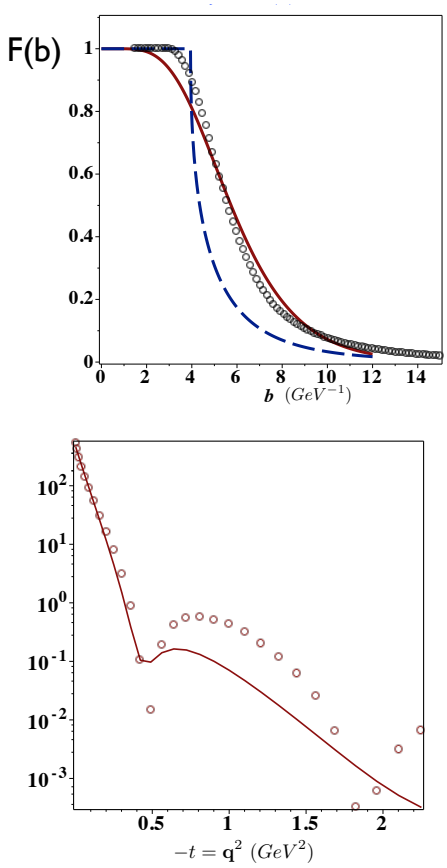

FIG. 51 (a) The solid line is the empirical LHC data parametrization. The dashed line is the shape corresponding to the "excited string" approximation for fixed sizes of the dipoles, while the circles correspond to the profile averaged over the fluctuating dipoles. (b) The corresponding elastic amplitude (the absolute value squared of the profile Bessel transform) as a function of the momentum transfer. Model prediction agrees with parameterization well at small t, up to the dip.

Fig.51(a) shows the elastic scattering profile, defined as the Fourier-Bessel transform of the imaginary part of the elastic amplitude. Shown by the dashed line is the prediction of the model with the basic first order transition occurring at fixed impact parameter, and fixed size of the colliding dipoles. The circles show a more realistic model, including averaging over certain distribution over the dipole sizes. The solid line is the empirical fit to the elastic scattering amplitude measured at he LHC. The difference between this empirical curve and the model (circles) is relatively small at plot (a), although it becomes more noticeable in plot (b) showing its Fourier-Bessel transform as a function of the momentum transfer Q. As one can see, beyond the minimum good agreement is lost. Apparently the "transition edge" in b predicted

by the first order transition model is a sharper than the corresponding change in the experimental data.

Brief summary: a decades-old Pomeron amplitude was finally derived, in a "stringy" AdS/QCD setting. Surprisingly, the Pomeron is related to thermally excited strings, with an effective temperature proportional to the inverse impact parameter. Rapid "phase transition" in scattering amplitude at some impact parameter, from nearly black disc to light gray, corresponds to the deconfinement transition. An intermediate regime corresponds to highly excited strings, known as "string-ball" regime. So far only the the elastic amplitude is calculated, die to tunneling (Euclidean) stage of the evolution. To work out subsequent evolution of the system, extending this theory to description of *inelastic* collisions, remains to be done.

D. Collisions at ultrahigh energies

Discussions about Pomeron regimes ultimately drive us to the old question: what happens at the ultrahigh energies, well above that of the LHC? The highest observed energies, by Pierre Auger Observatory and similar cosmic ray detectors, go until

$$E_{\rm lab} \lesssim E_{\rm max} \sim 10^{20}{\rm eV}\,. \tag{61}$$

where they are limited by the so-called Greisen-Zatsepin-Kuzmin (GZK) bound, due to their inelastic interaction with cosmic microwave background.

For comparison with the LHC, let us convert the laboratory energy into the center of mass frame, and use standard Mandelstam invariant. Assuming it is the *pp* collision, one finds

$$\sqrt{s_{\rm max}} = (2E_{\rm max}m_p)^{1/2} \approx 450\,{\rm TeV}\,. \tag{62}$$

While significantly higher than current LHC *pp* energy $\sqrt{s_{LHC}} = 8$ TeV, the jump to it from the LHC is comparable to that from the Tevatron $\sqrt{s} = 1$ TeV or RHIC $\sqrt{s_{RHIC}} = 0.5$ TeV. In view of smooth small-power s-dependence of many observables, the extrapolation to the LHC worked relatively well, and one might think that any further extrapolations may work as well. But, smooth extrapolations using standard event generators do *not* reproduce experimental data from the Pierre Auger collaboration.

Models aimed to resolved the contradiction were proposed. For example, (Farrar and Allen, 2013) suggested an exotic freezeout *without* chiral symmetry breaking, *without* multipion production. According to simulations presented in this work, if mostly nucleons are produced, the Pierre Auger data are explained.

A more modest (but still significant) change between LHC and the so called "ultrahigh" energies, has been proposed by (Kalaydzhyan and Shuryak, 2014b): at such energies $\sqrt{s_{\rm max}}$ even minimally biased *pp* collisions should be in the "explosive regime" we discussed above for central *pA* or rare ($P \sim 10^{-6}$) high multiplicity *pp* collisions at the LHC. This is simply caused by an increase in particle density dN/dy, by about factor 3. Another generic reason for this regime change is that both primary collisions and subsequent cascades in the Earth atmosphere have, as targets, light N, O nuclei. Furthermore, the projectiles themselves are also most likely are some mixture of nuclei, perhaps up to Fe.

Taking into account large *pp* cross section at ultra high energies, $\sim 150\,{\rm mb}$, one finds that its typical impact parameters $b \approx 2\,{\rm fm}$. Thus the range of the interaction in the transverse plane is comparable to the radius of the light nuclei (oxygen $R_O \approx 3\,{\rm fm}$) and therefore even in the *pO* collisions most of its 16 nucleons would become collision "participants". For light-light *AA* collisions like *OO* the number of participants changes from 32 (central) to zero. Accidentally, the average number of participants is comparable to the average number of participant nucleons $\langle N_p\rangle \approx 16$ in central *pPb* collisions at the LHC.

IX. ELECTROMAGNETIC PROBES

A. Brief summary

The sources of the dileptons are split into the following categories:
(i) instantaneous $\bar{q}q$ annihilation, known as the Drell-Yan partonic process;
(ii) $\bar{q}q$ annihilation at the pre-equilibrium stage, after the nuclei pass each other;
(iii) $\bar{q}q$ annihilation in the equilibrated sQGP ;
(iv) meson-meson annihilation at the (kinetically but not chemically) equilibrated hadronic stage;
(v) the so called "cocktail" contribution, consisting of leptonic decays of unstable secondaries. Electromagnetic and electroweak decays all occur long $after$ freezeout, so this component can be calculated from spectra and statistically subtracted. We will not discuss this component any longer.

The corresponding windows in the dilepton mass are, respectively: $M > 4GeV$ for (i), $1 < M < 3\,GeV$ for (iii) and $M < 1\,GeV$ for (iv). So the early stage dileptons mostly fall into the 3-4 GeV window[29].

Among the CERN SPS dilepton experiments the most successful was NA60, which quantified with the largest statistics the following phenomena:
(a) Large enhancement over the "cocktail" at dilepton masses $M < m_\rho$. The resulting spectral density of the

[29] This window of masses contains also prominent peaks due to $J/\psi, \psi', \psi''$ decays. Those, according to the definition used, belong to the "cocktail" one should also be subtracted.

electromagnetic current in QGP was quantitatively measured;
(b) By plotting the $p_\perp$ slope as a function of the dilepton mass M it was demonstrated that light ($M < 1\,GeV$) dileptons are produced when flow is fully developed, or near freezeout
(c) The intermediate mass dileptons (IMD) in the mass range $1\,GeV < M < 3\,GeV$ are entirely different: they produced early, when the flow is still absent;
(d) the IMD are mostly "prompt", coming from QGP thermal radiation, and not from the charm decays (as was suggested originally).

At RHIC: (a) Low mass dileptons are also enhanced over the cocktail. The exact magnitude of it is still somewhat disputed between STAR and PHENIX, for the the most central bin.
(b) IMD are well measured but the contribution from charm/bottom decays remains unknown. PHENIX is solving this problem with new vertex detector, STAR expect to use $e-\mu$ correlations based on new muon subsystem now in place;
(c) direct photons have spectra consistent with standard rates and hydrodynamics in shape, but not in absolute magnitude.
(d) unexpectedly large elliptic flow v_2 of direct photons persists.

At LHC the dilepton measurements are not yet as developed as hadronic ones. Photons measurements by ALICE include a confirmation of relatively large (and puzzling) value of the direct photon ellipticity, consistent with that originally observed by PHENIX. Fig. 52 shows comparison to theoretical models (curves): poor agreement is known as the "direct photon puzzle".

Theory of the electromagnetic observables follow tradition set up long ago (Shuryak, 1980), using mostly the production rates based on binary collisions of partons or hadrons. Now we know that similar approach fails to give viscosity, heavy quark diffusion coefficient or jet quenching parameter $\hat{q}$. So perhaps photon and dilepton production rates are larger numerically, and of more complicated non-perturbative origin. If large v_2 of the photons – measured so far with large error bars – will be confirmed, photons must be produced at the larger rate at late stage of the collisions.

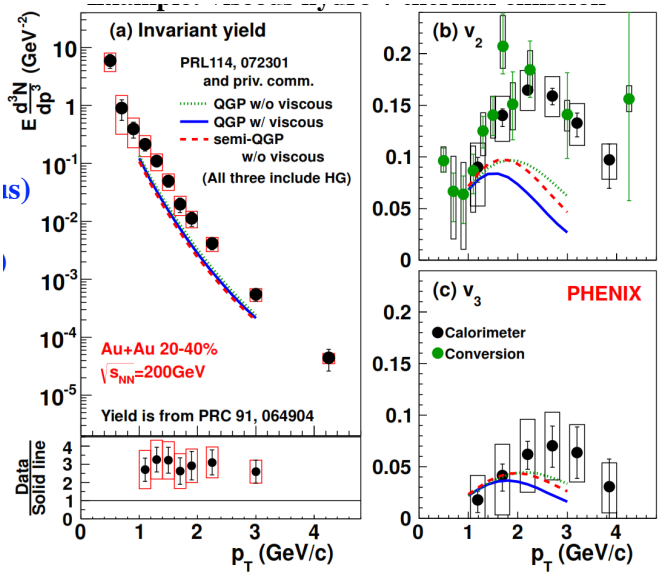

FIG. 52 Illustrations to "direct photon puzzle" (from A.Drees, PHENIX presentation at QM2015).
The yield (a), v_2 (b) and v_3 of the direct photons. Points are data and curves are from theory based on hydrodynamical model, the reference indicated on the figure.

B. New sources of photons/dileptons: multi-gluon or phonon+magnetic field

The production of photons and dileptons is tied to the presence of quarks, since gluons (and monopoles abundant near T_c) have no QED electric charge. The initial stages of the high energy collisions are believed to be dominated by gluons. Old perturbative arguments (Shuryak and Xiong, 1993) suggested that chemical equilibration via quark-antiquark pair production is relatively slow and should much later than thermal equilibration of the glue. This idea led to a "hot glue" scenario in which the quark/antiquark density at early stages is suppressed by powers of quark fugacity, $\xi_q < 1$. The basic process of the dilepton production

$$q + \bar{q} \to \gamma^* \to l_+ + l_- \tag{63}$$

is expected to be suppressed quadratically, $\sim \xi_q^2$.

This scenario has been recently challenged: higher order processes with *virtual quark loops* can produce electromagnetic effects as well, even without on-shell quarks. First, contrary to general expectations, the quark loop effect in GLASMA has been suggested to be significant (Chiu *et al.*, 2013), enhanced due to multigluon -to virtual quark loop -to dilepton processes such as e.g.

$$ggg \to (\text{quark loop}) \to \gamma^* \to l_+ + l_-. \tag{64}$$

The magnitude of the correction to production rates due to these processes still needs to be quantified.

An explicit calculation of the rate of two gluon to two photon transition $gg \to \gamma\gamma$ was done by (Basar *et al.*, 2014). One of the photons is assumed to be the ambient magnetic field at the time of collision, while both gluons are combined into a colorless stress tensor

$$T^\mu_\mu + \vec{B} \to (\text{quark loop}) \to \gamma^*(= dileptons) \tag{65}$$

The terminology introduced in this paper is as follows. The process in which glue appears as average matter stress tensor $< T_{\mu\nu} >$, producing photons (

real or virtual) due to time-dependent magnetic field, is called *Magneto-Thermo-Luminescence* (MTL). The average stress tensor is nearly constant over the whole fireball, and therefore its Fourier decomposition has very small momenta $p \sim 1/R$.

Individual events, however, also possess fluctuations of the matter stress tensor $\delta T_{\mu\nu}$, with chaotic spatial distribution, and thus with the Fourier transforms with non-negligible momenta. Since those are referred to as "sounds", their interaction with the ambient magnetic field is called *Magneto-Sono-Luminescence*, (MSL). If observed, the MSL process tests both the amplitudes of the short-wavelength sounds and also the magnitude of the magnetic field. We already discussed many uses of sounds above: let us here only comment on the magnetic field. It is easy to evaluate its early values, resulting from Maxwell equations and the currents due to the spectators in peripheral collisions. Since sQGP is believed to be a good conductor, these fields are expected to create currents capturing a fraction of the field inside the plasma (Tuchin, 2013), perhaps lasting for many fm/c. Magnetic field evolution is important to know for other applications as well, e.g. chiral magnetic effects and the like.

So far, luminosity and acceptance limitations had led experiments to focus on most luminous central collisions. In those, however, the ambient magnetic field is absent. Now it is perhaps time to look at dileptons in semi-peripheral collisions as well. To tell the effect of the ambient magnetic field from others, RHIC considers runs of isotopes with similar A but different Z, N values.

C. Dilepton polarization and the (early time) pressure anisotropy

It is well known that when spin-1/2 particles (such as quarks) annihilate and produce lepton pairs, the cross section is not isotropic but has the following form

$$\frac{d\sigma}{d\Omega_k} \sim (1 + a \cdot cos^2\theta_k) \tag{66}$$

where the subscript correspond to a momentum k of,say, the positively charged lepton and θ_k is its direction relative to the beam. The anisotropy parameter a in the Drell-Yan region – stage (i) in the terminology introduced at the beginning of this section– is produced by annihilation of the quark and antiquark partons, collinear to the beam. In this case, $a = 1$.

It was suggested (Shuryak, 2012a) that the parameter a can be used to control anisotropy of the early stage of the collision. In particular, if it is anisotropic so that longitudinal pressure is small relative to transverse, $p_l < p_t$, the annihilating quarks should mostly move *transversely* to the beam, which leads to *negative* $a < 0$. Such regime is expected due to a "self-sorting" process, in which partons with different rapidities automatically become spatially separated after the collision.

For illustration one can use a simple one-parameter angular distribution of quarks over their momenta p in a form

$$W \sim exp[-\alpha cos^2\theta_p] \tag{67}$$

and calculate $a(\alpha)$ resulting from it. It does show that a may reach negative values as low as -0.2 at stage (ii), before it vanishes, when equilibration is over, at stages (ii-iv).

X. HEAVY QUARKS AND QUARKONIA AS A SQGP PROBE

Physics of heavy flavor quark/hadron production is a rather large area, to which we cannot give full justice here; for a review see (Prino and Rapp, 2016). Heavy quarks provide interesting probes for matter properties, for a number of reasons. First of all, they are *not* produced by it, but by hard processes at the initial collision, which are under good theoretical control. Heavy quarks at the end are combined with light ones into heavy-flavor mesons and baryons, some identified by their decays. Leptons coming from c and b quark decays are also separately identified and studied. So, we know both the initial spectra, at the time of production, and the final ones.

Heavy quark motion inside matter is described by a number of tools, such as Langevin or Focker-Planck equations, or other kinetic approaches. There are two kinetic coefficients derived from these studies: (i) for small momenta, the diffusion coefficients $D_f(T), f = c, b$ and, (ii) for large momenta, the (flavor dependent) quenching parameter $\hat{q}_f$. Not going to specifics of the fits of heavy quark spectra, let us proceed directly to summary of the diffusion constant of the charm quark shown in Fig.53, (From (Prino and Rapp, 2016)). Like shear viscosity, the diffusion constant is *inversely* proportional to the scattering cross section. And, like shear viscosity, the diffusion constant seems to have a *minimum* at $T = T_c$.

There is a well known but persistent puzzle associated with these the diffusion constants, which is worth reminding. Perturbatively, the gluon quenching should to be stronger than that of the quarks, by the factor 9/4, due to color Casimir operators. Contrary to this simple prediction, the data indicate about *the same* magnitude of the suppression, for gluonic, light and heavy quarks! The mechanism which would explain this puzzle is not yet identified.

A. Quarkonium suppression

Quarkonia – bound states of $\bar{c}c$ or $\bar{b}b$ – are among the most discussed probes of matter properties. Initially discussed issue is the relative role of the real and imaginary

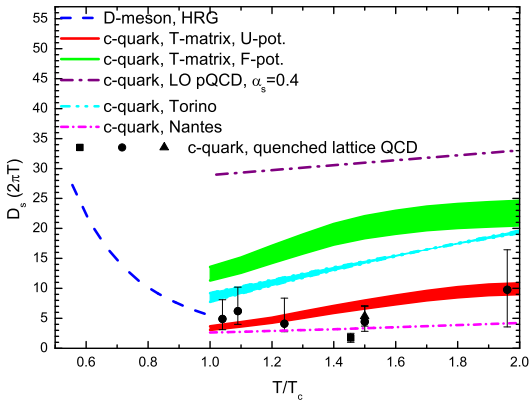

FIG. 53 The charm quark diffusion coefficients from quenched lQCD (circles , squares , and triangle) compared to model calculations based on different elastic interactions in the QGP (corresponding to the A(p=0) limit: T- matrix calculations with either free (green band) or internal energy (red band) as potential , pQCD Born calculations from HTL/pQCD matching using a reduced Debye mass and running coupling (Nantes , pink dash-dotted line) or with perturbative Debye mass and fixed coupling (Torino, cyan band), as well as schematic LO pQCD with fixed coupling and Debye mass mD=gT (purple dash-dotted line). The blue-dashed line below Tc is a calculation of D-meson diffusion in hadronic matter from elastic scattering off various mesons and anti-/baryons

parts of the potentials, binding them. Already the first paper on QGP signals (Shuryak, 1978) discussed an excitation process $J/\psi + g \to \bar{c}c$ in QGP, an analog of the photoeffect in atomic physics, with the conclusion that initially produced J/ψ would be partially killed by it. (Matsui and Satz, 1986) famously pointed out that, due to QGP screening, the real part of the potential is T-dependent, and therefore quarkonia binding diminishes with increasing temperature. They predicted sequential melting of the charmonia states, from highest to the ground state. Quantitative study of these potentials in weakly coupled QGP had been performed in (Laine *et al.*, 2007), for review see (Brambilla *et al.*, 2013). According to these works for $T > 300\,MeV$ the imaginary part of the potential exceeds the real part, $ImV > ReV$ and becomes dominant.

However, ImV describes excitation to all other states combined, and its knowledge is not sufficient if one needs to follow the system more closely. Its usage assumes that excited states are gone forever, completely ignoring transitions back to the ground state. But, without the balance between direct and inverse reactions, one cannot formulate the concept of thermal equilibrium, which is crucial for understanding of chemical freezeout.

Views on how QGP effects the quarkonia yield had changed in a complicated and confusing historical path. Instead of following it, we will proceed from simpler to more complicated settings, namely go thorough:
(0) static heavy quark potentials
(i) time independent equilibrium state of charmonia;
(ii) equilibration processes and rates;
(iii) heavy ion collisions.

(0) Static heavy quark potentials have been extensively studied on the lattice, at variable temperatures. A sample of 2-flavor QCD results, from (Kaczmarek and Zantow, 2006), is shown in Fig.54. Vacuum potential, at $T = 0$ is indicated at all plots, for comparison. The free energy measured can be related to entropy and thus the internal energy $V(T, r)$, by standard thermodynamic relations

$$V(T,r) = F(T,r) - T\frac{\partial F}{\partial T} = F(T,r) + TS(T,r) \quad (68)$$

One can see from Fig.54 that F and V are rather different. The force, also known as the string tension, has a maximum for U, reaching about $4\,GeV$ in magnitude. What are their physical meanings? Which one should be used as the potential in the quarkonium problem?

One explanation of these lattice findings proposed by (Liao and Shuryak, 2010) is based on the observation, that near T_c matter contains both "a dual superconductor" (Bose-condensed monopoles) as well as "normal" Bose gas of monopoles. Both components create currents around the electric flux tubes, terminating the field outside them. The size and tension of the flux tube thus depend on the densities of both components, which in turn are strongly T-dependent.

Its detailed discussion is out of context here, and we only mention a clarification of the entropy associated with the potential. Its generation is related with the level crossing phenomena, occurring while the separation between charges is changed. Suppose a pair of static charges (held by external hands) are slowly moved apart in thermal medium at certain speed $v = \dot{L}$. For each fixed L, there are multiple configurations of the medium populated thermally. When L is changed, the energies of these configurations are crossing each other, and at each level crossing there is certain probability to change or not to change the population of the states. These probabilities strongly depend on the speed $v = dL/dt$. For adiabatically slow motion all the level crossing processes happen with the probability 1. The adiabatic limit is to identified with the free energy $F(T, L)$.

If however the motion is very fast, transitions between crossing levels are suppressed. The internal energy $V(T, L)$, on the other hand, is different from $F(T, L)$ by subtracting the entropy term and thus it is probed in the extremely fast motion regime.

Such phenomena have multiple analogs in many other contexts in physics. The oldest example is the so called Landau-Zener theory of electron terms in the vibrational motion of the nuclei in a diatomic molecule. Specific

electron quantum states are defined at fixed L (the separation between the two nuclei) with energies $E_n(L)$, and certain levels cross each other as the value of L changes. Consider two levels with their energies given approximately by $E_1(L) = \sigma_1 L + C_1$ and $E_2(L) = \sigma_2 L + C_2$ near the crossing point. When the two nuclei approach the crossing point adiabatically slowly $v = dL/dt \to 0$, the electrons always change from the lowest state to the lowest other. But if dL/dt is finite, then the transition to *both* levels at crossing point may happen, with certain probability. This is how initially pure state becomes a mixture and entropy is produced. Landau and Zener gave the probability to remain in the original state at small velocity v in the following form

$$P = exp[-\frac{2\pi H_{12}}{v|\sigma_1 - \sigma_2|}] \tag{69}$$

where H_{12} is the off-diagonal matrix element of a two-level model Hamiltonian describing the transition between the two levels, and σ_i are slopes of the crossing levels. In the opposite limit of rapid crossing, the system remains in the original state, and no entropy is produced again. So, there should be a maximum of entropy production at some speed. For a discussion of the "entropic forces" in a heavy quark motion see e.g.(Kharzeev, 2014).

B. Quarkonia and lattice correlation functions

Suppose one puts one J/ψ in matter at some temperature T. Transitions from J/ψ to its excited states will happen first, eventually going into $\bar{D}D$, with charm quark separated. Since $\bar{D}D$ can eventually occupy an infinite volume, the separated states will win over the bound states. Thus, given enough time, any initial J/ψ will dissolve, at *any* T. On the other hand, thermal transitions may also proceed in the opposite direction as well. Starting from a certain density of separated charm quarks, charmonia and their ground states J/ψ are constantly re-generated. Given sufficient time, an equilibrium between $\bar{D}D$ and J/ψ will be reached. LHC data suggest that this regime is in fact reached for charm by the chemical freezeout (see below).

Heavy quarks c, b are produced in hard processes, not in thermal reactions. Since the heavy ion collision time is small compared to weak decays, c, b quarks are conserved, and thus c, b chemical potentials can be introduced. (It is *not* the one coupled to charm quantum number, but to c and $\bar{c}$ number separately.) This μ is such that charm fugacity is large, defining the equilibrium production of charmonium states.

Can "the density of certain quarkonia states" be defined at $T > T_c$? We know for a fact that it is not so: the evidence come from lattice static potentials described above. Already at $T \approx T_c$ there is a relatively large entropy associated with a quark $S = (U - F)(r \to \infty)/2T$,

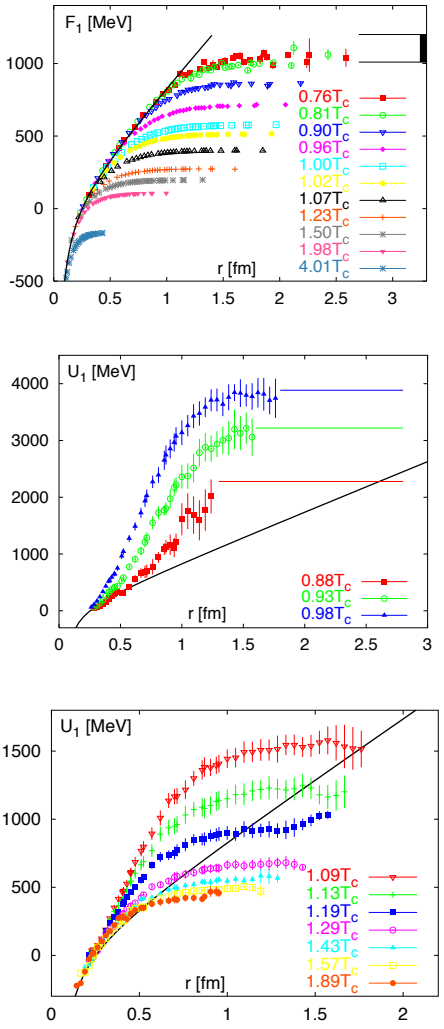

FIG. 54 from (Kaczmarek and Zantow, 2006). Free energy singlet potentials $F_1(T, r)$ (top plot) and the potential energy $U_1(T, r)$ below and above T_c. Note that the vertical scale is different.

corresponding to huge number of states $N \sim e^S$.

A well-defined field theory object is the correlation function of local gauge invariant operators

$$K(x, y) =< \bar{c}\Gamma c(x)\bar{c}\Gamma c(y) > \tag{70}$$

where the average is over the heat bath, and x or time $x^0 = t$ can be Minkowskian or Euclidean. In both cases the correlation function is related with the same *spectral density* $\tilde{K}(\omega, k)$, characterizing amplitude of excitation of states with given energy/momentum. At low T, one can find the individual states as certain peaks at the lines $\omega = \omega_i(k)$ in the spectral density, but with increasing T they all merge into a smooth continuum.

Euclidean correlation functions of such kind have been numerically calculated on the lattice: for a review see (Mocsy *et al.*, 2013). Unfortunately the problem of *spec-*

tral density reconstruction from those is, in practice, very difficult. Highly accurate (and very expensive) Euclidean correlation functions are converted into a relatively poorly defined spectral densities. Even when the individual states are seen, as some peaks in the spectral density, their widths are hardly quantifiable. Above a certain T all peaks corresponding to charmonium states merge into one "near-threshold bump", the imprint of the Sommerfeld-Gamow enhancement due to an attractive potential $\sim e^{-V/T} > 1$. .

C. Quarkonia and real time QFT formalism

A more detailed – time dependent – set of questions can be asked about *transition rates* in equilibrium matter. Those has been addressed (at least) at three levels, (a) real time QFT; (b) quantum mechanical; (c) classical diffusion.

Real time QFT, also known as Schwinger-Keldysh formalism, can follow a system from some initial to some final state using the full Hamiltonian

$$< i|Pexp(-\int_i^f dtH)|f > \tag{71}$$

which is viewed as a sum of that for the subsystem in question H_0 and matter perturbation V. Diagrammatic expansion, including two-time contours as well as Matsubara portion of an Euclidean time for thermal media are widely used in conduced matter problems, but they are not much used so far in the problem we discuss.

If H_0 corresponds to non relativistic quantum mechanical description of quarkonium, we will call it quantum mechanical approach. One can evaluate matrix elements of V over various quarkonia states. The first considered reactions were J/ψ *excitation* into unbound states of $\bar{c}c$ due to photoeffect-like reactions of one gluon absorption $J/\psi + g \to \bar{c}c$. For heavy quarkonia the *diagonal part* of the real and imaginary part of the perturbation V can be considered as a modified potential: for review see (Brambilla *et al.*, 2013). More generally, one can define transition rates between states and write a *rate equation*. The fundamental question here is of course whether the "matter perturbation" V is small or not. (We will argue below that at very low and very high T perturbative approach may work, but at least for charmonium in the near-T_c matter the answer to this question is negative).

Suppose the "perturbation" V is not small comparable with the interparticle interaction: then quantum quarkonium states are no longer special and one can as well use for H_0 just free particles. Using mass as large parameter, one can argue (Moore and Teaney, 2005; Svetitsky, 1988) that even in strong coupling setting the heavy quark motion should be described by classical stochastic equations, the Langevin or Fokker-Plank type. Let us only mention two crucial consequences of the argument. First, motion is diffusive, with $x \sim \sqrt{t}$ as it happens in random uncorrelated directions. Second, each step in space is very small. Suppose a perturbation delivers a kick of the order T to a heavy quark of mass $M \gg T$. Its velocity is changed little, by $\Delta v \sim T/M$ and by the time next kick comes $\Delta t \sim 1/T$ the shift in coordinate is small $\Delta x \sim 1/M$.

Suppose a quark needs to diffuse a distance large enough so that the gradient of the potential no longer pulls it toward the antiquark. From energy potentials V displayed above one can see that the distance it needs to go is about 1.5 fm, or $\sim 10\Delta x$ jumps it can make. However, since it is moving diffusively, to get that far the quark would need $\sim 10^2$ jumps, which can well be larger than time available. Quantitative study of classical diffusion in a charmonium (Young and Shuryak, 2009) confirmed that to climb out of the attractive potential in multiple small steps is hard. Contrary to common prejudice, using the realistic charm diffusion constant we found that the survival probability of J/ψ is not small but is of the order of 50 percents or so.

Finally, in order to model the fate of heavy quarks/ quarkonia in heavy ion collisions, one need to follow them all the way, from initial hard collisions to the freezeout. In classical diffusion approach one starts with pair distribution in the phase space, as defined by the parton model, and at the end project the resulting distribution to the charmonia states using their Wigner functions.

If the reader is insufficiently puzzled by all that, let us finish this section presenting two opposite answers to the question: What is the effect of the QGP production on the charmonium survival? In 1986 it was famously argued by (Matsui and Satz, 1986) that QGP, via the Debye screening of the color potential, *kills* charmonium states *sequentially*, excited states first and then eventually the ground states. In 2008 the opposite was argued by (Young and Shuryak, 2009): strongly coupled QGP helps to *preserve* charmonia. Small mean free path, and a specific bottleneck in the Focker-Planck solution, prevents $Q\bar{Q}$ to move far from each other. At the end of the process, $\bar{c}c$ pairs are projected back to the bound states, and the ground states of charmonia dominate if the distance between them is small.

D. Observed charmonium composition and chemical equilibration

The simplest, and also most radical, model of charmonium composition is a picture of its *statistical hadronization*, see (Andronic *et al.*, 2007) and references therein. It assumes that, like all light hadrons, charmonium states are produced in thermal equilibrium state at chemical freeze out. If so, issues discussed in the previous subsection are completely irrelevant: whatever charmonium history during the intermediate stages may be is simply forgotten in equilibrium.

The data at RHIC and LHC show that this is only partially true, and in fact there are two component of the charmonium population, the "survived" one and the products of the "recombination". Observations of the latter component are among of the most important results from heavy ion experiments.

Let us proceed to next order questions, related in particular with relative population of charmonium states. If all of them come the statistical hadronization at chemical freezeout, the consequence should be

$$\frac{N_{\psi'}}{N_{J/\psi}} = exp\left(-\frac{M_{\psi 2s} - M_{J/\psi}}{T_{ch}}\right) \tag{72}$$

(with similar expressions for other states). However if we have two out-of-equilibrium components, with different history, the answer should be different. The "survival" component, with its flow of probability from small to large r, should be richer in lower states. The "recombination" component flows the opposite way, and it should have more higher states instead. In general, two components have different centrality and p_t dependences, and in principle can be separated.

E. Are there some stationary quarkonia states in a strongly coupled medium?

Like in all other parts of heavy ion theory, there exist two points of view, a weakly coupled and a strongly coupled ones on the quarkonia dynamics. Which one is more adequate depends on the value of the quark mass. All approaches assume that it is very large compared to temperature $M \gg T$, so quarkonia are not thermally produced and are nonrelativistic, with $v/c \ll 1$.

If frequencies of the internal motion $\omega \sim v^2 M$ are small compared to those in ambient matter $\sim T$, one should be able to use static potentials from the lattice and calculate wave functions from the corresponding Schreodinger equation. Unfortunately, both for charmonia and bottomonia those frequencies are few hundreds of MeV, comparable to energies of medium constituents, so this condition cannot really be fulfilled. As we argued above, this implies that the appropriate potential to be used should be somewhat in between the free energy $F(T,r)$ and the potential energy $V(T,r)$, corresponding to slow and fast limits.

The weakly coupled point of view is valid at parametrically large M. In this case one may argue that quarkonia interact weakly with the matter. Excitations are rare and integrating imaginary part of the potential ImV (summarized e.g. by (Brambilla *et al.*, 2013)) over the collision time one obtains quarkonia suppression observed.

The opposite picture is that of very strong coupling assumes that transitions between quarkonium states are numerous, Large ImV exceeding the frequencies (distances between levels) makes the initial vacuum states meaningless. The spectral density of the correlator is smooth, without any peaks. Indeed, there are no 2-particle bound states in a dense plasma, just certain spatial correlations between the charges. In practice, classical approaches like Langevin or Focker-Planck (FP) equations are used. If one starts with close $\bar{c}c$ pair at $t = 0$, the solution to Langevin or Focker-Planck (FP) equations describe *positive* flow toward large relative distance $r \to \infty$. The opposite setting, describing quarkonium recombination, starts with originally unrelated $\bar{c}c$ at large r, and calculate the diffusion current directed toward small r. Both are followed for some time, the sQGP era, and at the freezeout the obtained distributions (in the phase space p, r) are projected to the vacuum quarkonia states, using their Wigner functions, see e.g. (Young and Shuryak, 2009).

Both the inward and outward diffusions turned out to be rather slow. The reason for that is quite interesting. The spatial distribution rapidly reaches a certain shape which persists with only slow growth of its tail. The example is shown in Fig. 55. (Note that in this case the attractive Coulomb-like potential has been complemented by a repulsive quantum effective potential $\sim \hbar^2/mr^2$ which generates the hole in the distribution at small r and prevents classical falling of the charge on the center.)

We called solutions with a nearly-permanent shape and small flux "quasi-equilibrium" solutions. This concept is – to my knowledge – not yet been noticed in this particular field[30] but it deserves to be. Let us show how quasi-equilibrium solutions appear in the quark diffusion problem, using the FP equation

$$\frac{\partial P}{\partial t} = \frac{\partial}{\partial \vec{r}} D\left(\frac{\partial P}{\partial \vec{r}} + \beta P \frac{\partial V}{\partial \vec{r}}\right) \tag{73}$$

where $P(t,\vec{r})$ is the distribution over the $\bar{c}c$ separation $\vec{r}$ at time t, D is the diffusion constant, $\beta = 1/T$ and $V(r)$ is the interquark potential. When $P \sim exp(-\beta V)$ the two terms in the r.h.s. bracket cancels, so the thermal equilibrium is of course time-independent. Note further, that if the bracket in the r.h.s. is nonzero but *constant*, its divergence is still zero, which makes the l.h.s. zero!

So, one has a family of stationary solutions, characterized by *constant fluxes*. The direction depends on the sign of the constant, it can be from small to large r as in charmonium suppression problem, or from large to small r for recombination. It is these stationary states which

[30] An example in a different but similar context is the so called globular clusters of stars inside Galaxies. It is well known that they are not in thermal equilibrium, but in a certain dynamical quasi-equilibrium, as the data for all of them show very similar phase space distributions. Depending on the environments, some are slowly evaporating, and some are growing instead, but with the net flux small.

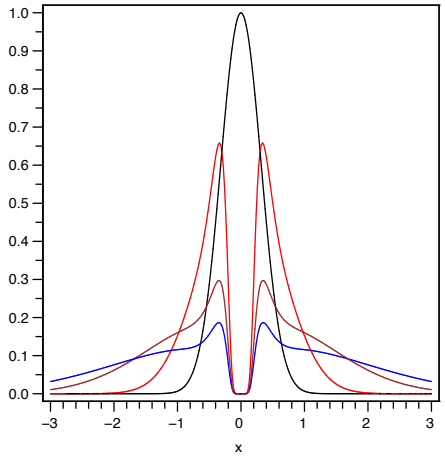

FIG. 55 from (Young and Shuryak, 2009): one-dimensional Fokker-Planck equation for an interacting c?c pair. The relaxation of the initial narrow Gaussian distri- bution is shown by curves (black, red,brown,green,blue, or top to bottom at r=0) corresponding to times t = 0, 1, 5, 10 fm, respectively.

can be called "quarkonium states in matter". (Note however, that constant flux needs to be supported at the ends: something should produce quarkonia at one end, and destroy them on the other.)

XI. JET QUENCHING

Jets are produced by hard collisions of partons, with momentum transfer $Q \gg 1\,GeV$, and constitute perturbative cascade from this scale down to on-shell hadrons. Hard collisions in QCD are described perturbatively, while the structure and fragmentation functions are non-perturbative objects treated so far phenomenologically.

By "jet quenching" one mean modification in jet yields and shape, due to interaction of the leading parton and subleading cascade with ambient matter. The cascade modification has specific features, due to the so called Landau-Pomeranchuck-Migdal (LPM) effect generalized from QED to QCD. We will not go into discussion of the large subject of gluon radiation, in vacuum and/or in matter, except of subsection XI.B on recent progress describing jets as a turbulent flow fixed points.

What will be the central focus of this chapter is possible usage of the jet quenching phenomenon as a matter probe. The jet quenching parameter $\hat{q}$ is defined as *the mean square of transverse momentum to a jet given to it due to scattering per unit of length.* It is a kinetic quantity proportional to the jet scattering cross section, in many respects similar to *invserse* viscosity-to-entropy density discussed above.

A. Is jet quenching dominated by the near-T_c matter?

Let us consider first a more general proposition: If the scattering of QGP quasiparticles and the scattering of jets (high $p_\perp$ partons) on the matter is similar, one may expect various related kinetic coefficients to have similar temperature dependence. In particular, one may expect that

$$\hat{q}(T) \sim \frac{s(T)}{\eta(T)} \tag{74}$$

As we know by now from hydrodynamical studies, the r.h.s. seem to have a peak at $T = T_c$. The main message from this subsection (Liao and Shuryak, 2009; Xu *et al.*, 2015) is that the l.h.s. seem to have a peak at $T = T_c$ as well!

There were two experimental hints which eventually led us to this conclusion. The first was the angular dependence of the jet quenching. At the very beginning of RHIC era it was noticed (Shuryak, 2002) that the simplest model, in which $\hat{q}$ was assumed to be a universal constant, cannot reproduce a direction-dependent (the ratio of in-reaction-plane to out-of-reaction-plane) data, or $v_2(large\, p_\perp)$. The relation between them is simply

$$R_{AA}^{in/out} = R_{AA}(1 \pm 2v_2) \tag{75}$$

The experimental value of v_2 was, from the very first PHENIX and STAR measurements, about twice larger than all simple quenching model predicts. It took years of slicing the matter distributions and trying various T-dependent $\hat{q}$ to find at least *one* possible solution to this puzzle (Liao and Shuryak, 2009): one can get close to the observed v_2 values if the jet quenching is strongly peaked near T_c. The reason being that the angular asymmetry of the corresponding shell of matter is sufficiently large.

The second hint was provided by the LHC jet data, showing that quenching at LHC is rather similar to that at RHIC, *in spite* of the fact that the multiplicity (and thus matter density) is twice larger there. Now we hope we understand it: shorter time spent near T_c at LHC, as compared to RHIC, compensates for twice more scatterers.

Now let us have a look at the angular distribution of jet quenching, Fig. 56 from (Xu *et al.*, 2015) , showing $v_2(large\, p_\perp)$ measurements at LHC. There are 3 upper (red) theory curves, and 3 lower (violet) ones. Only the former describe the data: those include the jet-monopole scattering. The latter, with $f_m = 0$ in the caption, ignore it and thus fail to describe the data. In Fig.57 we show the $\hat{q}(T)$ of the model for a jet with 20 GeV. The red curve marked pQCD+QGMP has a peak reaching $\hat{q}/T^3 \sim 50$ in the left upper corner, includes the scattering on monopoles (this is what M in the matter description is). Note that blue curve at the bottom marked pQCD+HTM, which includes quarks and gluon only in

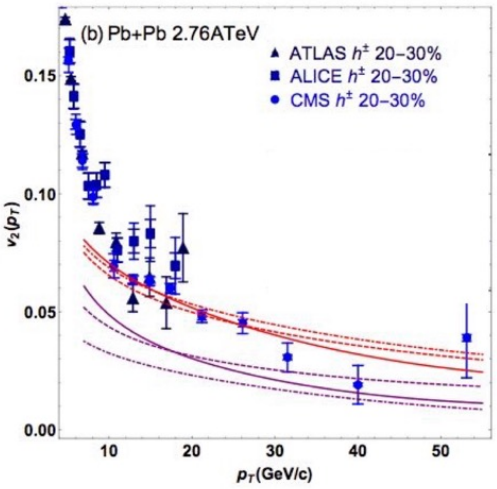

FIG. 56 (color online) From (Xu *et al.*, 2015): jet suppression and elliptic parameter v_2, data versus models.

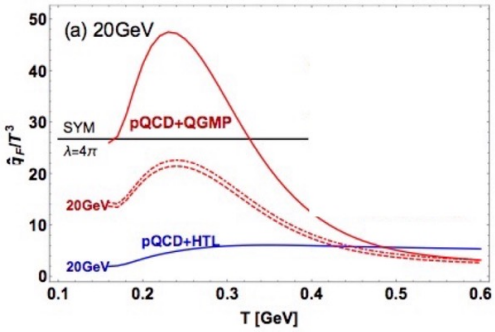

FIG. 57 (color online) the NTcE model with enhanced near-T_c quenching

hard thermal loop (HTL) approximation, has $\hat{q}/T^3 \sim 5$, an order of magnitude lower.

Another representation of the same information is given in the insert, in which $\hat{q}(T)$ is plotted in absolute scale. The maximal value of the red curve $\hat{q}(T) \approx 5GeV^2/fm$ is at $T \sim 300\,MeV$, while the blue perturbative curve reaches the same $\hat{q}(T)$ at much higher $T \approx 550\,MeV$ in the right upper corner.

This is a very concrete manifestation of what we discussed in the introduction, where we compared perturbative and non-perturbative effects. The perturbative amplitude has the gluon charge and the coupling $\alpha_s \sim g^2$, one g from a jet and one from the "scatterer". The non-perturbative amplitude still has a factor g from a jet, times[31] $(1/g)$ from the field of the monopole: thus there is no coupling.

[31] This $(1/g)$ can also be called the magnetic coupling constant, related to electric one by the Dirac condition.

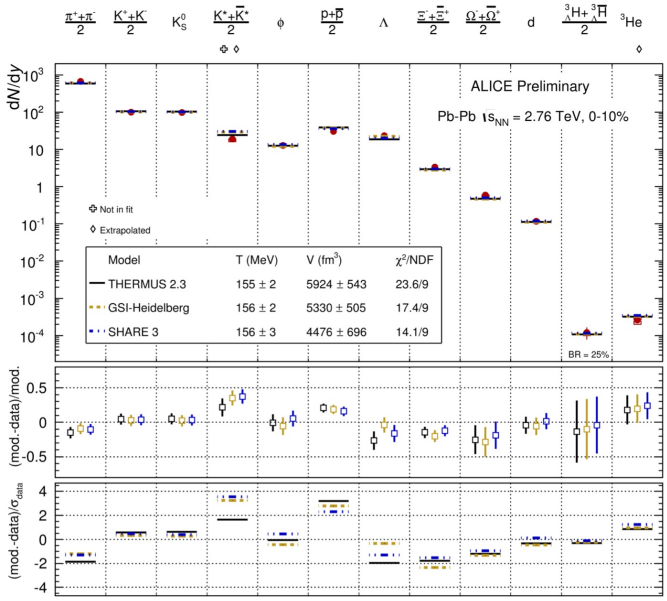

FIG. 58 Alice data on particle yields compared to thermal model (Andronic *et al.*, 2007). The main fit parameters are indicated in the upper plot.

B. "Fixed points" of the jet distributions

There have been important developments relating jet-in-matter with a general turbulence theory: our presentation follows (Blaizot *et al.*, 2015). For a large enough medium, successive gluon emissions can be considered as independent: multiple emissions can be treated as probabilistic branching processes, with the BDMPSZ spectrum playing the role of the elementary branching rate. The inclusive gluon distribution function

$$\frac{dN}{dlog(x)d^2\vec{k}} = \frac{D(x,\vec{k},t)}{(2\pi)^2} \tag{76}$$

satisfies certain diffusion-brunching equation. Integrating over transverse momentum one gets the zeroth moment $D(x,t) = \int_k D(x,k,t)$ on which we focus here, for simplicity. This moment satisfies the equation

$$t_* \frac{\partial D(x,t)}{\partial t} = \int dz K(z) \left[\sqrt{\frac{z}{x}} D(\frac{x}{z},t) - \frac{z}{\sqrt{x}} D(x,t) \right] \tag{77}$$

with the gain and the loss terms in the r.h.s. The details such as the shape of the kernel K and time parameter t_* can be found in ref.(Blaizot *et al.*, 2015): they are not really important. The central point is the analytic solution

$$D(x,t) = \frac{(t/t_*)}{\sqrt{x}(1-x)^{3/2}} exp(-\frac{\pi t^2}{t_*^2(1-x)}) \tag{78}$$

which balances the gain and the loss.

Note that an essential singularity at $x = 1$ is expected: it is known as the Sudakov suppression factor. The remarkable news is that apart of the exponent, the shape of the x-dependence remains the same at all times. Only the normalization changes. Let us see how it works in the most important small $x << 1$ region, where the leading $x^{-1/2}$ dependence is such that the gain and loss terms cancel. This is the "quasi-equilibrium solution" for the jets. As a result, jets in matter are expected to approach some universal shape, not determined by the particular initial conditions, but by the quasiequilibrium solution to which it gets attracted as the process proceeds.

It is essentially the same phenomenon as we have seen in Fig.55 for diffusing charmonium: the shape itself is dictated by the balance of the gain and loss. Both are "quasi-equilibrium" attractor solutions: their main feature is *constant flux* of certain quantity, from one end of the spectrum to the other. (The flux in decaying charmonium comes from small to large distance between quarks, in the jet case it comes from large to small x.) Once again, the constancy of the flux in such solutions is the key idea going back to Kholmogorov's theory of hydrodynamical turbulence, which I find quite remarkable. As Einstein once observed (approximate quote from memory): "... the number of good ideas in physics is so small, that they keep being repeated again and again in various contexts".

XII. NEAR THE PHASE BOUNDARY: FLUCTUATIONS AND THE FREEZEOUTS

A. Chemical freezeouts

The concept of two separate freeze outs is based on separation of elastic and inelastic rates at low T, in magnitude. Statistical equilibration is so famous success story, that we just show current ALICE data, with the corresponding thermal fits, in Fig.58. For a simple statistical model with two parameters, the quality of data description is extraordinary.

Note that even light nuclei – d, t, He^3 and their antiparticles are also included. One may wonder how d, with its $B = 2\,MeV$ binding energy, can be found in an environment with ambient temperature $T \sim 160\,MeV \gg B$. It is literally like finding a snowflake jumping out of a hot oven. Shouldn't d be instantly destroyed in it? The answer to this and similar questions is well known. Thermodynamics does not depend on the d lifetime. As one deuteron is destroyed, perhaps with some large rate, in equilibrium another one must be recreated, by the inverse process with *the same* rate. The average population is conserved, and it is what the statistical mechanics gives us.

Note that one deviation is K^*: the model predicts more than observed. This is expected: it is short lived resonance which decays when the density is still non-negligible, the products can be re-scattered and their invariant mass moved out of the peak. Corrections to that can be made using any cascade codes.

Another deviation is for $p + \bar{p}$. Some argued that one should take into account possible annihilation on the way out. As available practical tools people used cascade codes (RQMD, UrQMD or similar) and got very large effects. This puzzle was even much stronger at lower collision energies (AGS,SPS) at which the density of baryons is large and antibaryons were predicted to get nearly extinct, contrary to observations.

The puzzle was resolved by the observation by (Rapp and Shuryak, 2001): all cascade codes included the annihilation $p+\bar{p} \to n\pi, n \sim 5$ but *not* their inverse reactions. Contrary to popular beliefs, the inverse reactions are not suppressed. In fact at equilibrium their rates are exactly the same as that of the direct one.

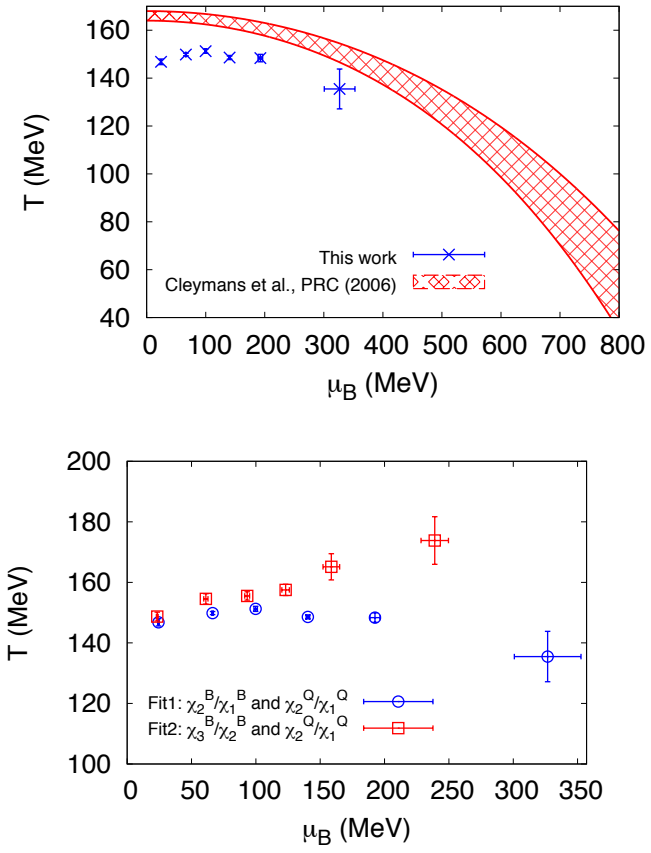

FIG. 59 (Color online) (a) Freeze-out parameters in the $(T - \mu_B)$ plane: comparison between the curve obtained in Cleymans et al (red band) and the values obtained in the present analysis from a combined fit for net-electric charge and net protons (blue symbols). (b) The freezeout parameters fitted from two different set of particle ratios, as shown in the plot

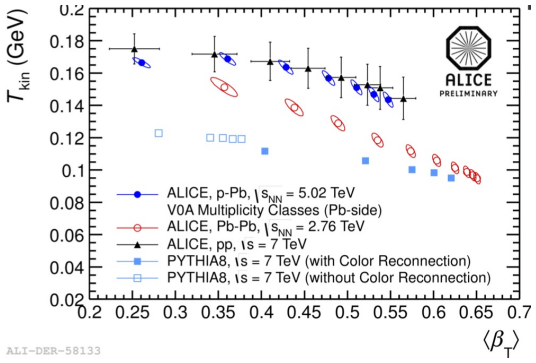

FIG. 60 (color online) The temperature of the kinetic freeze-out versus mean velocity of the radial flow, fitted to ALICE spectra of the identified secondaries $(\pi, K, p, \Lambda, \Xi, \Omega)$.

I would not show the freezeout points on the phase diagram, which has been done many times. Let us just remind that those seem to be remarkably close to the phase boundary, defined on the lattice. Why should this be the case? An answer suggested by Braun-Munzinger, Stachel and Wetterich (Braun-Munzinger *et al.*, 2004) is also related to the multiparticle reaction rates. Since those depend on a very high power of the temperature, they all should decouple very close to the critical line

$$\frac{|T_{ch} - T_c|}{T_c} \ll 1 \tag{79}$$

New trend in freezeout physics is focus of susceptibilities. As pointed out by (Shuryak, 1998) before RHIC era, information about them can be provided by measured event-by-event fluctuations. Since the susceptibilities are higher order derivatives of the free energy, over T or various chemical potentials, they are more sensitive to singularities. This idea was further applied toward location of the critical point in (Stephanov *et al.*, 1999), suggesting the low energy beam-scan program at RHIC. The results of the actual beam scan are however still not finalized enough to be reviewed here.

Both the measurements of event-by-event fluctuations in experiments and the calculation of susceptibilities on the lattice reached significant maturity. In fact comparison between them now allows the $T - \mu_B$ freezeout curve be reconstructed, even without using any particle ratios. An example by (Alba *et al.*, 2014) is shown in Fig.59. Fig(a) compares new set of freezeout parameters (points) compared to earlier one from the particle ratios. Fig.(b) shows that as μ grows a consistency between different ratios becomes worse. It is generally believed that the Hadron Resonance Gas model describes the QCD thermodynamics at chemical freezeout quite well.

B. From chemical to kinetic freezeouts

Separation in magnitude of the elastic and inelastic (low energy) hadronic reactions is the basis of the "two freezeouts" paradigm, with separate chemical T_{ch} and kinetic T_{kin} temperatures.

Its effectiveness became even more clear at LHC, which we illustrate in Fig.60 containing the "blast wave" fitted parameters to the ALICE spectra of . Unlike T_{ch}, the kinetic one T_{kin} strongly depends on centrality of PbPb collisions, decreasing to values below 0.1 GeV for the most central bins. Cooling from 0.16 to 0.1 GeV may not look so dramatic: but one should remember that pressure and energy density in this region are proportional to high power of T, and so we speak about a change by a factor 20 or so.

Let us discuss the dependences displayed in Fig.60 in more detail. The most central AA collisions produce the largest systems, which also have the highest T at the early stages. The fit displayed also shows that most central collisions produce the lowest T at the kinetic freezeout. Indeed, the larger is the system, the smaller is its expansion rate, and thus it freezeout at smaller collision rate, or smaller density.

Look now at the pp, pA data at Fig.60: for them both temperatures, T_{ch} and T_{kin}, are much closer. An explanation to that, discussed above, is based on strong radial flow related with higher expansion rates. These collisions definitely cannot support the hadronic phase.

In summary, there are evidence that in central AA collisions matter cools deep into the *hadronic phase*, retaining kinetic – but not chemical –equilibrium. This opens some interesting questions related to hadronic phase, which can now be addressed experimentally. Mentioning the relevant numbers: Cold fireballs created in central $PbPb$ have several thousands of particles and their kinetic freezeout time reaches 15 fm. The highest multiplicities in pp, pA still correspond to fireballs with order of magnitude less particles, and freezeout time/size of 3 fm or so.

Since between T_{ch} and T_{kin} the particle numbers are conserved, one should introduce new nonzero chemical potentials, not associated with conserved quantum numbers like charge and baryon number. In particular, there should be nonzero chemical potentials for pions. Whether there are nontrivial fugacity factors at the kinetic freezeout can be directly observed in the pion spectra, because in this case Bose enhancement can be measured. This idea is at least 20 years old (Bebie *et al.*, 1992): its experimental manifestation was also discussed by (Hung and Shuryak, 1998), see Fig.61(a). (The reference SS collisions is much smaller system than PbPb, and thus its chemical and kinetic freeze outs should be close.) Fig.61(b) shows that the same effect shows up, now at LHC. The fit *without* chemical equilibrium, with nonzero pion μ on top, provides a better description to the spectra

at small $p_t < 200\,MeV$.

Interesting that the parameter of the fit in this last work gives $\mu_\pi \approx m_\pi$, so the authors speculated if the conditions for pion Bose-Einstein Condensation (BEC) were actually reached. If this indeed becomes true, it has been many times suggested previously that the femtoscopy parameter λ should show it, as it is sensitive to "degree of coherence" of the pion source. Femtoscopy data on 2 and 3 identical pions from ALICE can be indeed fitted with a coherent source, with a fraction as large as 20%.

Do we actually witness the BEC formation at the LHC? In order to answer this question it is useful to recall BEC discovery in experiments with ultra cold atoms a decade ago. As the atomic system does evaporating cooling and its temperature decreases, the measurements of the momentum distribution (by switching off the trap) revealed appearance of new and much more narrow component. Unlike the usual thermal component, its width was independent of T, and related to the inverse spatial size of the BEC cloud.

This indeed sounds like what is observed in heavy ion collisions: as one goes to most central collisions and the kinetic freezeout T_{kin} get below 100 MeV, the p_t spectra do become enhanced at small momenta. The difference however is in the shape: we don't see a new Gaussian, as in the atomic experiments, but only some deformation of the spectrum, by $\mu \neq 0$.

If the condensate be produced, it should be a separate component, with μ being exactly m_π, independent on T. If BEC cloud contains about 1/4 of all pions, its diameter should be large, at least of the order of 2-3 fm. The corresponding width of momentum distribution, from uncertainty relation, should be as small as say $< p_t >< 0.1\,GeV$. Looking back to Fig.61(b) one however finds, that such soft secondaries seem to be *outside* of the acceptance. So, even if BEC component is there, we so far cannot see it, neither with ALICE nor with any other LHC detectors! How then can we get their influence in the femtoscopy?

This issue can perhaps be clarified by a short dedicated run, in which the ALICE detector switches to smaller (say 1/2 of the current value) magnetic field, to improve the low p_t acceptance. (Yes, recalculating all the efficiencies is a lot of extra work, but perhaps it is worth clarifying this interesting issue.)

C. The search for the critical point and RHIC low energy scan

The main idea of a scan aimed at the QCD critical point, (Stephanov *et al.*, 1999), is well known. The critical point – if it exists – should enhance the event-by-event fluctuations, similar to critical opalescence. known in many cases. Technically, various effects given by diagrams, can be classified according to a number of propagators of the critical modes, with each enhancing the effect due to large correlation lengths. It was quantified by (Stephanov, 2009). The n-particle correlators may contain up to n such propagators, 3 particle correlators are $\sim \xi^6$, 4-particle ones $\sim \xi^8$, see Fig.62, and so on. The wavy line at zero 4-momentum is $\sim 1/m_\sigma^2 \sim \xi^2$: but the prediction is not just the power of the propagators because the coupling of critical modes by itself vanishes as certain power of ξ given by the critical indices. The quartic one in the diagram considered is $\sim 1/\xi$ so the total power is 7, not 8.

It is possible to tell the same story in a somewhat simpler non-technical language. The critical field we here call σ should be viewed as some stochastic/fluctuating background field coupled to fluctuations in particle num-

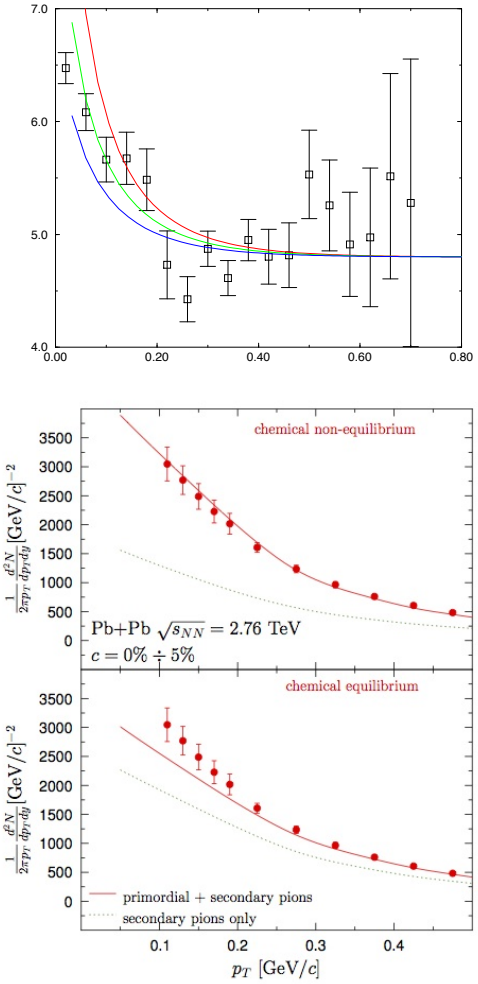

FIG. 61 (Color online) (a) Points show the ratio of *PbPb* to SS spectra, from NA44. Three curves are for pion chemical potential $\mu_\pi = 60, 80, 100\,MeV$, from (Hung and Shuryak, 1998). (b) (From (Begun *et al.*, 2014)) Dots are ALICE transverse momentum spectra of pions in the low-p_t region, compared to the model with (upper plot) and without (lower plot) pion chemical potential.

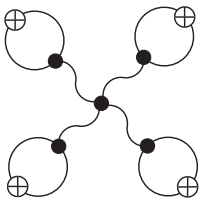

FIG. 62 The enhanced contribution to 4 particle correlator, from (Stephanov, 2009).

ber (circles with crosses in the diagram above). One can view it being proportional to some stochastic potential $\Delta V(x)$ which enters the probability in the usual way $P \sim exp(-\Delta V(x)/T)$, so that in its minima the probability is larger and more particles – e.g. four protons mentioned above – all gather there. The critical point is special in that the scale of the correlation length ξ of this potential increases, and thus more particles have a chance to get inside the correlation length.

Which particles one should observe? In principle sigma is scalar-isoscalar, coupled to any hadron. In our paper (Stephanov *et al.*, 1999) and in (Stephanov, 2009) the simplest coupling was considered as an example, the $\sigma\pi\pi$ one, and so the particles were pions. Yet one can argue that the nucleons should work better. First, the powers of the baryon density $n_B = N_N - N_{\bar{N}}$ correlated together are the susceptibilities calculated on the lattice as derivatives over μ_B. Second, we know from the nucleon forces – e.g. the simplest version of the Walecka model – that σ is the main component of the attractive nuclear potential which binds the nuclei.

$$\Delta V = \frac{g^2_{\sigma NN}}{4\pi r} exp(-m_\sigma r) \tag{80}$$

In vacuum the typical mass $m_\sigma \sim 600\, MeV$ and the inter-nucleon distance $r \sim 1.5 fm$ are combined into small suppression factor $\sim exp(-5) \ll 1$ explaining why the nuclear potential scale $\Delta V \sim -50\, MeV$ is much smaller than the nucleon mass, in spite of strong coupling. (At smaller distance r the repulsive omega contribution dominates the attractive sigma one.).

Can it be so, that at the QCD critical point $m_\sigma \to 0$ and this small exponent disappears? If so, one should expect much deeper ΔV, perhaps even larger than the freezeout temperature T. Furthermore, if say $\xi = 2\, fm$, the volume $4\pi\xi^3/3 \sim 40 fm^3$ is large enough to collect many nucleons, not just 3 or 4, as Stephanov suggested. So, such clustering of the nucleons should produce large nuclear fragments, a new cute signal of the critical point!

This argument, unfortunately, is still a bit naive. The critical mode which gets long-range is not just the σ field but – because we are at nonzero density – a certain combination of scalar σ with vector ω fields. Therefore the repulsive forces between the nucleons may become long-range as well. To tell what happens we need a reliable theory or some dedicated experiments. Fortunately, we can do it in the coming low energy scan. Isoscalar sigma interacts with scalar – net baryon – density $n_s = N_N + N_{\bar{N}}$, while omega interacts with $n_B = N_N - N_{\bar{N}}$. The powers of these differ by the non-diagonal terms such as nucleon-antinucleon correlators $C^{m,n} =< N_N^m N_{\bar{N}}^n >$ which can and should be measured. Perhaps restricting kinematics of all particles involved – rapidity and momenta differences – would further enhance the signal.

Let us now jump to the STAR data shown in Fig.63. The proton 4-point correlator has an interesting structure: a minimum at $\sqrt{s} = 20 - 30\, GeV$ and perhaps a maximum at low energy. Antiprotons have a similar shape but with much smaller amplitude. The structure qualitatively agree with theoretical predictions of an oscillatory behavior of the kurtosis near the critical point.

(However before getting excited by the new large signal – with large error bar – Let us remind that it appeared as a result of particle ID improvement, from $0.4 < p_\perp < 0.8\, GeV/c$ to now reaching $p_t = 2\, GeV/c$. The newly open kinematic window should be sensitive to hydrodynamic flow, and potentially to its fluctuations.)

Also near critical point one expect significant modification of attractive (sigma-related) nuclear forces: can those affect the 4-proton (antiprotons) correlations in question?

Clearly more data at the low energies are needed, to understand whether one has indeed located the QCD critical point or not.

XIII. SUMMARY AND DISCUSSION

A. Progress on the big questions

Before we summarize conclusions on the particular subjects, let us remind the reader "the big questions"

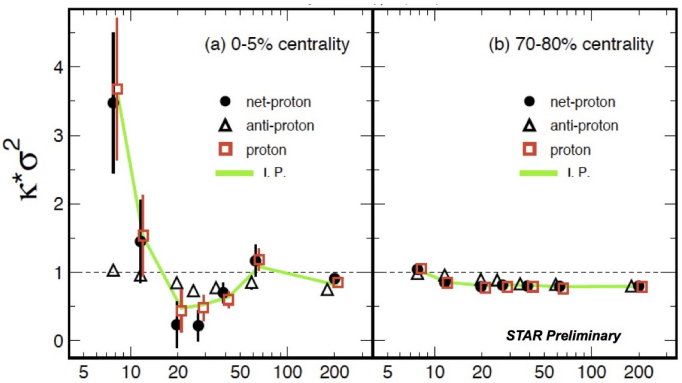

FIG. 63 The kurtosis – 4 particle correlator – in units of the width, as a function of the collision energy $\sqrt{s}, GeV$.

mentioned in the Introduction:

I.**Can one locate the "soft-to-hard" boundary**, where the transition from the strong to the weak coupling takes place?

II. **Can one locate the 'micro-to- macro" boundary**, where the transition from the ballistic to collective regime takes place?

III. **Can we experimentally identify signals of the QCD phase transition**, in particular locate the QCD critical point?

Somewhat surprisingly, the sharpest observed transition discussed is in the *profile of the pp elastic amplitude* shown in Fig.51(a). Although indirectly, this sharp transition from nearly black to light gray profile is claimed to be related to the phase transition from the deconfined (gluonic) to confined (stringy) regimes of the Pomeron. On one hand, the sharpness is surprising because it is associated with quite small system – the Pomeron or a pair of strings, rather than a macroscopic system. On the other, the analogy originates from the phase transition in gluodynamics (strings at early stage are considered excitable but not breakable, so no quarks), which is the first order transition.

The location of the micro-to-macro transition in pA and pp collisions, as a function of multiplicity, is debatable. Data on the mean $p_\perp$ and slopes shown in Fig.24 indicate smooth growth of the radial flow: but we now know that the radial flow can be "faked". At the same time, the $v_2\{2\}$ as a function of multiplicity are rather flat. Its version $v_2\{n\}, n > 2$, from multi-particle correlations, show changes, but their understanding of that is still missing. Calculations of v_n in dynamical models of the Pomeron are in progress: perhaps they will explain later the low multiplicity side.

The theoretical justification of successful hydrodynamical description for small systems is getting under control. A number of examples show rather effective cancellations of all higher-gradient corrections. Navier-Stokes approximation seem to be rather accurate, even in situations in which one hardly expects it to work.

The low energy scan at RHIC shows clear experimental evidences for "the softest point". Attempts to locate the effects of the QCD critical point are intriguing but not yet conclusive.

B. Sounds

The first triumph of hydrodynamics, at the onset of RHIC program, was description of the "Little Bang". The magnitude of the radial and elliptic flows were measured and calculated, as a function of $p_\perp$, centrality, rapidity, particle type and collision energy. Spectacularly successful description of higher azimuthal harmonics of the flow, with $m = 3 - 6$, had followed. As it has been repeatedly emphasized, these are sounds, propagating on top of the exploding fireball. The damping of these modes agrees with acoustic-inspired formulae.

Another phenomenon, well known for the Big Bang perturbations, is due to a presence of the "phase factor". Common freezeout time for all harmonics imply m-dependent phases. As m grows, the phases rotate, so one should see maxima/minima in the power spectrum. These are not observed: the only experimental indication for that is the triangular flow $m = 3$ stronger than the elliptic one $m = 2$ for the ultra-central bin.

We emphasized that we have only observed harmonics with $m < 7$ because the higher ones are damped too much by the freezeout time. Yet at the initial time the Glauber model produced equally well harmonics up to $m = 20$ or so, and GLASMA-based models predict harmonics to the hundreds. Most of them do not survive till freezeout: so, are there any observable manifestations of their existence? Magneto-Sono-Luminescence process, converting them into electromagnetic signals, is an example of that.

The damping of harmonics with $m > 6$ is also an opportunity to observe the sources of sounds other than the initial state, in particular from inhomogeneities at the phase transition.

Finally, even in equilibrium there must be fluctuations emitting sounds. Those generate nontrivial "loop corrections" to hydrodynamics. Observation of "sound background" in hadronic matter is another challenge of the field.

C. The conflicting views of the initial state

Perhaps the most important conceptual controversy in the field remains the conflicting conclusions coming from weakly coupled and strongly coupled scenarios of the initial state and equilibration.

Significant progress in the theory of a weakly coupled initial state is in the concept of *turbulent cascades*, with stationary and time-dependent self-similar solutions. Both classical glue simulations and parton cascades came up with out-of-equilibrium attractors possessing power spectra with certain indices, which are qualitatively different from equilibrium. From a practical perspective, these studies suggest that the stress tensor remains anisotropic for a long time. However, more recent works indicate that the nontrivial attractor is only approached if the coupling is unrealistically small.

Strongly coupled approaches, especially based on AdS/CFT and related models, view equilibration as a process dual to the *gravitational collapse* resulting in black hole production in the bulk of AdS_5. As soon as some trapped surface (a black hole) is present, the equilibration is very rapid: any kind of "debris" simply falls into it. Mathematically, the non-hydro modes have imaginary parts comparable to the real one, which nu-

merically are quite large (50). In this scenario, there are no cascades or even quasiparticles, the only propagating modes are sounds (dual to gravitons).

Whether the stress tensor remains anisotropic beyond the short initial period or not is still an open question. Theoretical efforts to combine hydrodynamics with out-of-equilibrium parameterization of the stress tensor were discussed above: the situation at any realistic anisotropy is thus under theoretical control.

In order to decide on the equilibration time and anisotropy, one needs to develop experimental observables sensitive to the early stage. (My specific proposal – the dilepton polarization – has been discussed in section IX.C.)

D. The smallest drops of sQGP

The major experimental discovery from the first years of LHC operation was the observation of collective anisotropies in "small systems": central pA and high multiplicity pp collisions.

One point of view – admittedly advocated above – is that these are exploding fireballs. While smaller then those produced in AA collisions, they are still "macroscopically large" and can be described hydrodynamically. Hydrodynamical description of strong radial and elliptic flows in those systems is very successful.

The opposite point of view is that, from the smallest to the highest multiplicity bins, the pA and pp collisions produce microscopic systems which can be discussed dynamically. The models are the same as used for minimally biased pp, and the issue is sometimes known as "the shape of Pomeron". Recall that the Pomeron is cased on the pQCD ladder diagrams in weak coupling, or "stringy" in confining models. Both need to be developed much further to predict v_n correlations. While experiments at RHIC with d and He^3 beams disfavor such scenarios for large multiplicities, at lower ones they should be applicable.

A very positive development is that groups working on all scenarios try now to figure out the limits of their approaches. Inside hydrodynamics, for example, one study higher gradients and their effect. In the string-based picture, we discussed a string-string interaction – ignored for long time by event generators.

Meanwhile, phenomenologists describe the data. Hydrodynamical treatment of high multiplicity pA, pp events seem to be rather successful. They require very small initial sizes and rather high temperatures. But we do not really understand how such systems can be produced. In particular, the case of central pA collisions is contested between the IP-glasma model and a string-based initial state picture. So far one has very little theoretical control over the initial state of the high multiplicity pp : if it exists anywhere, glasma should be there. It is difficult to study this system, for statistical reasons, but since this is the highest density system we have, it should be pursued.

E. Heavy quarks and quarkonia

LHC data confirmed what has been already hinted by the RHIC data: a significant fraction of the observed charmonia comes from *recombination* of charm quarks at the chemical freezeout . The "surviving charmonia" fraction continue to be reduced. Such major change in charm quark behavior, from "heavy-like" to "light-quark-like" is clearly an important discovery.

It remains true that c, b quarks are produced differently from the light ones, namely in the initial partonic processes. Yet their interaction with the ambient matter is strong. At large p_t we observe quenching $R_{AA}^{c,b}$ comparable to that of gluons/light quarks. At small p_t we observe an elliptic flow of open charm and changes in spectra.

Langevin/Fokker-Planck studies however suggest that c quarks are not moving with the flow. At early time c, b quarks are produced with large $p_\perp$ and start decelerating, due to drag, while the matter is slowly accelerating due to pressure gradients: their velocities move toward each other, yet they do not match even by the end. As a result, charm radial/elliptic flows are *not* given by the Cooper-Frye expression. The recombinant charmonia may perhaps be an exception. Whether they actually co-move with the flow still needs to be established.

On the theory front, Langevin/Fokker-Planck studies induced new conceptual developments. In particular, we discussed a new set of solutions of those for charmonia, the quasi-equilibrium attractors with constant particle flux. Those states, not the original bound states like $J/\psi, \psi'$ etc, provide a convenient basis for evaluation of the speed of relaxation and out-of-equilibrium corrections to current charm hadronization models.

F. Jets

The theory of hard processes – jets, charm/bottom production – were based on factorization theorems and a concept of structure functions. It is a solid foundation, but a very restrictive one. When one asks questions about jets in high multiplicity bins of pp collisions, one soon realizes the "corresponding structure functions" do not exist: that concept has only been defined for the minimally biased (untouched) proton in strictly inclusive setting. Universal structure functions, measured rather than calculated, have served us since 1970's, but now they cannot be used anymore. If a certain fluctuation of a nucleon is selected, new models and much more measurements are needed.

Unfortunately, there are severe practical limits: hard processes reduce probability by several orders of magnitude, on top of 5% trigger for central pA. Yet high LHC luminosity plus specialized triggers should be enough to get to some of those issues in the near future. Current jet quenching data even for min.bias pA remains to be understood. Scaling arguments, like the ones we used for hydro in smaller-but-hotter systems, can and should be developed and compared with the data.

We argued above that in AA collisions jet quenching parameter $\hat{q}$ seem to be strongly enhanced at the near-critical $T \approx T_c$ region. Small systems are more explosive and pass near-freezeout stage rapidly: this should play a significant role in jet quenching.

Acknowledgements. This paper is a summary from multiple conversations with colleagues, at seminars, workshops and conferences. They are too many to attempt to name them here (see long list of references below), but still I need to thank them for patiently teaching me about this or that idea or experimental findings. This work was supported in part by the U.S. Department of Energy, Office of Science, under Contract No. DE-FG-88ER40388.

Appendix A: Heavy ion terminology

"Ion" in physics refers to atoms with some of its electrons missing. While at various stages of the acceleration process the degree of ionization varies, all of it is unimportant for the collisions, which always are done with nuclei fully stripped.

By **"heavy ions"** we mean gold Au^{197} (the only stable isotope in natural gold, and a favorite of BNL) or lead Pb^{208} (the double magic nucleus used at CERN). Some experiments with uranium U has been also done, but not because of its size but rather due to its strong deformation.

Collision centrality in physics is defined usually via an *impact parameter* b, the minimal distance between the centers of two objects. It is a classical concept, and in quantum mechanics channels with *integer* angular momentum $l = L/\hbar$ (in units of Plank constant) are used. However, collisions at very high energy have high angular momentum and uncertainty in b is small. Standard way of thinking about centrality is to divide any observed distribution – e.g. over the multiplicity P_n – into the so called *centrality classes*, histogram bins with a fixed fraction of events rather than width. For example, many plots in the review say something like "centrality 20-30%": This means that total sum $\sum_n P_n$ is taken to be 100%, the events are split into say 10 bins, numerated 0-10,10-20,20-30 etc %, and only events from a particular one are used on the plot under consideration. The most central bins have the largest multiplicity and are always recorded, the more peripheral ones (say 80-100%) often are not used or even recorded. While the observables – like mean multiplicity – decreases with centrality b monotonically, it is not true for individual events. Multiple possible definitions of the centrality classes may sound complicated, but it is not, and simple models like Glauber nucleon scattering give quite good description of all these distributions, so in practice any centrality measure can safely be used.

The number of participant nucleons N_p plus the number of "spectators" is the total number of nucleons $2A$. The number of spectators (usually only the neutrons) propagating along the beam direction are typically recorded by special small-angle calorimeters in both directions. Two-dimensional distributions over signals of both such calorimeters are cut into bins of special shapes, also in a way that each bin keeps fixed percentage of the total. Small corrections for nucleons suffering only small angle elastic and diffractive scatterings – not counted as "participants" are also made.

Overlap region is a region in the transverse space in which the participant nucleons are located at the moment of the collision. Note that dues to relativistic contraction, high energy nuclei can be viewed as purely 2-d object, with longitudinal size reduced practically to zero: therefore the collision moment is well defined and is the same for all nucleons.

Flow harmonics are Fourier coefficient of the expansion in azimuthal angle ϕ

$$\frac{dN}{dydp_\perp^2 d\phi} = \frac{dN}{dydp_\perp^2}\left[1 + 2\sum_m v_m(p_\perp)cos(m\phi)\right] \quad \text{(A1)}$$

Its measurements require knowing the direction of the impact parameter vector $\vec{b}$, from which the azimuthal angle ϕ is counted. The direction of $\vec{b}$ and the beam define the so called *collision plane*. The direction of $\vec{b}$ in transverse plane is traditionally denoted by x, the orthogonal direction by y and the beam direction by z.

In practice this either comes from separate "near beam" calorimeters, recording "spectator" nucleons, or from correlation with other particles. The flow harmonics are often introduced as a response on the system to the asymmetry parameters ϵ_m describing Fourier components of matter distribution in ϕ. Note that v_m relates to momentum distribution and ϵ_m to that in space: connection between the two is non-trivial.

Collectivity of flow. Flow harmonics were originally derived from 2-particle correlations in relative angle, to which they enter as mean square

$$v_n^2\{2\} = < e^{in(\phi_1-\phi_2)} > = < |v_n|^2 > \quad \text{(A2)}$$

Alternatively, it can be derived from multi-hadron correlation functions: for example those for 4 and 6 particles mostly used are

$$v_n^4\{4\} = 2 < |v_n|^2 >^2 - < |v_n|^4 > \quad \text{(A3)}$$

$$v_n^6\{6\} = \frac{1}{4}(< |v_n|^6 > -9 < |v_n|^2 >< |v_n|^4 > +12 < |v_n|^2 >^3) \quad \text{(A4)}$$

By "collectivity" one mean the fact that all of such measurements produce nearly the same values of the harmonic v_n. In contrast to that, the "non-flow" effects – e.g. production of resonances – basically only affect the binary correlator $v_n\{2\}$ but not the others.

Soft and hard secondaries mentioned in the main text indicate their dynamical origin. "Soft" come from thermal heat bath, modified by collective flows, while the "hard" ones from partonic reactions and jet decay. The boundary is not well established and depend on the reaction: "soft" are with $p_\perp < 4\,GeV$ while "hard" is perhaps with $p_\perp < 10\,GeV$.

Rapidity y is defined mostly for longitudinal motion, via the longitudinal velocity being $v_z = tanh(y)$. There is also the so called space-time rapidity $\eta = (1/2)log[(t+z)/(t-z)]$ (which should not be mixed with viscosity, also designated by η) used in hydrodynamics. Both transform additively under the longitudinal Lorentz boost.

Sometimes one also uses transverse rapidity, $v_\perp = tanh(y_\perp)$. Pseudorapidity variable is an approximate substitute for rapidity y, used when particle identification is not available.

Chemical and kinetic freezeouts refer to stages of the explosion at which the rates of the *inelastic* and *elastic* collisions become smaller than the rate of expansion. The chemical freezeout is called so because at this stage particle composition, somewhat resembling a chemical composition of matter, is finalized. The kinetic or final freezeout is where the last rescattering happen: it is similar to photosphere of the Sun or to CMB photon freezeout in cosmology. The time-like surfaces of the chemical and kinetic freezeouts are usually approximated by isotherms with certain temperatures. The final particle spectrum is usually defined as the so called Cooper-Frye integral of thermal distribution over the kinetic freezeout surface.

Femtoscopy or HBT interferometry method came from radio astronomy: HBT is abbreviation for Hanbury-Brown and Twiss who developed it there. The influence of Bose symmetrization of the wave function of the observed mesons in particle physics was first emphasized in (Goldhaber *et al.*, 1960) and applied to proton-antiproton annihilation. Its use for the determination of the size/duration of the particle production processes had been proposed back in 1970's (Kopylov and Podgoretsky, 1974; Shuryak, 1973). With the advent of heavy ion collisions this "femtoscopy" technique had grew into a large industry. Early applications for RHIC heavy ion collisions were in certain tension with the hydrodynamical models, although this issue was later resolved, see e.g. (Pratt, 2009).

QCD thermodynamics on the lattice is the calculation of the thermodynamical observables from the first principles, the QCD Lagrangian, using numerical simulations of he gauge and quark fields discretized on a 4-dimensional lattice in Euclidean time. For a recent review see e.g.(Ding *et al.*, 2015), from which we took Fig. 64. The first thing to note is that quantities plotted are all normalized to corresponding powers of the temperature given by its dimension: so scale-invariant matter corresponds to T-independent constants at this plot. An indeed, the curves seem to approach constant at its right side (high T). The second thing to note is that these constants seem to be lower than the dashed line at high temperatures, corresponding to a non-interacting quark-gluon gas. Interesting that the value for infinitely strongly interacting supersymmetric plasma is predicted to be 3/4 of this non-interacting value.

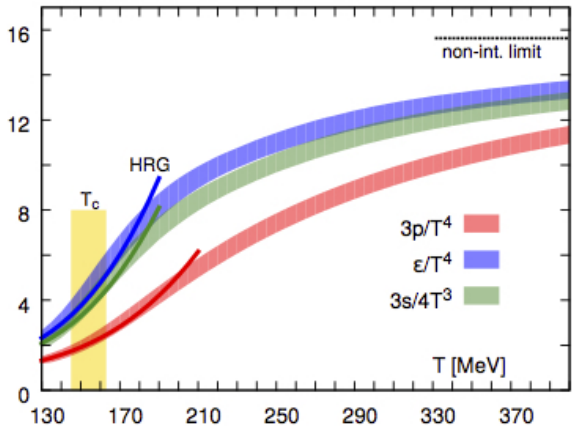

FIG. 64 Continuum extrapolated results for pressure, energy density and entropy density obtained with the HISQ action. Solid lines on the low temperature side correspond to results obtained from hadron resonance gas (HRG) model calculations. The (yellow) band marked T_c indicate the phase transition region for deconfinement and chiral symmetry restoration.

Confinement and deconfinement: The term is an abbreviated version of "color-electric confinement phenomenon", a condition that any object with (electric) color charge cannot be in the spectrum of states in the QCD vacuum, since it must be produced accompanied by a flux tube which carries the electric flux to another – oppositely color charged – object. These flux tubes are dual to those observed in superconductors: they carry electric flux, not a magnetic one. Stability of flux tubes in superconductors against transverse expansion is produced by a "coil" with *supercurrent*, made by (electrically charged) Cooper pairs running around the tube. The QCD flux tubes also have a coil with supercurrent around them, also dual, made by magnetically

charged objects. Detailed studies of these tubes has been made by lattice numerical simulations. Also like superconductivity, confinement goes away at sufficiently large temperatures $T > T_c$: this phenomenon is called "deconfinement".

Chiral symmetry breaking and restoration: The quark mass term is the only one in QCD Lagrangian connecting right- and left-handed polarizations of the quark fields. For light u, d, s quarks one can, as an approximation, neglect the masses: in this case $U(3)$ flavor rotation symmetry is doubled to $U(3)_{left} \times U(3)_{right}$ larger symmetry. Extra new symmetry created by relative counter-rotations of left and right parts is known as the *chiral symmetries*, divided into an overall phase $U(1)_{axial}$ and rotations $SU(3)_{axial}$. The former one is not actually a symmetry since it is violated by axial anomaly (instantons). The second one is broken *spontaneously* in the QCD vacuum, by quark-antiquark pairing. At sufficiently high temperatures $T > T_\chi$ the condensate created by pairing disappears, this phenomenon is called "chiral symmetry restoration". In real-world QCD with quarks we have it turned out that T_c of deconfinement and T_χ are too close to tell the difference, so both are mentioned in the text simply as T_c. However, for QCD-like theories with different number or color charge of the quarks lattice studies had found that these two phase transition can be separate, sometimes by a large factor.

Temperature range scanned in heavy ion experiments The matter produced at RHIC/LHC has the initial temperature $T \approx 2T_c$, and the final one, at the kinetic freezeouts of the largest systems, is low as $T \approx 0.5T_c$. Thus the near-T_c phenomena play a very significant role.

Appendix B: Relativistic hydrodynamics

Describe collective effects which are absent in elementary processes, like say e^+e^- annihilation into hadrons or (min.bias) pp collisions. The explosion seen in heavy ion collisions are often called "The little Bang", in analogy to the "Big Bang" in cosmology, with which it shares many concepts. One of them is an idea of "smooth average behavior" on top of which there "perturbations", different on event-by-even basis in the little Bang and on specific location in the Big Bang. The former is described by "full hydrodynamics" and the latter, sometimes, by a linearized version on top of the smooth solution.

The conceptual basis of the hydrodynamics is very simple: it is just a set of local conservation laws for the stress tensor ($T^{\mu\nu}$) and for the conserved currents (J_i^μ),

$$\begin{aligned} \partial_\mu T^{\mu\nu} &= 0 \\ \partial_\mu J_i^\mu &= 0 \end{aligned} \tag{B1}$$

In equilibrium, $T^{\mu\nu}$ and J_i^μ are related to the bulk properties of the fluid by the relations,

$$\begin{aligned} T^{\mu\nu} &= (\epsilon + p)u^\mu u^\nu - p g^{\mu\nu} \\ J_i^\mu &= n_i u^\mu \end{aligned} \tag{B2}$$

Here ϵ is the energy density, p is the pressure, n_i is the number density of the corresponding current, and $u^\mu = \gamma(1, \mathbf{v})$ is the proper velocity of the fluid. In strong interactions, the conserved currents are isospin (J_I^μ), strangeness (J_S^μ), and baryon number (J_B^μ). For the hydrodynamic evolution, isospin symmetry is assumed and the net strangeness is set to zero; therefore only the baryon current J_B is considered below.

In order to close up this set of equations, one needs also the equation of state (EoS) $p(\epsilon)$. One should also be aware of two thermodynamical differentials

$$d\epsilon = T ds \qquad dp = s dT \tag{B3}$$

and the definition of the sound velocity

$$c_s^2 = \frac{\partial p}{\partial \epsilon} = \frac{s}{T}\frac{\partial T}{\partial s} \tag{B4}$$

and that $\epsilon + p = Ts$. Using these equations and the thermodynamical relations in the form

$$\frac{\partial_\mu \epsilon}{\epsilon + p} = \frac{\partial_\mu s}{s} \tag{B5}$$

one may show that these equations imply another non-trivial conservation law, namely, the conservation of the entropy

$$\partial_\mu (s u_\mu) = 0 \tag{B6}$$

Therefore in the idealized adiabatic flow all the entropy is produced only in the discontinuities such as shock waves.

In an arbitrary coordinate system the equations of motion can be written as

$$T^{mn}{}_{;m} = 0\,, \qquad j^m{}_{;m} = 0\,, \tag{B7}$$

where the semicolon indicates a covariant derivative. For tensors of rank 1 and 2 it reads explicitly

$$j^i_{;p} = j^i_{,p} + \Gamma^i_{pk} j^k\,, \tag{B8}$$

$$T^{ik}{}_{;p} = T^{ik}{}_{,p} + \Gamma^i_{pm} T^{mk} + \Gamma^k_{pm} T^{im}\,, \tag{B9}$$

where the comma denotes a simple partial derivative and the Christoffel symbols Γ^s_{ij} are given by derivatives of the metric tensor $g^{ab}(x)$:

$$\Gamma^s_{ij} = (1/2) g^{ks}\big(g_{ik,j} + g_{jk,i} - g_{ij,k}\big)\,. \tag{B10}$$

As an example, let us do the following transformation from Cartesian to light cone coordinates:

$$x^\mu = (t, x, y, z) \longrightarrow \bar{x}^m = (\tau, x, y, \eta)$$

$$t = \tau \cosh\eta \qquad \tau = \sqrt{t^2 - z^2} \tag{B11}$$

$$z = \tau \sinh\eta \qquad \eta = (1/2)\ln\frac{t+z}{t-z}\,. \tag{B12}$$

In the new coordinate system the velocity field (after inserting $v_z = z/t$) is given by

$$\bar{u}^m = \bar{\gamma}(1, \bar{v}_x, \bar{v}_y, 0) \tag{B13}$$

with $\bar{v}_i \equiv v_i \cosh\eta$, $i = x, y$, and $\bar{\gamma} \equiv 1/\sqrt{1-\bar{v}_x^2-\bar{v}_y^2}$.

Now we turn to the metric of the new system. We have

$$\begin{aligned} ds^2 = g_{\mu\nu}dx^\mu dx^\nu &= dt^2 - dx^2 - dy^2 - dz^2 \\ &= d\tau^2 - dx^2 - dy^2 - \tau^2 d\eta^2 \end{aligned} \tag{B14}$$

and therefore

$$g_{mn} = \begin{pmatrix} 1 & 0 & 0 & 0 \\ 0 & -1 & 0 & 0 \\ 0 & 0 & -1 & 0 \\ 0 & 0 & 0 & -\tau^2 \end{pmatrix}, \tag{B15}$$

The only non-vanishing Christoffel symbols are

$$\Gamma^\eta_{\eta\tau} = \Gamma^\eta_{\tau\eta} = \frac{1}{\tau}, \qquad \Gamma^\tau_{\eta\eta} = \tau\,. \tag{B16}$$

Dissipative corrections to the stress tensor and the current can be written as follows

$$\delta T_{\mu\nu} = \eta(\nabla_\mu u_\nu + \nabla_\nu u_\mu - \frac{2}{3}\Delta_{\mu\nu}\nabla_\rho u_\rho) + \xi(\Delta_{\mu\nu}\nabla_\rho u_\rho) \tag{B17}$$

$$\delta J_\mu = k(\frac{\eta T}{\epsilon + p})^2 \nabla_\mu(\mu_B/T) \tag{B18}$$

where the three coefficients η, ξ, k are called the shear and the bulk viscosities and the heat conductivity, respectively. In this equation the following projection operator onto the matter rest frame was used:

$$\nabla_\mu \equiv \Delta_{\mu\nu}\partial_\nu, \;\; \Delta_{\mu\nu} \equiv g_{\mu\nu} - u_\mu u_\nu \tag{B19}$$

It is further useful to relate the magnitude of the viscosity coefficient η to a more physical observable. As such one can use the sound attenuation length. If a sound wave have frequency ω and the wave vector $\vec{q}$, its dispersion law (the pole position) is

$$\omega = c_s q - \frac{i}{2}\vec{q}^2\Gamma_s, \qquad \Gamma_s \equiv \frac{4}{3}\frac{\eta}{\epsilon + p} \tag{B20}$$

Navier-Stokes term is the first order expansion in gradients: it has some issues with causality and in practice some second-order hydrodynamic equations are used, for more information see e.g. (Romatschke, 2010). Attempts to do resummation of all gradient terms (Lublinsky and Shuryak, 2009) are discussed in the section on holography.

The original Landau paper focused on "longitudinal" flow and what we now call rapidity distribution. In heavy ion domain we focus mostly on a "splash" in the transverse plane: a collective transverse velocity of up to $.8\,c$ is observed, and thus it also require relativistic hydrodynamics.

1. Bjorken flow

The idea of rapidity-independent "scaling" distribution of secondaries originates from Feynman's early discussion of the parton model, around 1970. The existence of rapidity-independent hydrodynamic solution was perhaps first noticed by Landau, who used rapidity variable in his classic paper, as a somewhat trivial case. The space-time picture connected with such scaling regime was discussed in refs (Chiu *et al.*, 1975; Gorenshtein *et al.*, 1978) before Bjorken's famous paper (Bjorken, 1983) in which the solution was spelled out explicitly.

It is instructive first to describe it in the original Cartesian coordinates. There is no dependence on transverse coordinates x, y, only on time t and longitudinal coordinate z. The 1+1d equations $\partial_\mu T^{\mu\nu} = 0$ can be re-written in the following way

$$\frac{\partial}{\partial t}(s\,\cosh y) + \frac{\partial}{\partial z}(s\,\sinh y) = 0 \tag{B21}$$

$$\frac{\partial}{\partial t}(T\,\sinh y) + \frac{\partial}{\partial z}(T\,\cosh y) = 0 \tag{B22}$$

where $u_\mu = (cosh(y), sinh(y)$, and T, s are the temperature and the energy density. The first equation manifests the entropy conservation.

The central point is the 1-d-Hubble ansatz for the 4-velocity

$$u_\mu = (t, 0, 0, z)/\tau \tag{B23}$$

where $\tau^2 = t^2 - z^2$ is the proper time. Note that all volume elements are expanded linearly with time and move along straight lines from the collision point. The spatial $\eta = \tanh^{-1}(z/t)$ and the momentum rapidities $y = \tanh^{-1} v$ are just equal to each other. Exactly as in the Big Bang, for each "observer" (the volume element) the picture is just the same, with the pressure from the left compensated by that from the right. The history is also the same for all volume elements, if it is expressed in its own proper time τ. Thus one has $s(\tau), T(\tau)$. Using this ansatz, the entropy conservation becomes an ordinary differential equation in proper time τ

$$\frac{ds(\tau)}{d\tau} + \frac{s}{\tau} = 0 \tag{B24}$$

with an obvious solution

$$s = \frac{const}{\tau} \tag{B25}$$

So far all dissipative phenomena were ignored. Including first dissipative terms into our equations one finds the following source for the entropy current

$$\frac{1}{\epsilon + p}\frac{d\epsilon}{d\tau} = \frac{1}{s}\frac{ds}{d\tau} = -\frac{1}{\tau}\left(1 - \frac{(4/3)\eta + \xi}{(\epsilon + p)\tau}\right) \tag{B26}$$

with shear and bulk viscosities η, ξ, which tells us that one has to abandon ideal hydrodynamics at sufficiently early time.

Alternatively, one can start with curved coordinates τ, η from the beginning, and look for η-independent solution. Those are co-moving coordinates, in those $u_\mu = (1, 0, 0, 0)$ but the equations obtain extra term from Christoffel symbols.

2. Gubser flow

The Gubser flow (Gubser, 2010; Gubser and Yarom, 2011) is a solution which keeps the boost-invariance and the axial symmetry in the transverse plane of the Bjorken flow, but replaces the translational invariance in the transverse plane by symmetry under special conformal transformation. Therefore, one restriction is that the matter is required to be conformal, with the EOS $\epsilon = 3p$. Another is that the colliding systems has to be of a particular shape, corresponding to conformal map of the sphere onto the transverse plane.

The solution of ideal hydrodynamics has three parameters: One is dimensional q, it defines the size of the system (and is roughly corresponding to the radii of the colliding nuclei). The other two are dimensionless, f^* characterizes the number of degrees of freedom in the matter, and $\hat{\epsilon}_0$ the amount of entropy in the system.

The original setting uses the coordinates we used above, the proper time -spatial rapidity - transverse radius - azimuthal angle $(\bar{\tau}, \eta, \bar{r}, \phi)$ with the metric

$$ds^2 = -d\bar{\tau}^2 + \bar{\tau}^2 d\eta^2 + d\bar{r}^2 + \bar{r}^2 d\phi^2, \qquad \text{(B27)}$$

The dimensionless coordinates $\bar{\tau} = q\tau, \bar{r} = qr$ are rescaled versions of the actual coordinates.

Looking for solutions independent on both "angles" η, ϕ and using transverse rapidity

$$u_\mu = (-\cosh\kappa(\tau, r), 0, \sinh\kappa(\tau, r), 0) \qquad \text{(B28)}$$

Gubser obtained the following solution

$$v_\perp = \tanh\kappa(\tau, r) = \left(\frac{2q^2\tau r}{1 + q^2\tau^2 + q^2 r^2}\right) \qquad \text{(B29)}$$

$$\epsilon = \frac{\hat{\epsilon}_0 (2q)^{8/3}}{\tau^{4/3}\left(1 + 2q^2(\tau^2 + r^2) + q^4(\tau^2 - r^2)^2\right)^{4/3}} \qquad \text{(B30)}$$

where $\hat{\epsilon}_0$ is the second parameter. In (Gubser and Yarom, 2011) Gubser and Yarom re-derived the same solution by going into the co-moving frame. In order to do so they rescaled the metric

$$ds^2 = \tau^2 d\hat{s}^2 \qquad \text{(B31)}$$

and performed a coordinate transformation from the τ, r to a new set ρ, θ given by:

$$\sinh\rho = -\frac{1 - q^2\tau^2 + q^2 r^2}{2q\tau} \qquad \text{(B32)}$$

$$\tan\theta = \frac{2qr}{1 + q^2\tau^2 - q^2 r^2} \qquad \text{(B33)}$$

In the new coordinates the rescaled metric reads:

$$d\hat{s}^2 = -d\rho^2 + \cosh^2\rho\left(d\theta^2 + \sin^2\theta d\phi^2\right) + d\eta^2 \qquad \text{(B34)}$$

and we will use ρ as the "new time" coordinate and θ as a new "space" coordinate. In the new coordinates the fluid is at rest.

The relation between the velocity in Minkowski space in the (τ, r, ϕ, η) coordinates and the one in the rescaled metric in $(\rho, \theta, \phi, \eta)$ coordinates corresponds to:

$$u_\mu = \tau \frac{\partial \hat{x}^\nu}{\partial \hat{x}^\mu} \hat{u}_\nu \,, \qquad \text{(B35)}$$

while the energy density transforms as: $\epsilon = \tau^{-4}\hat{\epsilon}$.

The temperature (in the rescaled frame, $\hat{T} = \tau f_*^{1/4} T$, with $f_* = \epsilon/T^4 = 11$ as in (Gubser, 2010)) is now dependent only on the new time ρ, in the case with nonzero viscosity the solution is

$$\hat{T} = \frac{\hat{T}_0}{(\cosh\rho)^{2/3}} + \frac{H_0 \sinh^3\rho}{9(\cosh\rho)^{2/3}} \, {}_2F_1\left(\frac{3}{2}, \frac{7}{6}; \frac{5}{2}, -\sinh^2\rho\right) \qquad \text{(B36)}$$

where H_0 is a dimensionless constant made out of the shear viscosity and the temperature, $\eta = H_0 T^3$ and ${}_2F_1$ is the hypergeometric function. In the inviscid case the solution is just the first term of expression (B36), and of course it also conserves the entropy in this case. The picture of the explosion is obtained by transformation from this expression back to τ, r coordinates.

Small perturbations to the Gubser flow obey linearized equations which have also been derived in (Gubser and Yarom, 2011). We start with the zero viscosity case, so that the background temperature (now to be called T_0) will be given by just the first term in (B36). The perturbations over the previous solution are defined by

$$\hat{T} = \hat{T}_0(1 + \delta) \qquad \text{(B37)}$$

$$u_\mu = u_{0\,\mu} + u_{1\mu} \qquad \text{(B38)}$$

with

$$\hat{u}_{0\,\mu} = (-1, 0, 0, 0) \qquad \text{(B39)}$$

$$\hat{u}_{1\mu} = (0, u_\theta(\rho, \theta, \phi), u_\phi(\rho, \theta, \phi), 0) \qquad \text{(B40)}$$

$$\delta = \delta(\rho, \theta, \phi) \qquad \text{(B41)}$$

Plugging expressions (B37),(B38) into the hydrodynamic equations and only keeping linear terms in the perturbation, one can get a system of coupled 1-st order differential equations. Furthermore, if one ignores the viscosity terms, one may exclude velocity and get the

following (second order) closed equation for the temperature perturbation.

$$\frac{\partial^2\delta}{\partial\rho^2}-\frac{1}{3\cosh^2\rho}\left(\frac{\partial^2\delta}{\partial\theta^2}+\frac{1}{\tan\theta}\frac{\partial\delta}{\partial\theta}+\frac{1}{\sin^2\theta}\frac{\partial^2\delta}{\partial\phi^2}\right)+\frac{4}{3}\tanh\rho\frac{\partial\delta}{\partial\rho}=0 \quad \text{(B42)}$$

(Since the initial perturbations are assumed to be rapidity-independent, we also ignored this coordinate here.)

It has a number of remarkable properties: all 4 coordinates can be separated $\delta(\rho,\theta,\phi)=R(\rho)\Theta(\theta)\Phi(\theta)$ and a general solution is given by

$$\begin{aligned}R(\rho)&=\frac{C_1}{(\cosh\rho)^{2/3}}P^{2/3}_{-\frac{1}{2}+\frac{1}{6}\sqrt{12\lambda+1}}(\tanh\rho)\\&\quad+\frac{C_2}{(\cosh\rho)^{2/3}}Q^{2/3}_{-\frac{1}{2}+\frac{1}{6}\sqrt{12\lambda+1}}(\tanh\rho\\\Theta(\theta)&=C_3P^m_l(\cos\theta)+C_4Q^m_l(\cos\theta)\\\Phi(\phi)&=C_5e^{im\phi}+C_6e^{-im\phi}\end{aligned} \quad \text{(B43)}$$

where $\lambda=l(l+1)$ and P and Q are associated Legendre polynomials. The part of the solution depending on θ and ϕ can be combined in order to form spherical harmonics $Y_{lm}(\theta,\phi)$, such that $\delta(\rho,\theta,\phi)\propto R_l(\rho)Y_{lm}(\theta,\phi)$. This property should have been anticipated, as one of the main ideas of Gubser has been to introduce a coordinate which together with ϕ make a map on a 2-d sphere.

Gubser flow was used as a theoretical laboratory ever since. A complete Green function has been constructed (Staig and Shuryak, 2011b), leading to pictures of sound circles we discussed at the beginning of this review. Generalization to perturbations by the quenching jets, with the sounds propagating in the rapidity direction, was done in (Shuryak and Staig, 2013a). For the second order (the Israel-Stuart version) of the hydrodynamics in it has been done in (Marrochio *et al.*, 2015; Pang *et al.*, 2015). Boltzmann equation (in tau-approximation) has also been solved in such setting, see (Denicol *et al.*, 2014) and discussion in section IV.C.

There are also a number of phenomenological applications. Without going into those, Let us just comment that those are limited by the fact that at large r the power tail of the solution is completely inadequate for heavy ion collisions. So to say, Gubser solution is like an explosion in atmosphere, while the real ones are in vacuum. As a result, in applications one basically needs to amputate the unphysical regions by hand.

Appendix C: Introduction to gauge-gravity duality

The starting point of this development was (i) the discovery AdS/CFT correspondence (Maldacena, 1999), which a decade later became an important tool of the Nuclear Theorists, as well as a prime examples of the "applications" in the string theory community. Here we briefly outline for non-specialists the logics of several important developments, whose understanding is needed to understand the main text section devoted to gauge-gravity calculations. Those include (ii) the thermodynamics of strongly coupled N=4 plasma (**?**) and (iii) the transport properties derived from the linearized hydrodynamics, (**?**). Another significant achievement (iv) was general derivation of the full nonlinear hydrodynamics, from the gradient expansion of the Einstein equations in (Natsuume and Okamura, 2008; **?**; **?**).

(i) The AdS/CFT correspondence has been discovered in studies of certain string theory construction. While strings have one coordinate along them, and thus their world-volume has co-dimension 2, usually parametrized by "internal coordinates" τ,σ, their dynamics is for certain consistency reasons is studied in space-times with much higher number of "external dimensions" D. String theory actually admit solitons called "branes" with certain intermediate number of dimensions, e.g. D_3 branes with 3+1 internal dimensions. The original construction contained N_c such D_3 branes stacked together at the same location in $D=10$space-time.

Closed string massless excitations are known to include states with spin up to 2, described by certain supergravity. At large N_c the original stack generates a strong gravity described by classical GR. A particular solution of Einstein equation called $AdS_5\times S^5$ where AdS_5 is anti-de-Sitter 5-dimensional space and S^5 is a 5-dimensional sphere. The metric of AdS_5 does not depend on 4 coordinates of the brane space-time, but only on the 5-th coordinate called z, and at $z=0$ it has a 4-dimensional boundary. Maldacena (Maldacena, 1999) had conjectured that since symmetries of conformal $\mathcal{N}$=4 supersymmetric Yang-Mills (SYM) theory on this 4-d boundary and of the AdS_5 solution match uniquely, there must be certain "holographic" correspondence between them. In particular, gauge invariant colorless operators in the boundary theory (e.g. the stress tensor $T_{\mu\nu}$) should be related to fields in the 5-dimensional "bulk" (such as the metric $g_{\mu\nu}$). Testing the conjecture was popular occupation in late 1990's: people calculated correlators in the $\mathcal{N}$=4 SYM theory and compared those with gravity calculations of certain propagators and multi-point Green functions: all tests were positive and the conjecture were considered true. The important observation is that in certain limit the gauge theory has infinite 't Hooft coupling $\lambda=g^2N_c$ while the bulk theory is weakly coupled, since bulk fields are uncolored.

This discovery created large industry, which is divided into two directions. The"top down" one looks for exact correspondence involving theories other than the $\mathcal{N}$=4 SYM theory: yet it seems to be impossible to find sufficiently convenient correspondence for non-supersymmetric QCD-like theories. The " down up" approach, also known as AdS/QCD, builds holographic

models for any theories, without string theory solution in the background. For a review of this approach see e.g. (Gursoy and Kiritsis, 2008). One bulk field in 5-d – dilatons or gravity – generates many "radial excitations" of hadrons and their Regge trajectories. Such models include confinement and chiral symmetry breaking, and to certain accuracy they do reproduce the spectroscopy of mesons and glueballs.

(ii) The AdS_5 GR solution resembles Schwarzschiled one for a black hole, with obvious change of 4-d Coulomb factors to 6-d ones: these 6 dimensions are what is left from 10 dimensions minus 4 on which no dependence is present. But the main difference is that string theory branes happen to have charges which make them "charged black holes", with certain vector fields added. Moreover, they are "extreme" black holes, with maximal allowed charge, as a result of which their horizon area (and thus entropy) vanishes. This is how it msy be, since we intend to describe a vacuum state of the gauge theory on the boundary, and it should not be degendrate and have any entropy.

It was further found that excited states of the brane construction are described by non-extreme black holes with a nonzero horizon. Since metric still depends on the 5-th coordinate only, the horizon sits at some value z_h, and the physical region ranges from $z = 0$ to z_h. Schwarzschiled black holes emit Hawking radiation, and in 4d flat Universe they therefore must eventually emit all their energy and disapper. The "black brane" AdS_5 GR solution has a different fate: Hawking radiation heats up the Universe, including to its boundary, to certain equilibrium static case.

Projecting this solution to gauge theory one finds thermodynamics of strongly coupled N=4 plasma at nonzero temperature T. Unlike QCD-like theories (which develops scale Λ_{QCD} via running coupling), the N=4 SYM has zero beta function and thus has no scale of its own. So its properties must obey trivial scaling given by the dimension, e.g. the energy density can only be $\epsilon = C(g)T^4$ with some dimensionless coefficient depending on the coupling. At zero coupling one has non-interacting gas or Stephan-Botzmann generalization of thermal radiation famously explained by Plank. It was found that (Gubser *et al.*, 1996)

$$C(g^2N_c \to \infty) = \frac{3}{4}C(0) \tag{C1}$$

The coefficient 3/4 is in fact in better agreement with lattice equation of state, than 1 of ideal QGP.

(iii) The transport properties of derived in a number of ways. Small perturbations around thermal AdS solution are elementary excitations of static plasma, such as sounds or transverse dissipative modes. Linearized perturbations of Einstein equations in the bulk corres pond to solutions of the linearized hydrodynamics on the boundary theory. Therefore one can find (Policastro *et al.*, 2001) the dissipation rate of these modes and thus the *shear viscosity*. (Bulk viscosity is zero because of scale-invariance.) Since its dimension T^3 is the same as entropy density, people quote the famous value of their ratio

$$\frac{\eta}{s}|_{g^2N_c\to\infty} = \frac{1}{4\pi} \tag{C2}$$

In gravity setting it is clear what happens: the excitaions are gravity waves which are simply falling into the black hole. On the gauge theory side we have no intuition of how this small number appears, but it is not far from experiment!

(iv) In the 19th century the hydrodynamics was a very advanced theoretical field, teaching how to work with partial differential equations, potentials and rotational flows. Stokes was one of Maxwell's teachers, and electrodynamics clearly has benefited from hydrodynamical methods. Landau had introduced relativistic hydrodynamics into the field of high energy collisions. Yet from 1970's to about 2000, hydrodynamics was ridiculed by high energy theorists, as simplistic approach incompatible with QCD and QFT's in general.

Apparently, this is no longer so, and one is allowed to mention it in high society. In particular, relativistic hydrodynamics of strongly coupled N=4 plasma was derived by (Natsuume and Okamura, 2008; **?**) as a solution to Einstein equation with gradient expansion method. If the scale of inhomogenuity R is large compare to the horizon location z_h, one can think of smoothly varying horizon $z_h(x^\mu), \mu = 0, 1, 2, 3$. This variation may or may not be small: in the latter case all nonlinear terms of hydrodynamics naturally appear as they should. And, last but not least, unlike phenomenological hydrodynamics (say, of water), all the kinetic coefficients, order by order, got their definite values! About a dozen of them have been calculated so far.

REFERENCES

Aamodt, K., *et al.* (ALICE) (2011a), Phys. Rev. **D84**, 112004, arXiv:1101.3665 [hep-ex].

Aamodt, K., *et al.* (ALICE) (2011b), Phys. Rev. Lett. **107**, 032301, arXiv:1105.3865 [nucl-ex].

Adcox, K., *et al.* (PHENIX) (2005), Nucl. Phys. **A757**, 184, arXiv:nucl-ex/0410003 [nucl-ex].

Ade, P. A. R., *et al.* (Planck) (2014), Astron. Astrophys. **571**, A15, arXiv:1303.5075 [astro-ph.CO].

Adler, S. S., *et al.* (PHENIX) (2014), Phys. Rev. **C89** (4), 044905, arXiv:1312.6676 [nucl-ex].

Alba, P., W. Alberico, R. Bellwied, M. Bluhm, V. Mantovani Sarti, and Nahrgang (2014), Phys. Lett. **B738**, 305, arXiv:1403.4903 [hep-ph].

Andronic, A., P. Braun-Munzinger, K. Redlich, and J. Stachel (2007), *Proceedings, 4th International Workshop on Critical point and onset of deconfinement (CPOD07)*, PoS **CPOD07**, 044, arXiv:0710.1851 [nucl-th].

Arean, D., I. Iatrakis, M. Jarvinen, and E. Kiritsis (2013), JHEP **11**, 068, arXiv:1309.2286 [hep-ph].

Arnold, P. B., G. D. Moore, and L. G. Yaffe (2003), JHEP **05**, 051, arXiv:hep-ph/0302165 [hep-ph].

Baier, R., A. H. Mueller, D. Schiff, and D. T. Son (2001), Phys. Lett. **B502**, 51, arXiv:hep-ph/0009237 [hep-ph].

Baker, M., J. S. Ball, and F. Zachariasen (1997), Phys. Rev. **D56**, 4400, arXiv:hep-ph/9705207 [hep-ph].

Balasubramanian, V., A. Bernamonti, J. de Boer, N. Copland, B. Craps, E. Keski-Vakkuri, B. Muller, A. Schafer, M. Shigemori, and W. Staessens (2011), Phys. Rev. **D84**, 026010, arXiv:1103.2683 [hep-th].

Basar, G., D. E. Kharzeev, and E. V. Shuryak (2014), Phys. Rev. **C90** (1), 014905, arXiv:1402.2286 [hep-ph].

Basar, G., D. E. Kharzeev, H.-U. Yee, and I. Zahed (2012), Phys. Rev. **D85**, 105005, arXiv:1202.0831 [hep-th].

Baar, G., and D. Teaney (2014), Phys. Rev. **C90** (5), 054903, arXiv:1312.6770 [nucl-th].

Bebie, H., P. Gerber, J. L. Goity, and H. Leutwyler (1992), Nucl. Phys. **B378**, 95.

Begun, V., W. Florkowski, and M. Rybczynski (2014), Phys. Rev. **C90** (1), 014906, arXiv:1312.1487 [nucl-th].

Bellwied, R. (STAR) (2005), *Nuclear physics. Proceedings, 22nd International Conference, INPC 2004, Goeteborg, Sweden, June 27-July 2, 2004*, Nucl. Phys. **A752**, 398.

Berges, J., K. Boguslavski, S. Schlichting, and R. Venugopalan (2015), arXiv:1508.03073 [hep-ph].

Bhalerao, R. S., and J.-Y. Ollitrault (2006), Phys. Lett. **B641**, 260, arXiv:nucl-th/0607009 [nucl-th].

Bhattacharyya, S., V. E. Hubeny, S. Minwalla, and M. Rangamani (2008), JHEP **02**, 045, arXiv:0712.2456 [hep-th].

Bjorken, J. D. (1982), .

Bjorken, J. D. (1983), Phys. Rev. **D27**, 140.

Bjorken, J. D., S. J. Brodsky, and A. Scharff Goldhaber (2013), Phys. Lett. **B726**, 344, arXiv:1308.1435 [hep-ph].

Blaizot, J.-P., Y. Mehtar-Tani, and M. A. C. Torres (2015), Phys. Rev. Lett. **114** (22), 222002, arXiv:1407.0326 [hep-ph].

Blaizot, J.-P., and J.-Y. Ollitrault (1990), Adv. Ser. Direct. High Energy Phys. **6**, 393.

Boulware, D. G., L. S. Brown, R. N. Cahn, S. D. Ellis, and C.-k. Lee (1976), Phys. Rev. **D14**, 2708.

Bozek, P. (2012), Phys. Rev. **C85**, 014911, arXiv:1112.0915 [hep-ph].

Bozek, P., and W. Broniowski (2014), Phys. Lett. **B739**, 308, arXiv:1409.2160 [nucl-th].

Brambilla, N., M. A. Escobedo, J. Ghiglieri, and A. Vairo (2013), JHEP **05**, 130, arXiv:1303.6097 [hep-ph].

Braun-Munzinger, P., J. Stachel, and C. Wetterich (2004), Phys. Lett. **B596**, 61, arXiv:nucl-th/0311005 [nucl-th].

de Cassagnac, R. (CMS) (2014), *Proceedings, 24th International Conference on Ultra-Relativistic Nucleus-Nucleus Collisions (Quark Matter 2014)*, Nucl. Phys. **A931**, 22.

Chatrchyan, S., *et al.* (CMS) (2013), Phys. Lett. **B718**, 795, arXiv:1210.5482 [nucl-ex].

Chatrchyan, S., *et al.* (CMS) (2014), Eur. Phys. J. **C74** (6), 2847, arXiv:1307.3442 [hep-ex].

Chesler, P. M., and L. G. Yaffe (2014), JHEP **07**, 086, arXiv:1309.1439 [hep-th].

Chiu, C. B., E. C. G. Sudarshan, and K.-H. Wang (1975), Phys. Rev. **D12**, 902.

Chiu, M., T. K. Hemmick, V. Khachatryan, A. Leonidov, J. Liao, and L. McLerran (2013), Nucl. Phys. **A900**, 16, arXiv:1202.3679 [nucl-th].

Csernai, L. P., F. Becattini, and D. J. Wang (2014), *Proceedings, 14th International Conference on Strangeness in Quark Matter (SQM 2013)*, J. Phys. Conf. Ser. **509**, 012054.

Csernai, L. P., J. Kapusta, and L. D. McLerran (2006), Phys. Rev. Lett. **97**, 152303, arXiv:nucl-th/0604032 [nucl-th].

D'Alessandro, A., M. D'Elia, and E. V. Shuryak (2010), Phys. Rev. **D81**, 094501, arXiv:1002.4161 [hep-lat].

Denicol, G. S., U. W. Heinz, M. Martinez, J. Noronha, and M. Strickland (2014), Phys. Rev. **D90** (12), 125026, arXiv:1408.7048 [hep-ph].

Ding, H.-T., F. Karsch, and S. Mukherjee (2015), Int. J. Mod. Phys. **E24** (10), 1530007, arXiv:1504.05274 [hep-lat].

Dirac, P. A. M. (1931), Proc. Roy. Soc. Lond. **A133**, 60.

Epelbaum, T. (2014), *Proceedings, 24th International Conference on Ultra-Relativistic Nucleus-Nucleus Collisions (Quark Matter 2014)*, Nucl. Phys. **A931**, 337.

Ewerz, C., P. Lebiedowicz, O. Nachtmann, and A. Szczurek (2016), Phys. Lett. **B763**, 382, arXiv:1606.08067 [hep-ph].

Farrar, G. R., and J. D. Allen (2013), *Proceedings, International Symposium on Future Directions in UHECR Physics (UHECR2012)*, EPJ Web Conf. **53**, 07007, arXiv:1307.2322 [hep-ph].

Fermi, E. (1951), Phys. Rev. **81**, 683.

Floerchinger, S., and U. A. Wiedemann (2011), JHEP **11**, 100, arXiv:1108.5535 [nucl-th].

Florkowski, W., and R. Ryblewski (2011), Phys. Rev. **C83**, 034907, arXiv:1007.0130 [nucl-th].

Florkowski, W., and R. Ryblewski (2014), *Proceedings, 24th International Conference on Ultra-Relativistic Nucleus-Nucleus Collisions (Quark Matter 2014)*, Nucl. Phys. **A931**, 343, arXiv:1407.3557 [hep-ph].

Gelman, B. A., E. V. Shuryak, and I. Zahed (2006a), Phys. Rev. **C74**, 044908, arXiv:nucl-th/0601029 [nucl-th].

Gelman, B. A., E. V. Shuryak, and I. Zahed (2006b), Phys. Rev. **C74**, 044909, arXiv:nucl-th/0605046 [nucl-th].

Goldhaber, G., S. Goldhaber, W.-Y. Lee, and A. Pais (1960), Phys. Rev. **120**, 300.

Gorda, T., and P. Romatschke (2014), Phys. Rev. **C90** (5), 054908, arXiv:1406.6405 [nucl-th].

Gorenshtein, M., V. A. Zhdanov, and Y. M. Sinjukov (1978), ZhET **74**, 833.

Gross, D. J., R. D. Pisarski, and L. G. Yaffe (1981), Rev. Mod. Phys. **53**, 43.

Grosse-Oetringhaus, J. F. (ALICE) (2014), *Proceedings, 24th International Conference on Ultra-Relativistic Nucleus-Nucleus Collisions (Quark Matter 2014)*, Nucl. Phys. **A931**, 22, arXiv:1408.0414 [nucl-ex].

Gubser, S. S. (2010), Phys. Rev. **D82**, 085027, arXiv:1006.0006 [hep-th].

Gubser, S. S., I. R. Klebanov, and A. W. Peet (1996), Phys. Rev. **D54**, 3915, arXiv:hep-th/9602135 [hep-th].

Gubser, S. S., S. S. Pufu, and A. Yarom (2008), Phys. Rev. **D78**, 066014, arXiv:0805.1551 [hep-th].

Gubser, S. S., S. S. Pufu, and A. Yarom (2009), JHEP **11**, 050, arXiv:0902.4062 [hep-th].

Gubser, S. S., and A. Yarom (2011), Nucl. Phys. **B846**, 469, arXiv:1012.1314 [hep-th].

Gursoy, U., and E. Kiritsis (2008), JHEP **02**, 032, arXiv:0707.1324 [hep-th].

Gursoy, U., E. Kiritsis, and F. Nitti (2008), JHEP **02**, 019, arXiv:0707.1349 [hep-th].

Heinz, U., and R. Snellings (2013), Ann. Rev. Nucl. Part.

Sci. **63**, 123, arXiv:1301.2826 [nucl-th].
Heller, M. P., R. A. Janik, and P. Witaszczyk (2012), Phys. Rev. **D85**, 126002, arXiv:1203.0755 [hep-th].
Hidaka, Y., and R. D. Pisarski (2008), Phys. Rev. **D78**, 071501, arXiv:0803.0453 [hep-ph].
Hirano, T., U. W. Heinz, D. Kharzeev, R. Lacey, and Y. Nara (2006), Phys. Lett. **B636**, 299, arXiv:nucl-th/0511046 [nucl-th].
Hirono, Y., and E. Shuryak (2015), Phys. Rev. **C91** (5), 054915, arXiv:1412.0063 [hep-ph].
't Hooft, G. (1974), Nucl. Phys. **B79**, 276.
't Hooft, G. (1978), Nucl. Phys. **B138**, 1.
Hung, C. M., and E. V. Shuryak (1998), Phys. Rev. **C57**, 1891, arXiv:hep-ph/9709264 [hep-ph].
Iatrakis, I., A. Ramamurti, and E. Shuryak (2015a), Phys. Rev. **D92** (1), 014011, arXiv:1503.04759 [hep-ph].
Iatrakis, I., A. Ramamurti, and E. Shuryak (2015b), Phys. Rev. **D92** (1), 014011, arXiv:1503.04759 [hep-ph].
Iatrakis, I., A. Ramamurti, and E. Shuryak (2016), Phys. Rev. **D94** (4), 045005, arXiv:1602.05014 [hep-ph].
Iritani, T., G. Cossu, and S. Hashimoto (2014), *Proceedings, 31st International Symposium on Lattice Field Theory (Lattice 2013)*, PoS **LATTICE2013**, 376, arXiv:1311.0218 [hep-lat].
Janik, R. A., and R. B. Peschanski (2006), Phys. Rev. **D73**, 045013, arXiv:hep-th/0512162 [hep-th].
Jia, J. (ATLAS) (2011), *Quark matter. Proceedings, 22nd International Conference on Ultra-Relativistic Nucleus-Nucleus Collisions, Quark Matter 2011, Annecy, France, May 23-28, 2011*, J. Phys. **G38**, 124012, arXiv:1107.1468 [nucl-ex].
Kaczmarek, O., and F. Zantow (2006), *Proceedings, 23rd International Symposium on Lattice field theory (Lattice 2005)*, PoS **LAT2005**, 192, arXiv:hep-lat/0510094 [hep-lat].
Kajantie, K., M. Laine, K. Rummukainen, and Y. Schroder (2003), Phys. Rev. **D67**, 105008, arXiv:hep-ph/0211321 [hep-ph].
Kalaydzhyan, T., and E. Shuryak (2014a), Phys. Rev. **C90** (1), 014901, arXiv:1404.1888 [hep-ph].
Kalaydzhyan, T., and E. Shuryak (2014b), arXiv:1407.3270 [hep-ph].
Kalaydzhyan, T., and E. Shuryak (2014c), Phys. Rev. **D90** (2), 025031, arXiv:1402.7363 [hep-ph].
Kalaydzhyan, T., and E. Shuryak (2015), Phys. Rev. **D91** (8), 083502, arXiv:1412.5147 [hep-ph].
Keegan, L., A. Kurkela, A. Mazeliauskas, and D. Teaney (2016), JHEP **08**, 171, arXiv:1605.04287 [hep-ph].
Khachatryan, V., *et al.* (CMS) (2010), JHEP **09**, 091, arXiv:1009.4122 [hep-ex].
Kharzeev, D. E. (2014), Phys. Rev. **D90** (7), 074007, arXiv:1409.2496 [hep-ph].
Kopylov, G. I., and M. I. Podgoretsky (1974), Sov. J. Nucl. Phys. **18**, 336, [Yad. Fiz.18,656(1973)].
Kovtun, P. (2012), *INT Summer School on Applications of String Theory Seattle, Washington, USA, July 18-29, 2011*, J. Phys. **A45**, 473001, arXiv:1205.5040 [hep-th].
Kovtun, P., G. D. Moore, and P. Romatschke (2011), Phys. Rev. **D84**, 025006, arXiv:1104.1586 [hep-ph].
Kovtun, P. K., and A. O. Starinets (2005), Phys. Rev. **D72**, 086009, arXiv:hep-th/0506184 [hep-th].
Kraan, T. C., and P. van Baal (1998), Phys. Lett. **B435**, 389, arXiv:hep-th/9806034 [hep-th].
Kuraev, E. A., L. N. Lipatov, and V. S. Fadin (1977), Sov. Phys. JETP **45**, 199, [Zh. Eksp. Teor. Fiz.72,377(1977)].
Kurkela, A., and Y. Zhu (2015), Phys. Rev. Lett. **115** (18), 182301, arXiv:1506.06647 [hep-ph].
Lacey, R. A., Y. Gu, X. Gong, D. Reynolds, N. N. Ajitanand, J. M. Alexander, A. Mwai, and A. Taranenko (2013), arXiv:1301.0165.
Laine, M., O. Philipsen, P. Romatschke, and M. Tassler (2007), JHEP **03**, 054, arXiv:hep-ph/0611300 [hep-ph].
Landau, L. D. (1953), Izv. Akad. Nauk Ser. Fiz. **17**, 51.
Lappi, T., A. Dumitru, and Y. Nara (2014), *Proceedings, 24th International Conference on Ultra-Relativistic Nucleus-Nucleus Collisions (Quark Matter 2014)*, Nucl. Phys. **A931**, 354, arXiv:1407.8549 [hep-ph].
Larsen, R., and E. Shuryak (2016), Phys. Rev. **D93** (5), 054029, arXiv:1511.02237 [hep-ph].
Lee, K.-M., and C.-h. Lu (1998), Phys. Rev. **D58**, 025011, arXiv:hep-th/9802108 [hep-th].
Liao, J., and E. Shuryak (2007), Phys. Rev. **C75**, 054907, arXiv:hep-ph/0611131 [hep-ph].
Liao, J., and E. Shuryak (2008), Phys. Rev. Lett. **101**, 162302, arXiv:0804.0255 [hep-ph].
Liao, J., and E. Shuryak (2009), Phys. Rev. Lett. **102**, 202302, arXiv:0810.4116 [nucl-th].
Liao, J., and E. Shuryak (2010), Phys. Rev. **D82**, 094007, arXiv:0804.4890 [hep-ph].
Lin, S., and E. Shuryak (2008a), Phys. Rev. **D77**, 085014, arXiv:0711.0736 [hep-th].
Lin, S., and E. Shuryak (2008b), Phys. Rev. **D78**, 125018, arXiv:0808.0910 [hep-th].
Lin, S., and E. Shuryak (2008c), Phys. Rev. **D77**, 085013, arXiv:hep-ph/0610168 [hep-ph].
Lin, S., and E. Shuryak (2009), Phys. Rev. **D79**, 124015, arXiv:0902.1508 [hep-th].
Lin, S., and E. Shuryak (2011), Phys. Rev. **D83**, 045025, arXiv:1011.1918 [hep-th].
Liu, Y., E. Shuryak, and I. Zahed (2015), Phys. Rev. **D92** (8), 085007, arXiv:1503.09148 [hep-ph].
Lublinsky, M., and E. Shuryak (2009), Phys. Rev. **D80**, 065026, arXiv:0905.4069 [hep-ph].
Lublinsky, M., and E. Shuryak (2011), Phys. Rev. **C84**, 061901, arXiv:1108.3972 [hep-ph].
Makhlin, A. N., and Yu. M. Sinyukov (1988), Z. Phys. **C39**, 69.
Maldacena, J. M. (1999), Int. J. Theor. Phys. **38**, 1113, [Adv. Theor. Math. Phys.2,231(1998)], arXiv:hep-th/9711200 [hep-th].
Mandelstam, S. (1976), *Phys. Rep. 23 (1976) 245-249, In *Gervais, J.L. (Ed.), Jacob, M. (Ed.): Non-linear and Collective Phenomena In Quantum Physics*, 12-16*, Phys. Rept. **23**, 245.
Marrochio, H., J. Noronha, G. S. Denicol, M. Luzum, S. Jeon, and C. Gale (2015), Phys. Rev. **C91** (1), 014903, arXiv:1307.6130 [nucl-th].
Martinez, M., and M. Strickland (2010), Phys. Rev. **C81**, 024906, arXiv:0909.0264 [hep-ph].
Matsui, T., and H. Satz (1986), Phys. Lett. **B178**, 416.
Mazeliauskas, A., and D. Teaney (2015), Phys. Rev. **C91** (4), 044902, arXiv:1501.03138 [nucl-th].
McLerran, L. D., and R. Venugopalan (1994), Phys. Rev. **D49**, 3352, arXiv:hep-ph/9311205 [hep-ph].
Mocsy, A., P. Petreczky, and M. Strickland (2013), Int. J. Mod. Phys. **A28**, 1340012, arXiv:1302.2180 [hep-ph].
Molnar, D., and P. Huovinen (2005), Phys. Rev. Lett. **94**, 012302, arXiv:nucl-th/0404065 [nucl-th].

Moore, G. D., and D. Teaney (2005), Phys. Rev. **C71**, 064904, arXiv:hep-ph/0412346 [hep-ph].

Nagle, J., A. Adare, S. Beckman, T. Koblesky, J. O. Koop, D. McGlinchey, P. Romatschke, J. Carlson, J. Lynn, and M. McCumber (2014), Phys. Rev. Lett. **113** (11), 112301, arXiv:1312.4565 [nucl-th].

Nakamura, A., and S. Sakai (2005), Phys. Rev. Lett. **94**, 072305, arXiv:hep-lat/0406009 [hep-lat].

Natsuume, M., and T. Okamura (2008), Phys. Rev. **D77**, 066014, [Erratum: Phys. Rev.D78,089902(2008)], arXiv:0712.2916 [hep-th].

Novikov, V. A., M. A. Shifman, A. I. Vainshtein, and V. I. Zakharov (1981), Nucl. Phys. **B191**, 301.

Pang, L.-G., Y. Hatta, X.-N. Wang, and B.-W. Xiao (2015), Phys. Rev. **D91** (7), 074027, arXiv:1411.7767 [hep-ph].

Policastro, G., D. T. Son, and A. O. Starinets (2001), Phys. Rev. Lett. **87**, 081601, arXiv:hep-th/0104066 [hep-th].

Polyakov, A. M. (1974), JETP Lett. **20**, 194, [Pisma Zh. Eksp. Teor. Fiz.20,430(1974)].

Polyakov, A. M. (1977), Nucl. Phys. **B120**, 429.

Pomeranchuk, I. Ya. (1951), Dokl. Akad. Nauk Ser. Fiz. **78**, 889.

Prakash, M., M. Prakash, R. Venugopalan, and G. Welke (1993), Phys. Rept. **227**, 321.

Pratt, S. (2009), Phys. Rev. Lett. **102**, 232301, arXiv:0811.3363 [nucl-th].

Prino, F., and R. Rapp (2016), arXiv:1603.00529 [nucl-ex].

Rapp, R., and E. V. Shuryak (2001), Phys. Rev. Lett. **86**, 2980, arXiv:hep-ph/0008326 [hep-ph].

Ratti, C., and E. Shuryak (2009), Phys. Rev. **D80**, 034004, arXiv:0811.4174 [hep-ph].

Romatschke, P. (2010), Int. J. Mod. Phys. **E19**, 1, arXiv:0902.3663 [hep-ph].

Romatschke, P. (2015), Eur. Phys. J. **C75** (9), 429, arXiv:1504.02529 [nucl-th].

Romatschke, P. (2016), arXiv:1609.02820 [nucl-th].

Rose, J.-B., J.-F. Paquet, G. S. Denicol, M. Luzum, B. Schenke, S. Jeon, and C. Gale (2014), *Proceedings, 24th International Conference on Ultra-Relativistic Nucleus-Nucleus Collisions (Quark Matter 2014)*, Nucl. Phys. **A931**, 926, arXiv:1408.0024 [nucl-th].

Schafer, T., and E. V. Shuryak (1998), Rev. Mod. Phys. **70**, 323, arXiv:hep-ph/9610451 [hep-ph].

Schenke, B., and R. Venugopalan (2014), Phys. Rev. Lett. **113**, 102301, arXiv:1405.3605 [nucl-th].

Schwinger, J. S., K. A. Milton, W.-y. Tsai, L. L. DeRaad, Jr., and D. C. Clark (1976), Annals Phys. **101**, 451.

Seiberg, N., and E. Witten (1994), Nucl. Phys. **B426**, 19, [Erratum: Nucl. Phys.B430,485(1994)], arXiv:hep-th/9407087 [hep-th].

Shuryak, E. (2012a), arXiv:1203.1012 [nucl-th].

Shuryak, E. (2012b), Phys. Rev. **C86**, 024907, arXiv:1203.6614 [hep-ph].

Shuryak, E. (2016), arXiv:1610.08789 [nucl-th].

Shuryak, E., S.-J. Sin, and I. Zahed (2007), J. Korean Phys. Soc. **50**, 384, arXiv:hep-th/0511199 [hep-th].

Shuryak, E., and P. Staig (2013a), Phys. Rev. **C88** (5), 054903, arXiv:1307.2568.

Shuryak, E., and P. Staig (2013b), Phys. Rev. **C88** (6), 064905, arXiv:1306.2938 [nucl-th].

Shuryak, E., and I. Zahed (2013), Phys. Rev. **C88** (4), 044915, arXiv:1301.4470 [hep-ph].

Shuryak, E., and I. Zahed (2014), Phys. Rev. **D89** (9), 094001, arXiv:1311.0836 [hep-ph].

Shuryak, E. V. (1973), Yad. Fiz. **18**, 1302.

Shuryak, E. V. (1978), Phys. Lett. **B78**, 150, [Yad. Fiz.28,796(1978)].

Shuryak, E. V. (1980), Phys. Rept. **61**, 71.

Shuryak, E. V. (1998), Phys. Lett. **B423**, 9, arXiv:hep-ph/9704456 [hep-ph].

Shuryak, E. V. (2002), Phys. Rev. **C66**, 027902, arXiv:nucl-th/0112042 [nucl-th].

Shuryak, E. V., and L. Xiong (1993), Phys. Rev. Lett. **70**, 2241, arXiv:hep-ph/9301218 [hep-ph].

Shuryak, E. V., and O. V. Zhirov (1979), Phys. Lett. **B89**, 253.

Spalinski, M. (2016), Phys. Rev. **D94** (8), 085002, arXiv:1607.06381 [nucl-th].

Staig, P., and E. Shuryak (2011a), Phys. Rev. **C84**, 034908, arXiv:1008.3139 [nucl-th].

Staig, P., and E. Shuryak (2011b), Phys. Rev. **C84**, 044912, arXiv:1105.0676 [nucl-th].

Stephanov, M. A. (2009), Phys. Rev. Lett. **102**, 032301, arXiv:0809.3450 [hep-ph].

Stephanov, M. A., K. Rajagopal, and E. V. Shuryak (1999), Phys. Rev. **D60**, 114028, arXiv:hep-ph/9903292 [hep-ph].

Stoffers, A., and I. Zahed (2013), Phys. Rev. **D87**, 075023, arXiv:1205.3223 [hep-ph].

Svetitsky, B. (1988), Phys. Rev. **D37**, 2484.

Tannenbaum, M. (2014), Nucl. Phys. **A931**, c877.

Teaney, D. (2003), Phys. Rev. **C68**, 034913, arXiv:nucl-th/0301099 [nucl-th].

Teaney, D., J. Lauret, and E. V. Shuryak (2001a), arXiv:nucl-th/0110037 [nucl-th].

Teaney, D., J. Lauret, and E. V. Shuryak (2001b), Phys. Rev. Lett. **86**, 4783, arXiv:nucl-th/0011058 [nucl-th].

Teaney, D., and L. Yan (2012), Phys. Rev. **C86**, 044908, arXiv:1206.1905 [nucl-th].

Tuchin, K. (2013), Phys. Rev. **C88** (2), 024911, arXiv:1305.5806 [hep-ph].

Xu, J., J. Liao, and M. Gyulassy (2015), arXiv:1508.00552 [hep-ph].

Xu, Z., and C. Greiner (2005), Phys. Rev. **C71**, 064901, arXiv:hep-ph/0406278 [hep-ph].

Young, C., J. I. Kapusta, C. Gale, and B. Jeon, S.and Schenke (2015), Phys. Rev. **C91** (4), 044901, arXiv:1407.1077 [nucl-th].

Young, C., and E. Shuryak (2009), Phys. Rev. **C79**, 034907, arXiv:0803.2866 [nucl-th].